AUTONOMOUS COOPERATIVE ASSEMBLY BY FORCE FEEDBACK USING A CONTROL BASIS APPROACH

By

JUAN L. ROJAS

Dissertation

Submitted to the Faculty of the

Graduate School of Vanderbilt University

In partial fulfillment of the requirements

for the degree of

DOCTOR OF PHILOSOPHY

in

Electrical Engineering

May, 2009

Nashville, Tennessee

Approved:

Richard Alan Peters II

Kazuhiko Kawamura

Mitch Wilkes

Julie Adams

Michael Goldfarb

ACKNOWEDGEMENTS

I am ever so grateful to the gift that was given me in being able to attend Vanderbilt University not only for my Ph.D. but for my entire college career. This has been a deeply transformational time in all aspects of my life. I thank God for such a blessing.

I would also like to give my deepest thank to my advisor Dr. Peters. I consider myself very fortunate to have had Dr. Peters as my advisor. His support and belief in me from the very beginning cannot be understated. From the time I started my graduate career to the last day of my doctorate, he has always believed in me. I am also indebted to his commitment to true scholarship, desiring for his students to learn, even if learning takes unconventional roads. I appreciate his deep insights into the application of mathematics to the field of robotics and his help in expanding my understanding identifying unique problems and solutions. I appreciate his courage to start a company and work on development again – this period led to great cooperation working in the development of solutions in robotics. I would like to thank Dr. Wilkes for his ability to simplify complex problems and his love for knowledge. I appreciate Dr. Kawamura's support and partnership over the years. He has helped me understand important aspects on advancing research. This dissertation would not have been possible without the invaluable help of Dr. Adams and Dr. Goldfarb. Dr. Adams has a passion for excellence and has taught me to persist in refining my work and always seek ways to improve my work. Dr. Goldfarb has been a great role model. Both a great teacher and researcher, Dr. Goldfarb has a great passion for scholarly work and helped add great depth to my work.

Special thanks to Christina Campbell, one of the smartest minds I know, without her support in the development of the software architecture none of this would be possible. Gratitude is also due to Dr. Cook who helped me understand the nature of Jacobian's in robotics. A special thank is also due to all the members of the Cognitive Robotics Lab that assisted me over the years: Tamara Rogers, Kim Hambuchen, Palis Ratanaswasd, Stephen Gordon, Erdem Erdemir, Jonathan Hunter, Baris Ulutas, and Esubalew Tamirat. This work was supported by NASA grant NNX07AF04G.

Finally I would like to thank my family. Quisiera darle gracias a mi familia. A mi querido papa que ya no esta conmigo. A ti ma que has sacrificado

tanto desde hace tantos aos. No solo en lo econmico, sino tambin en lo emocional, al estar separados durante tanto tiempo. Gracias por perseverar y junto a mi papa darme tan bonita oportunidad. Estoy muy muy agradecido! A mi hermano y a mi hermana. Siento que estos aos me hayan prevenido pasar mas tiempo con ustedes. Sin embargo, estoy contento de que podamos estar unidos. Los quiero mucho!

TABLE OF CONTENTS

LIST OF FIGURES

LIST OF TABLES

CHAPTER I

INTRODUCTION

Motivation

As part of the new frontiers in space exploration innovative robotic control is sought to enable robotic teams to perform autonomous assembly operations. The advent of robotics has brought many benefits to society. For example, robots have increased the productivity and lowered the costs in wide ranging fields such as the automotive industry, materials handling, food processing, microchip fabrication, circuit board assembly, and pharmaceutical production [Brogardh, 2007]. This has made a vast range of products not only available, but also affordable, to many people and (ostensibly) increased the quality of their lives. The current state of the art in industrial robotics is characterized by the mass produced machine (*e.g.* , articulated arm, conveyor system, autonomous guided vehicle) with a high degree of accuracy and repeatability with a large mean time between failures [Brogardh, 2007]. The industrial robot is limited; however, to highly controlled environments and the repetition of point-to-point algorithms. Sensors if used at all, are mainly to compensate for the small variations that exist in such environments. Sensors are also used to recognize a small set of objects and perform a number of different preprogrammed actions on them. Within the research environment, robots tend to be custom made, one-of-a-kind machines that are notoriously fragile. It is on these prototypical robots; however, that the state-of-the-art in robotics is advanced [Pires and da Costa, 1998]. The porting of advanced technologies from laboratory to to industrial robots poses many interesting challenges that have yet to be addressed.

Robots can project human activity into dangerous environments such as war zones, hazardous material spills, natural disasters, the deep seas, and outer space. The latter is of particular interest in this work because the special needs of space exploration present for robotics, interesting problems whose solutions will significantly expand the capabilities of their terrestrial counterparts as well.[1] In 2004, NASA launched a program to send human beings back to the Moon and later to Mars. NASA requires innovative technologies to develop and build the infrastructure that can support human habitation and exploration in space and on other worlds [OḰeefe, 2004]. The Moon and Mars missions presuppose the deployment of robots that can do just that. It is planned to have robots construct the habitats and prepare them for life support prior to the arrival of astronauts. The robots work will include the assembly of modular structures such as solar arrays, radiators, antennas, propellant tanks, and habitation modules [Rojas and Peters II, 2009].

NASA has carried out several in-depth studies to determine the most suitable hardware for the construction of extraterrestrial mission support systems [Doggett, 2002]. Modular truss structures have repeatedly been selected as the hardware of choice in keeping with the vision of implementing flexible, affordable, and sustainable structures [Diftler et al., 2005, Rhodes et al., 1990]. Therefore among other tasks, robots will have to assemble trusses, which requires them to hold, manipulate, and connect the parts through insertion, twisting, and snapping [NASA, 2007]. These tasks require robots that can work *cooperatively* with other robots to assemble complex structures, and do so robustly. The assembly tasks are suited for force control. Force control by two or more robots, is facilitated if each can take on the roles of leader or subordinate as needed [Boon-Cheong and Chutatape, 1992]. In

[1]This work was sponsored by NASA.

fact, NASA needs robots with reliability that exceeds that of industrial machines and skills that exceed the current state-of-the-art of research machines [Angelo, 2007].

The teleoperation of robots or teams of robots to perform tasks like assembly seems like a reasonable approach. However, latencies in space communications limit the use of teleoperation. In [Angelo, 2007], Angelo states,

> Future robots with suitable design and instrumentation will also allow a human controller to perform hazardous planetary exploration from the comfort of a permanent lunar base or Mars surface base.... The major limitation of using this technique in space exploration will be the speed-of-light distance between the human participant and the collaborative robot that mimics human behaviors. This distance should not exceed a few light-seconds, or else the human being will not be able to respond properly.... In situations with more than five-second time delays in the communications loop, the brain of the human controller might not have time to recognize a serious problem and respond before the at-risk collaborative robot would have become toast-that is, have injured itself or destroyed itself [Angelo, 2007].

The communications latencies across such long distances[2] preclude instantaneous teleoperation of the kind that would be required to control such a team of robots and is now used to control, for example, the NASA Robonaut.

To control Robonaut, a teleoperator dons a VR helmet, data gloves, and other position sensors that connect to the robot so that the operators motions are reflected by the robot concurrently with effectively no time delay [Peters II et al., 2006]. Even without a delay, such minute teleoperation is

[2]The round-trip signal latency between the Earth and the Moon is about 2.3 seconds.

difficult, tedious, tiring, and prone to errors that often lead to several attempts at a task before it is completed [Peters II et al., 2003a]. It is tiring because the operator must pay close attention to even his slightest moves and the resultant moves by the robot. Seemingly simple behaviors that a person rarely thinks about, such as grasping an object, become the focus of intense concentration that rapidly wears the operator out. Moreover, the object of manipulation is usually under the complete control of a single robot. A team of robots individually teleoperated by a number of operators tasked to jointly handle objects would greatly magnify those problems along with the challenges associated in coordinating the contributions of all teleoperators. Time latency challenges would render the approach close to impossible. Fully autonomous robots capable of cooperative assembly do not yet exist and are unlikely to be developed soon enough for the NASA missions.

Researchers are implementing a framework where an operator and a robot can vary the degrees of autonomy and do so in a way to maximize the success rate of the task. Heger, Hiatt, Simmons, Sellner, and Singh have researched how to optimize human involvement and increase task efficiency and robustness while supervising a robotic team [Heger et al., 2005]. This so-called "sliding autonomy" –wherein a teleoperator tasks a robot at a level above basic manipulation– ameliorates both the problems of tedium and of time delay. A teleoperator could, for example, guide a robot to an optimal position where grasp or assembly can take place. Then the robot slides to autonomous mode and performs the lower-level task that is so tiring to teleoperate and hard to coordinate. If the duration of autonomous behavior is on the order of the communications latency, then higher-level tasking becomes possible. Sliding autonomy is the focus of current research and is likely to be developed sufficiently for deployment on the missions [Simmons et al., 2007].

The full-autonomy problem is reduced to one of consecutive periods of short-term autonomy. And the short-term behaviors related to assembly can be implemented with a combination of position and force control (*i.e.* , hybrid control). Therefore, to meet the preassembly goals of the upcoming missions, NASA needs robots that can act *autonomously* using hybrid controllers for periods of time on the order of seconds to minutes. To date, this has been an open problem; in the literature, there appear to be no teams of heterogeneous robots that perform joint assembly tasks in open environments.

The goal of the research presented herein was to develop controllers that, at once, enable short term autonomy and cooperative assembly by two robots of highly differing morphology. The work advances the capabilities of heterogeneous robots to cooperate on some of the low-level tasks necessary for autonomous assembly. It presents a control strategy that allows independent robots in loosely structured environments to carry out beginning-to-end insertion tasks. The approach is to modularize and encapsulate the control problem by recasting it in terms of locally robust and reactive controllers. The controllers do not require explicit planning, rather through sensory stimuli and force control they drive the system to optimal state configurations: two separate parts joined together.

Contributions

This work takes a distributed approach to the short-term control of teams of heterogeneous robots so they can perform modular-truss assembly tasks cooperatively and autonomously. The system uses a *control basis* approach that allows both sequential and concurrent execution of position, force, and moment control primitives in two robots to generate force-driven joint assembly in an open environment. Experiments with two heterogeneous robots

to join two parts into a stable, rigid configuration have been conducted and are reported on here. This work is the first of its type and is intended to solve useful and necessary problems as part of the future developments in space exploration.

In short, the novel contributions of this work are the following:

1. The design and implementation of controllers that allow the autonomous joining of two mating parts by two independent, sensory-guided heterogeneous robots with articulated arms that operate in an uncalibrated environment.

2. The use of independent control bases by two robots, in which controllers reduce contact forces by displacing parts in response to local force, moment, and position feedback.

3. The coordination of a pneumatically actuated and highly compliant humanoid robot with a rigid industrial manipulator.

4. The implementation of reactive behaviors on a decidedly non-reactive, point-to-point, pre-programmable, industrial robot arm.

5. The ability to swap leader and subordinate roles in coordination schemes. Active-active and active-static coordination schemes are implemented through inter-robot communication.

It was found that a small set of basis controllers consisting of moment, force, and position primitives are able to implement simple low-level assembly tasks through force sensing. It was concluded that through appropriately defined and sequenced control laws, a vast array of tasks can be achieved. Tasks can be completed individually or through cooperation and under different coordination schemes across robots.

Based on experimental results, the principal strengths of this work are decreased task completion times when performed by two active robots as compared to times obtained by active-static coordination schemes or individual robots; and increased fault tolerance as a result of using a compliant robot. Particularly in cases where jamming occurred. Weaknesses of this system include an explicit dependance of the robot's responsiveness to the sensory stimuli on manually derived controller gains. This dependance limits the ease and flexibility with which the system is deployed across different robotic testbeds. Also, while the artificial muscles ease the accommodation of parts, the stiction associated with the elastic nature of the muscles can slow the task execution and increase experienced forces in the assembly task.

Document Overview

This document presents the implementation of the control basis and its application to joint cooperative assemblies. Chapter II presents prior related work in the fields of space robotics, multiple-robot manipulators, and autonomous assembly. Chapter III overviews the theory behind the Control Basis Approach and presents a formal framework for the generation of a primitive controller as well as a compound controller. An optimization technique for multiple objectives across controllers is also presented. Chapter IV defines controllers relevant to the execution of assembly tasks. The first section describes primitive controllers from which composite controllers are built. Then, composite controllers used to perform insertion operations in both robots is described. Chapter V shows experiments that demonstrate the performance of the basis controllers introduced in Chapter IV, with one and two robots. Analysis of the efficiency and effectiveness of the system is

carried out and comparative evaluations of the performance of the assembly tasks in the different scenarios. Finally, Chapter VI presents concluding remarks and unsolved problems.

CHAPTER II

PREVIOUS WORK

The near-term future of space robotics will require both partial autonomy and multi-robot cooperation [Angelo, 2007]. The study of semi-autonomous cooperative assembly draws concepts from both multi-robot coordination and autonomous robotic assembly. This chapter reviews previous work in space robotics, multi manipulator control, and autonomous assembly is presented.

Space Robots

The development of space robotics has occurred over the past 50 years. The roles robots have played has been predominantly ones of virtual laboratories that analyze the extraterrestrial objects through instrumentation. New roles have emerged and use robots as assembly manipulators and human assistants. The near future holds even a wider variety of uses in space construction and exploration. To such ends, prototype cranes, humanoids, and heterogeneous robots are being tested and analyzed [Ambrose et al., 2000, Simmons et al., 2007]. This section presents relevant examples to assembly as described in [Angelo, 2007] and a more comprehensive overview can be found in Appendix C.

In 1997, Japan launched a satellite that used a tele-operated robotic manipulator in space. The ETS-VI1 space craft was used for a number of experiments to exchange equipment and supply fuel. The inclusion of the manipulator affected the navigation dynamics of the systems, and so, researchers carried out detailed analysis of how this new equipment affected the system [Oda, 2000].

In 2001, Canada developed the second version of the Canada Arm originally deployed in 1981. The original mechanical arm was part of space shuttle remote manipulator system and served to maneuver payloads. The second generation of the arm, the *Mobile Servicing System* was part of the International Space Station (ISS) and consisted of three parts: the Canadarm2, the mobile base system, and the special purpose dexterous manipulator. The 3-part system allows the very large robotic manipulator (17.6 meters when the robot arm is fully extended) to move about the ISS via rails or trusses positioned in the station. The purpose of the teleoperated crane is to maneuver payloads around the ISS, carry out assembly tasks, and also repair operations [NASA, 2006a]. The CandaArm has been essential in the creation of the international space station. The use of a similar system that is autonomous and mobile on planetary surfaces would greatly benefit surface missions for future space launches.

NASA scientists have created rovers, which are mobile robots that explore planetary surfaces. In 2003, NASAs deployed the Mars Exploration Rovers: Spirit and Opportunity. Both rovers successfully are completing a teleoperated surface exploration mission under the supervision of mission controllers at NASA's Jet Propulsion Laboratory [Angelo, 2007]. Communication with these robots is intermittent yet they are able to complete a variety of experiments that analyze the martian surface. Similar robots with the ability to perform manipulation and assembly tasks are sought for future missions.

NASA scientists are also developing a humanoid robot, known as Robonaut [NASA, 2006b]. The goal of this humanoid robot is to work as an assistant to astronauts during space missions. Other uses for the robot are to prepare a work-site prior to the arrival of an astronaut. The robot is currently tele-operated and learning to automate tasks like manipulation and grasping

[Culbert et al., 2003, Peters II et al., 2003b, Diftler et al., 2005, Peters II et al., 2006, Peters II and Jenkins, 2006]. This project is focused on a human-robot collaboration. Our work focuses on autonomous robot-robot collaborations for space construction.

Looking ahead, NASA is devising a new types of extra-vehicular robots that take advantage of microgravity environments to perform a variety of jobs: a) a minimally invasive tendril for inspection tasks, b) an arachnid climber for transportation tasks c) a lemur for fine assembly and tool-related tasks (cutting and fastening), and d) free-flying nanosatellite cameras to guide systems [Rehnmark et al., 2003, Rehnmark et al., 2005].

This dissertation aims at furthering the capabilities of robots in outer space. The research done advances the possibility of teams of robots working together as they are supervised by human operators through teleoperation. The goal is to facilitate the creation of modular space structures used for construction and exploration through the use of a control basis for joint assemblies.

Multi-Robot Manipulators in Assembly Tasks

After the inception of computer-controlled robotic manipulators in the late 1960's [Whitney, 1987], it was not long before researchers began to work with multiple robotic arms simultaneously. It was evident that working with a number of robotic arms permits increased flexibility and reduces time-to-completion of tasks, higher load capacities, amongst others benefits [Brogardh, 2007]. Multiple robot-arm coordination has been investigated for nearly four decades amassing a large research literature. Challenges involve the control of position and/or force in the face of uncertainty in the robot, the manipulated object, or the environment. Historically, control

schemes have been applied first to single robots and then extended to multi-manipulators. Such research has been applied to the fields of manufacturing, object manipulation, parts assembly, and more recently servicing tasks in space [Namvar and Aghili, 2005]. In the literature, multiple robot coordination has been predominantly between two identical robots, although the inclusion of more robots is present in simulation [Sun and Mills, 2002]. Recently, cooperation across heterogeneous robots has been explored along with a number of coordination schemes to improve task performance across multiple manipulators. The term robot control will be considered synonymous with manipulator control in this section. A summary of the development of key efforts to solve dexterous manipulation challenges leading to assembly tasks through the use of heterogeneous cooperative robots is presented.

Homogeneous Multi-Robot Manipulators

This section reviews the inception and development of position and force control in single and multiple robot manipulator systems, which includes the development of homogeneous robot control, coordination schemes, and their application to insertion tasks.

Multi-arm robot control research is divided into three different coordination approaches: the master/slave scheme, the centralized scheme, and the decentralized scheme [Ishida, 1977, Prisma Lab, 2007]. The master/slave scheme selects one robotic manipulator as a leader and the other one as a follower [Arimoto et al., 1987]. This technique has been applied to tasks requiring simple joint motions, but it exhibited a time-lag by the subordinate manipulator. The centralized systems characterize a number of robotic systems as one entity, sharing one controller for all robots, and exerting tight coordination between them. Such systems produce high throughput

in strictly controlled environments but are susceptible to failure if a single localized fault occurs [Brookshire et al., 2004]. When the robots have a high number of degrees of freedom the system suffers from a complicated architecture [Liu et al., 1996]. The decentralized system, on the other hand, requires robots to work independently without higher-level coordination. Decentralized systems are primarily distributed systems that use communication protocols to message each other. The manipulators interact physically at the task level, where each robot has its own controller, thus rendering the system more fault tolerant and flexible. However, tight coordination is challenging [Xi et al., 96].

Master-Slave Schemes

The earliest types of multiple robot controllers were master/slave architectures. Ishida implemented one of the first systems [Ishida, 1977]. He coordinated two arms to manipulate an object in free space by using parallel and rotational motions. The master arm used position control while the slave used compliance control. Issues of load distribution and stability were not considered. Alford and Beylen followed with a similar approach were both robots used position control [Alford and Belyeu, 1984]. The slave arm was shown to follow the master arm harmoniously without manipulating an object [Alford and Belyeu, 1984]. Later, Arimoto, Miyazaki, and Kawamura extended the system to a multi-fingered hand [Arimoto et al., 1987]. The hand consisted of one master finger and two slave fingers that held an object forming a tight and closed kinematic chain. Spring characteristics were conidered between fingers in the control problem yielding asymptotically stable behavior. These initial experiments were a first step in robot coordination using pre-established trajectories and no force sensing.

Hybrid Position and Force Control

In 1981, Mason presented his seminal work on compliance and force control [Mason, 1981]. Raibert and Craig implemented this theoretical work on a two joint manipulator [Raibert and Craig, 1981], and a few years later, Hayati, extended this framework to two cooperating arms [Hayati, 1986]. Mason's seminal paper established the theoretical framework to implement a hybrid position and force controller. The position and contact forces generated at the end-effector were controlled in concert to achieve compliance. The premise was to identify a set of existing position and force constraints in the task space. It was proposed that any job can be decomposed into two orthogonal sets of constraints, denominated as the *natural* and *artificial* constraints. The former consists of the position and force elements that are inherently constrained by the mechanical and geometrical characteristics of the task. The latter are desired reference values that can be specified by the user. The theory can be illustrated by considering an example where a peg is inserted into a hole. First, a reference coordinate frame in world coordinates must be selected and labeled as: *C-frame* [Asada and Leonard, 2005]. Second, the natural physical constraints are identified. In this case the peg is unable to move or rotate in the $\vec{x}$ and $\vec{y}$ directions as seen in Figure 1. These four parameters $v_x, v_y, w_x,$ and w_y form part of the set of natural constraints. On the other hand, the peg can move and rotate in the z-direction: v_z, w_z. These values are determined by the user and are considered artificial constraints. No net force or torque is generated about z (assuming a frictionless surface). Hence f_z is a natural constraint. The forces and torques about the x and y direction can be arbitrarily assigned by the user and belong to the set of artificial constraints: f_x, f_y. After all sets of constraints have been established, two diagonal and binary matrices: S and $(1-S)$ are used by the

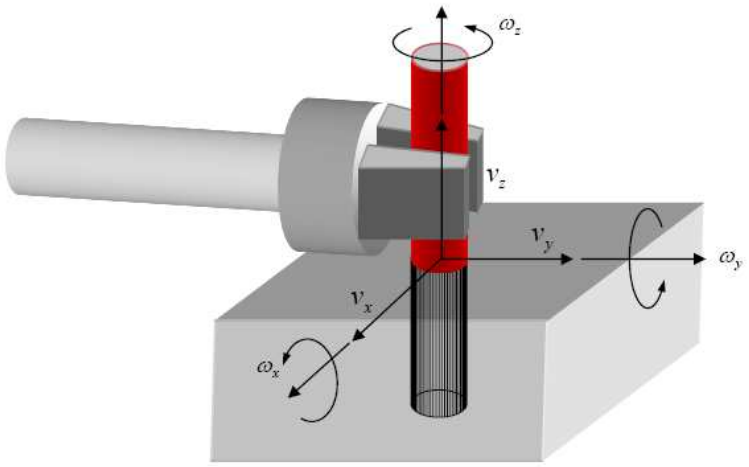

Figure 1: Assignment of the C-frame [Asada and Leonard, 2005]

controller to encode the natural and artificial constraints such that the goal of the task is achieved without negative interference from physical constraints. A hybrid force-position controller works by computing force and position errors and filtering them through the constraint matrices via two separate force and position feedback loops. The result is an update motion in joint space that achieves the desired force and position goals. While many modern force control strategies use this foundational theory in their work, the technique is limited to specific situations and requires the manual elaboration of the constraint matrices ahead of time [Yuan, 2006].

Hayati extended Mason's theory to include multiple manipulators [Hayati, 1986]. In Mason's work, multiple robots rigidly held and manipulated an object. Natural and artificial constraints were defined for each manipulator and to determine the position of the object through the controller. In contrast to a single manipulator, additional constraints are necessary to guarantee coordination and prevent undesired forces across robots. This issue is known as load distribution and is important in cooperative robotic tasks. Hayati used one

set of constraints and one common *C-frame* for all manipulators to simplify assigning constraints. A centralized controller divided the task space into a position and force subspace. Position distribution was determined on the basis of mass and inertia tensors of the links. Force distribution was computed by minimizing a weighted error function. The stability of the controller was guaranteed as long as the mass of the arms and the object were accurately known. Mason's work suffers the same limitations as Hayati's. Constraint parameters and load distribution parameters must be defined ahead of time for a specific task and robot. This prerequisite makes it difficult to the deploy the architecture across different robots and to succeed in scenarios were task conditions are dynamic.

To increase the accuracy and responsiveness of the system, Yoshikawa [Yoshikawa, 1987] extended Raibert and Craig's work by including manipulator dynamics into the hybrid position-force controller. The inclusion of dynamics established a theoretical framework that derived the joint torque necessary to achieve both position and force goals – a condition not previously guaranteed. Yoshikawa used hypersurfaces to define the constrained motion of an object. The surfaces were represented by a unit vectors normal and tangent to a surface. These surfaces essentially implemented normal and artificial constraints for the task. The hypersurfaces along with reference position and force values were used to compute necessary joint torques to complete the task. Yoshikawa extended his approach to include the coordination of a constrained object by a pair of 2 DoF planar robots [Yoshikawa, 1993]. Like Hayati, Yoshikawa coordinated robots by explicitly defining the amount of force each manipulator would apply to the object (also known as the internal force) [Yoshikawa and Nagai, 1987, Kumar and Waldron, 1988, Nakamura et al., 1989].

The total force experienced by a manipulator is a function of the desired constraint force and the internal force. The latter is projected onto the null space of the constraint force to prevent hindrances of the desired motion. Once the constraint hypersurfaces are determined, the desired position and force are used in conjunction with the measured internal force to determine the dynamics of the manipulator and to compute the joint torques necessary to complete the task. The projection of one vector quantity onto another can be used in the optimization of a goal. In this case, the most important goal is the constraint force. The force applied by each robot to the object must be subordinate to that of the entire system. While this technique allows two robots to coordinate, it is rigid in that it can only be applied between the constraint force and the internal force. This approach produces finer joint control at the expense of a more complicated derivation of manipulator dynamics. Manipulator dynamics are not trivial. Highly complex control-models depend on the accuracy of the dynamics for their stability. This dependence limits the system's robustness in the presence of uncertainty, which is common in dynamic environments. The control basis approach, on the other hand, generates reactive and robust behavior without off-line planning or requiring the manual setting of parameters. Primitive controllers can be combined without the need for complex modeling to achieve multiple tasks in an optimal way. Chapter III describes the approach in detail.

Adaptive Techniques

Up until that point in time, researchers had derived continuous control models that assumed precise system knowledge. In these cases, system stability is dependent on the accuracy of the system model. Model-based systems

are particularly vulnerable to dynamic environments which often are complex, highly non-linear, and stochastic. Hence, monolithic control laws are of limited applicability to complex tasks and environments [Walker, 1990, Huber, 2000]. Due to the complexity of calculating system and environment parameters, researchers turned to adaptive control methods. These have been applied to both single and multiple manipulator domains with positive results.

Jean and Fu, applied adaptive control techniques to perform motion tracking and internal force computations on simulated multimanipulator systems moving an object [Jong-Hann and Li-Chen, 1993]. They established a dynamic equation of motion that considered the contributions of participating robots and a manipulated object. The authors introduced an adaptive control law that estimated the dynamic parameters of two, three degree of freedom, planar, joint manipulators. Global convergence in trajectory tracking errors and internal force errors was achieved. With respect to the environment, Namvar and Aghili, estimated object parameters when its geometry was unknown [Namvar and Aghili, 2005]. They implemented an adaptive control strategy that used adaptive observers and parameter update laws to estimate the stiffness and geometry of the environment for a 2 DoF manipulator in simulation. The controller generated force torque signals that asymptotically tracked desired forces and motion trajectories [Namvar and Aghili, 2006]. Adaptive strategies relax the dependency on highly accurate system parameters. Yet adaptive control laws are still constrained to the structure of the model used. The same adaptive control law is generally inapplicable across robots and tasks. One of the key strengths of the control basis approach is its flexibility. A control basis is composed of a number of primitive controllers that are locally-robust. If the constituent

primitive controllers are defined appropriately, a small set of basis controllers are able to generate robust behavior in multiple tasks and environments. The control basis approach effectively decomposes a control problem into a number of interconnected concurrent controllers, where each controller or group of controllers achieves specific goals and maintains stability [Brock et al., 2005].

Intelligent Control Schemes

Cooperative control of two or more robots is challenging; extending solutions from single manipulators is not trivial. Research surveyed thus far has covered position and force control, including internal forces and load distribution, and adaptive estimation of system and environmental parameters. These techniques challenge roboticists to look for intelligent but simplified ways to control and coordinate robotic manipulators. Mukiyama designed a simple cooperative scheme that used hybrid position-force controllers to manipulate an object [Mukaiyama et al., 1996]. A decentralized leader-follower scheme was implemented where the leader established the goal of the task using position control and the follower reacted through force-feedback, which represents an extension of prior master/slave systems but now included force-feedback. The scheme sought to overcome time lags encountered in inter-robot communication. However, the force controller, exhibited a slow response, creating undesired time lags. Interestingly this approach seeks to achieve object manipulation by separating position and force control, not within a controller loop, but across robots. The approach ensures that regardless of where the leader robot moves, the subordinate robot does not impede the motion of the leader. The control basis approach uses this idea and applies it across control primitives. The methodology allows multiple objectives to be optimized within a control policy, which eases automation

and yields a greater flexibility to achieve different tasks. Section III presents more details on multiple objective composition.

Another intelligent control scheme is found in [Xi et al., 96]. Xi, Tarn, and Bejczy developed an event-based, decentralized, hybrid position/force controller for multi-robot coordination. This scheme used a planner combined with the current state of a system (*i.e.* the desired position and force of each robot) within the controller's closed loop in real-time. Decentralized communication was used to implement hybrid controllers that used nonlinear feedback to linearize and decouple the output in generalized space coordinates. A projection vector was used to transform the generalized coordinates to the task space for the robot. The method efficiently coordinated a dual-arm system that held cardboard boxes of different sizes. This design enabled tasks to be described in the task space of each robot while the structures of the controllers were task independent. The feedback scheme also allowed sensory information, robot planning, and the system control to be integrated more easily. Like Xi *et al.* 's work [Xi et al., 96], the control basis is deployed through a distributed multi-agent software system that allows for inter-robot communication with no planning necessary across a team of heterogeneous robots.

Later, Sun and Mills designed a scheme that although simple to set up, was applicable to a wide range of applications [Sun and Mills, 2002]. They observed that a coordination task required manipulators to maintain a synchronous motion with their immediate neighbors. An error criteria was established that considered not only the position error, but also the differential position error across neighboring robots [Sun and Mills, 2002]. The authors derived a synchronization method known as cross-coupling and embedded

it into an adaptive controller that used the feedback of position and synchronization error. They guaranteed the asymptotic convergence to zero of position and synchronization errors when they coordinated the trajectories of two 6 DoF industrial manipulators. They also used this scheme to simulate the interaction of four 2 DoF planar manipulators [Sun and Mills, 2002]. The adaptive synchronized method yielded satisfactory convergence for the position tracking and good performance for the position synchronization. While the manipulation of an object may be encoded through differential motion, assembly tasks often are more convoluted. Robot motion results from experienced forces during insertion. The control architecture must be able to compensate for local disturbances and drive the assembly using force sensing. In 2006, Yuan carried out an assembly task using force-sensing across two identical industrial robots [Yuan, 2006]. To the best of the author's knowledge this is the only published work that shows multi-manipulator assembly using force sensing (see Figure 2). The main contribution of the paper was the use of a self-tuning proportionalintegralderivative (PID) controller that scheduled tasks adaptively based on the state of the process [Yuan, 2006]. Yuan used a real-time force/torque leading controller that included robot dynamics and admission control to guide force assembly in a peg-in-a-hole experiment. The admission matrix helped to correct misalignments in insertion and was designed from the requirements of the task. Yuan compared force readings of assemblies executed with one robot with those executed with two robots. Results suggested that force signatures vary greatly in these tasks and that force sensing must be used to successfully execute an assembly. Yuan's work follows a model-based approach like some of the work reviewed earlier in this section including manipulator dynamics and an admittance matrix. The assembly is controlled through a task sequencer in which a leading robot drives

the assembly. As part of joint assemblies, Yuan's robots always acted independently and contributed to the task in some way. The work reported in this dissertation involves two robots in active-static and active-active control configuations. Interactions in active-active scenarios are uncalibrated and unplanned. Both robots behave autonomously and reactivly to cooperate in the insertion task.

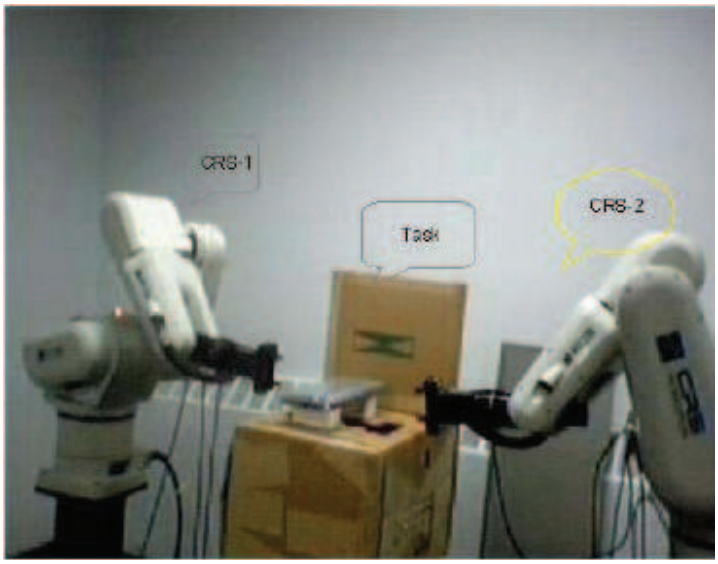

Figure 2: Image of two homogeneous robots attempting assembly through an adaptive PID scheduler [Yuan, 2006].

Finally, NASA's Johnson Space Center (JSC) and Jet Propulsion Laboratory (JPL) are developing a system that is designed to be low weight and requires low power [Stroupe et al., 2006]. NASA researchers are working on an autonomous Robotic Construction Crew (RCC) that consists of two mobile robots, each equipped with a 4 degree of freedom (DoF) arm, a 3-axis force-torque sensor, and a stereo camera pair (Figure II). The RCC coordinates motion to manipulate, transport, and place a beam on a stanchion. The robots use their visual system to locate a fiducial that marks pick-up and drop-off positions. During transport, force data corrects misalignments of the robots by updating the velocity of the robot designated as follower

[Huntsberger et al., 2005]. It is worth noting that force feedback is not used for insertion tasks, but only for coordination during transport. As with our work, the control basis uses a visual system to determine reference positions for the insertions fiducially marked. Force sensing is used by each robot to optimize pose and alignment to successfully drive the insertion.

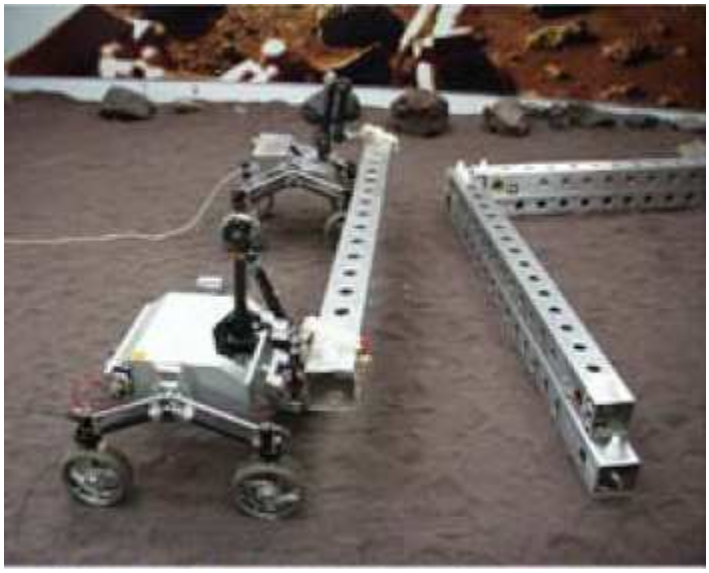

Figure 3: Two mobile robots, the RCC, coordinate to transport a beam [Stroupe et al., 2006]

More recently heterogeneous robots for manipulation, transportation, and assembly have been used. The next section reviews key literature in this area.

Heterogeneous Multi-Robot Manipulators

Teaming up heterogeneous robots to accomplish a task extends the capabilities of the robotic team and increases robustness [Heger et al., 2005]. Humans often create teams of individuals with specific skill sets, experience, or

abilities to accomplish a goal. In space construction for example, the environment forces systems to be low weight and low power. Robots need to endure hazardous climates and yet be able to assemble modular habitats and systems. As proposed by NASA's Human-Robotics working group, teams of heterogeneous robots coupled with human operators will be most effective in completing necessary space missions [Culbert et al., 2003].

The use of heterogeneous robots for autonomous assembly tasks has been studied by two groups: one at the Robotics Institute at the Carnegie Mellon University (CMU) and another at NASA's Jet Propulsion Laboratory and Johnson Space Center. At CMU, research on varying degrees of autonomy has been ongoing for a number of years. Generally, robotic tasks are executed through teleoperation or automation. The latter can suffer from environmental contingencies and complications, while the former can suffer from communication latencies, constricted bandwidth, and human limitations. For these reasons, the CMU team designed a system that allowed operator intervention at varying degrees of autonomy and coined the term "Sliding Autonomy" [Brookshire et al., 2004, Simmons et al., 2007]. The CMU team of heterogeneous robots consisted of a roving eye for localization; a 6 DoF crane for heavy lifting; and a mobile manipulator for fine manipulation tasks. This diverse team executed tasks in different configurations. All tasks consisted of docking suspended beams on top of stanchions. Within a task, each robot had a specific role. The rover eye detected objects using fiducial marks and communicated goal positions to the rest of the team. The crane moved the beams to general locations. The mobile manipulator was responsible for docking the beams on the stanchions [Sellner et al., 2005]. Figure 4 shows the robots at work at the CMU site. This dissertation studies collaboration

across robots for specific assembly tasks. Different collaborative strategies are presented to study force dynamics in insertions.

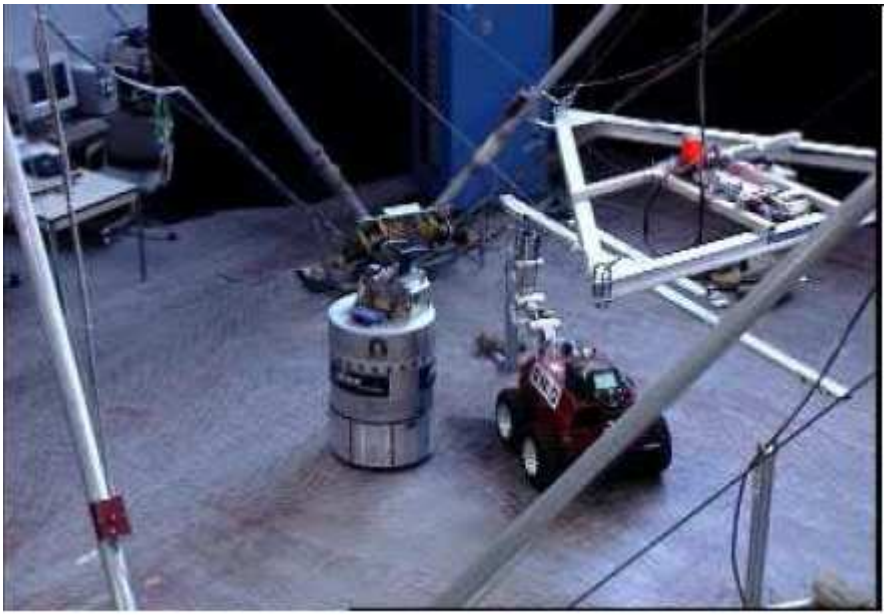

Figure 4: Two mobile robots coordinate to transport beam [Simmons et al., 2007]

Finally, researchers at JPL and JSC are prototyping a new generation of space vehicles and platforms that are flexible and extensible to support extended human missions and scientific observations. New robotic archetypes are envisioned to assist in the construction and maintenance of such systems. The robots may be remotely controlled or automated and are to be technologically capable of achieving part mating, connecting ancillary equipment, and verification of assembly completion, amongst other tasks [Rehnmark et al., 2005]. Three novel robotic prototypes were created and are currently being updated. An arachnid climber boasts light and smooth gaits to aid in material transport. A fine manipulation specialist handles

a wide range of assembly and maintenance tasks with minimal limb reconfiguration. A minimally invasive tendril loaded with sensors was devised to inspect and repair worksites with difficult access and to ensure their structural integrity.

Autonomous Assembly Strategies

The study of parts assembly can be understood as the mating, connection, or insertion of one part into another. Assembly processes are used extensively in manufacturing and automotive industries, for fastening parts, and circuit board assembly. The problem of assembly has been understood as a problem of mating strategies and contact dynamics [Gottschlich and Kak, 1989]. On the one had, mating is a function of two kinds of motions: *guarded motions* and *compliant motions* [Inuoe, 1981]. The former is related to the approach prior to contact, the latter is related to the insertion motion after contact. On the other hand, assembly motions are influenced by the external forces exerted on contact. Contact mechanics describe the nature of impacts and sliding that can help successful insertions, error detection, and error recovery [Donald, 1987]. Important challenges in autonomous assembly consist of: misalignment of parts, geometric uncertainties of fixtures, instability of the system, inaccuracies in control or system parameters, friction, and damage prevention for the robot or the environment [Mathewson, 1994].

Early research on assembly involved the development of passive and active compliant devices. Passive compliant devices are capable of adjusting to slight misalignments in the assembly tasks and to minimize wedging or jamming [Asada and Kakumoto, 1988, Peshkin, 1990, Watson, 1981]. They were designed to respond favorably to the common challenges encountered in assembly motions. Compliant devices came to be known as Remote Center

Compliance (RCC) devices. RCC devices commonly used chamfers to facilitate insertion and to prevent the system from jamming or wedging. The experiments in this dissertation do not use an RCC, rather a pneumatically driven humanoid robot, whose muscles are inherently compliant. We have found no litereature on compliant robots used to perform assemblies. This dissertation studies the combination of a stiff industrial robot with a compliant pneumatic robot. The findings are reported in Chapter V.

Active compliance, uses low-level force-feedback to perform force control explicitly. Force control can be implemented in either cartesian or joint space and can servo the robot with respect to position, velocity, or torque [Maples and Becker, 1986]. Active compliance typically is coupled with high-level strategies that generate planned motions as a function of the force readings. Examples of high-level strategies are: the use of force-cones, contact dynamics, and conditional probability strategies. These approaches require planning strategies for insertion and precise knowledge of part specifications. The strategies are successful in driving assembly tasks for specific environments but are limited in their applicability to situations where the environment changes. Planning is done *a priori* and may include the derivation of governing equations of motion and force-cone conditions to insure optimal contact configurations [Gottschlich and Kak, 1989, Shahinpoor and Zohoor, 1991, Lee and Smith, 1984].

Another method termed 'Accommodation control' used force readings to produce corrective velocity commands and to ensure the proper mating of a workpiece with its corresponding fixture [Schimmels and Peshkin, 1990]. The technique guides force control to correct misalignments in automated

assembly. Accommodation, however, must be constrained to low force-feedback gains to insure stability in high-stiffness environments. The constraint on the gains slows assemblies [Mathewson, 1994]. Others attempted to increase accommodation gains while lowering velocity gains to enhance the response of the system, but that increased internal friction and the stiction of the fixture due to increased internal friction. Continued efforts on accommodation control led to a more advanced level of servo control known as Natural Admittance Control (NAC) [Hogan, 1985]. NAC suppressed coulomb friction and was more responsive and stable under a variety of stiffness conditions [Glosser and Newman, 1994]. Since then, a variety of intelligent strategies have been implemented that incorporate admittance control [Chen et al., 2007]. The design of virtual attracting regions and an optimization algorithm was used in [Newman et al., 2001a]. Virtual attraction points were generated computationally to create nominal trajectories from end-effector positions to attractor points. A genetic algorithm was used to select a multi-dimensional vector trajectory and system dynamics parameters to reduce the time-to-completion of the assembly process. Results yielded better performance than a human worker doing the assembly. Similar efforts defined and manipulated regions of attraction, where a part was geometrically partitioned and analyzed to estimate the best trajectory for an insertion. An impedance controller was used to push and align a part compliantly [Stemmer et al., 2007]. This dissertation proposes a similar approach, where the primitive control elements of the basis set are scalar potential functions. Using greedy descent, each primitive converges to basin attractor regions over time to generate autonomous and locally-robust behavior.

Neural networks have been used to study force-moment patterns in assemblies to guide intelligent searches [Newman et al., 2001b]. Scientists interpreted moment data and computed corrective motions for the end-effector. Others used an advanced visual system to perform tight-tolerance, high-precision assemblies [Chen et al., 2007]. The visual system in this dissertation does not provide very accurate position estimations. The uncertainties of an dynamic environment are present. The basis controllers, however, compensate for bounded disturbances in the environment.

Computer aided design (CAD) models have been used recently. Thomas, designed a system that performed offline planning for complex part assembly [Thomas et al., 2005]. Model information was derived from CAD data and used to render a series of virtual steps to perform an assembly. Assembly plans were performed offline through a series of connected skill primitives that allowed the sequential construction of a trajectory for the mating of each set of parts. In [Thomas et al., 2007], the planning process was automated by using CAD designs and derived force-torque maps of the configuration space. As in [Thomas et al., 2005], the control basis requires control policies that sequence composite or primitive controllers to achieve beginning-to-end behavior. The sequencing of controllers is learned by the designers' experience although a control language and learning scheme exist to automate this process [Platt, 2006]. The correct sequence of controllers is indispensable to generate asymptotically stable behavior through the task.

While research in robotic assembly has had success creating advanced execution strategies and control methods, most of the implemented systems remain bound to the laboratory or the assembly line. Some of these approaches require the complete modeling of the environmental dynamics as well as the interactions between the robot and the fixture. Stability analysis,

such as the one presented in [Stemmer et al., 2007], requires precise knowledge of the system or is forced to make simplifying assumptions. As stated by Huber [Huber, 2000], the robustness of control policies is limited in the presence of uncertainty. The challenging process of modeling complex robots with precision, limits the scalability of the approach to a smaller set of tasks and environments than one might like.

Similarly, model-based planning solutions suffer some of the same challenges. They require *a priori* geometrical information, or the partitioning of a path into sub trajectories to generate a functional path. While some of these planning methodologies offer corrective measures in the presence of position error, the presence of uncertainty often leads to failure.

Using a control basis approach in the assembly process can overcome the aforementioned limitations. The control basis approach, introduced by Coelho and Grupen [Coelho and Grupen, 1997] partitions the control space into lower-dimensional, local control laws that are asymptotically stable under local perturbations and can be run concurrently. This technique requires no explicit planning to create trajectories, since the system moves to good configurations reactively.

Summary

Space robotics is advancing at a rapid pace. A new generation of robot archetypes will be necessary to fulfill future space construction and exploration missions, particularly robots that are able to fulfill their tasks over the latencies of space communications.

Multi-manipulator robotics has seen significant developments in modeling and control under constrained environments. As the complexity of robots and goal tasks have increased, a greater reliance on adaptive and simple yet

effective control methods have also been evaluated. Methods to increase the overall efficiency and effectiveness of partially supervised robot teams are being studied. The future of space robotics will undoubtedly see a more frequent occurrence of such teams.

Similarly, in assembly research, most solutions require accurate knowledge of system dynamics and planning strategies. Such requirements significantly limit the deployment of such systems in dynamic environments. Simple and flexible automated strategies are desired so they can be applied in a variety of environments to tasks and can function robustly in the presence of uncertainty.

CHAPTER III

THE CONTROL BASIS APPROACH

The control basis is a primitive organizational structure composed of parametric closed-loop controllers. The approach decomposes a complex control system into a series of modular control elements that when connected appropriately synthesize a variety of behaviors. The approach is rooted in closed-loop control for the following reasons: (i) nearly all actions in robotics are encompassed under closed-loop control, (ii) it is a basis for error suppression, and (iii) the interaction between the robot and the world is modeled as a dynamical system [Huber, 2000, Brock et al., 2005]. This approach was originally suggested by Coelho and Grupen [Coelho and Grupen, 1997]. A basis comprises a number of closed loop controllers, which represent primitive actions, and can be derived from a set of control laws. While similar approaches appear in the literature [Son et al., 1996, Jameson and Leifer, 1987], the way that a control basis factors objectives and captures the declarative structure of a solution was novel when first proposed [Brock et al., 2005]. In other words, each controller in the basis represents a single objective that is achieved from sensory inputs and effector (or commonly actuator) outputs. Single, closed-loop controllers can be referred to as segmental actions, and are exemplified by spinal cord reflexes, as Brock *et al.* states:

> These reflexes are specific stimulus response mappings in service to a single objective like the withdrawal reflex that extracts ones hand from a fire. They can be coupled in intersegmental arrangements such as the contralateral extension reflex that can accompany the withdrawal reflex. These arrangements serve two,

> concurrent objectives: one to extract a limb receiving a painful stimulus, and another to extend the other limb in a protective behavior [Brock et al., 2005].

Each controller in the set is a primitive that synthesizes on-line behavior by limiting the closed-loop response to specific stimuli and by engaging specific effector resources on low-dimensional subspaces of the system state-space. Complex behavior is generated by combining and sequencing a number of the primitive closed-loop controllers. The sequence is in effect an "instruction set" for performing complex tasks and provides a structure for larger-scale control policies. This approach prevents the generation of a monolithic controller, which is of limited applicability in dynamic environments, it also increases robustness by reducing the need for complete and accurate system models [Huber, 2000].

The feedback controllers are derived combinatorially from control laws. These laws are designed to yield asymptotically stable and predictable behavior under different robotic platforms and contexts. The careful selection of a small set of control laws permits flexible solutions for a wide variety of tasks. Such has been demonstrated by the implementation of grasp control, dexterous manipulation, whole body grasping, bipedal walking and other behaviors [Huber, 2000, Platt et al., 2006]. Asymptotic stability implies that the control laws partition the underlying continuous space into discrete basins of attraction. Each control law, ϕ_i in a set Φ is designed from a scalar potential function that maps independent configuration space variables to real numbers. Figure 5 illustrates a two dimensional representation of equipotential lines across two potential surfaces. Using greedy descent on a given potential surface, the system converges to the attractor within the basin that holds the current state. Within a given basin, a control law compensates for

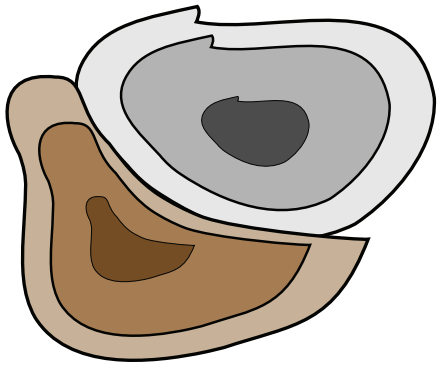

Figure 5: The task space is partitioned into a number of basins of attraction used to drive locally stable controllers [Huber, 2000]

limited perturbations and uncertainty while still converging to the attractor. Asymptotic stability, as asserted by Huber [Huber, 2000], is then a function of the design of the potential surface and the dynamics of the robot.

Controller Synthesis

As part of the control basis approach, a controller, $\phi_{\mathbf{i}}$, is synthesized when parameterized in terms of a sensor transform s_i and an output effector transform e_j. The binding of a potential surface function to sensory inputs and effecter outputs is designed to bind the objective of the controller to specific sensor resources and to use specific actuators to accomplish that objective.

The *sensor transform*, s_i, effectively represents a mapping from a limited set of available input control resources, $\Gamma_i \in \Gamma$ to a specified domain space, X_i. That is to say, an input control resource, such as a position or force sensor, will actually deliver a cartesian position or force reading:

$$s_i : \Gamma_i \rightarrow X_i \tag{1}$$

The artificial potential function then represents a native objective for the system and can be realized in a number of ways depending on how it is bound

with possible input sensory resources and output motors. It is important to select domain general potential functions that prevent the system from being constrained to specific strategies and allows tasks to adapt during run-time [Brock et al., 2005]. As such, the shape of the potential function depends on the input and output resources that are engaged. Each objective function is optimized by descending the gradient of the surface error through greedy descent of the form $\triangle q = -K * \nabla_{X_i} \phi_i$, where

$$\nabla_{X_i} \phi_i = \frac{\partial \phi_i(s)}{\partial X_i} \tag{2}$$

Finally, the *effector transform*, e_k, maps the error result in terms of a subset of the output control resources, $\Gamma_k \in \Gamma$, to the output space, Y_k. This is typically done through a Jacobian matrix that converts either position or force gradient data into the robot's joint space:

$$e_k(\Gamma_k) = \left(\frac{\partial \mathbf{x}_{\gamma_1}}{\partial \mathbf{y}_k}, \frac{\partial \mathbf{x}_{\gamma_2}}{\partial \mathbf{y}_k}, ..., \frac{\partial \mathbf{x}_{\gamma_{|S_k|}}}{\partial \mathbf{y}_k} \right)^T \tag{3}$$

where $\mathbf{x}_{\gamma_1}$ represents the configuration of control resource γ_i. y_k is a point in the output space (i.e. an element of the six DoF joint space vector), and $\Gamma_k = \{\mathbf{y}_1, \mathbf{y}_2, ..., \mathbf{y}_{|\Gamma_k|}\} \in \Gamma$ is a subset of the control resources (i.e. selecting one contact finger from a set of two that are available in a multi-fingered hand).

In summary, the closed-loop controller is implemented by binding an artificial potential gradient, $\nabla_{x_i} \phi_i$, with a sensor transform, $s_j(\Gamma_j)$, and an effector transform, $e_k(\Gamma_k)$. The input data must be of the same domain type as the artificial potential function, and the effector transform must have the same dimensions as the potential function in order to map the result into the convening output space.

Examples

Examples for cartesian and force control in a robotic manipulator were originally presented in [Platt, 2006], the cartesian controller is shown to illustrate the concept. The same feed-back loops are applied to assembly in this work and Chapter IV presents detailed descriptions of the synthesis of basis controllers for this work.

A commonly referenced form of cartesian position control is implemented through the Jacobian transpose control method. In assembly, cartesian control is used to displace the tip of a mating part to a reference location set by the six-element vector x, y, z, r, p, y. The controller computes the position error and multiples it by a gain and the transpose of the manipulator Jacobian. The result is a vector of joint angle updates. The updated positions are then passed to a low-level joint angle controller that actuates the robot to the desired position. The last step uses forward kinematics to transform the output into desired cartesian coordinates. The loop is shown in Figure 6.

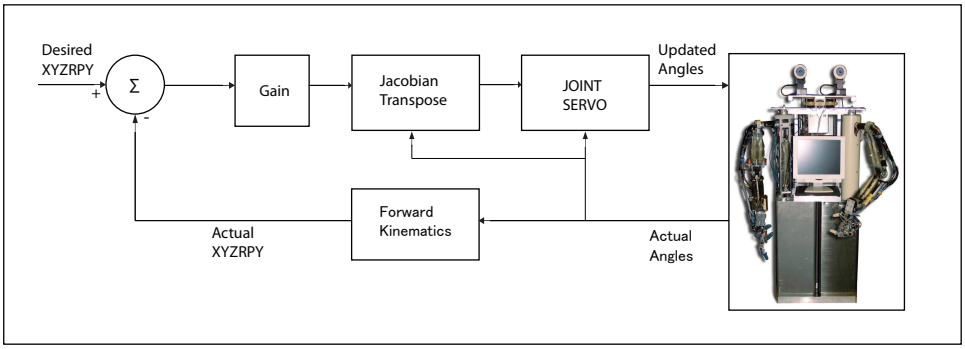

Figure 6: Diagrammatic representation of a position controller as part of the Control Basis set.

The controller referenced above is a primitive in the set of basis controllers used in this work. In the position primitive, the Jacobian transform serves as the sensor transform and the forward kinematics serve as the effector

transform. The difference between desired position and actual position is the error measure for the controller: $\phi_i(\mathbf{x}_{ref} - s_j(\Gamma_j))$, and the controller descends this potential through greedy descent $\nabla_{x_i}\phi_i$. This basis primitive is mathematically described as:

$$\nabla_{y_k}\phi_i = e_k(\Gamma_k)^T \nabla_{x_i}\phi_i(\mathbf{x}_{ref} - s_j(\Gamma_j)) \tag{4}$$

Throughout the rest of this thesis, this mathematical notation is represented for simplicity as:

$$\phi_i \,|_{e_k(\Gamma_k)}^{s_j(\Gamma_j)}\, (\mathbf{x}_{ref}) \tag{5}$$

Note that the reference input in the controller can also be the output of another basis controller as long as the task space is the same. This allows for nested controllers to be implemented:

$$\phi_1 \,|_{e_1(\Gamma_1)}^{s_1(\Gamma_1)}\, \left(\phi_2 \,|_{e_2(\Gamma_2)}^{s_2(\Gamma_2)}\right) \tag{6}$$

When more than one controller is embedded in a system, multiple goal states are required from the robot's actuators. This situation can lead to detrimental results if not managed appropriately. The next section discusses a technique to ensure the optimization for multiple objectives.

Multi-Objective Composition

Often when robotic systems are asked to execute a task, robots use an excess of sensory and motor degrees of freedom. This redundancy can be used to achieve a number of varying goals. In so doing, one must be careful to ensure that the pursuit of one goal does not affect the execution of another

goal. For such an end, the Moore-Penrose pseudo inverse has been a foundational mathematical tool [Brock et al., 2005]. This concept was originally used to optimize secondary objectives across controllers [Platt et al., 2002]. The pseudo-inverse method can be used to project the gradient result of the secondary objective onto the equipotential manifold of the primary objective, thereby achieving two simultaneous goals. Figure 7, illustrates the case where at different states of the primary controller objective, the number of states for the secondary controller are possible and allow to optimize the goals of each.

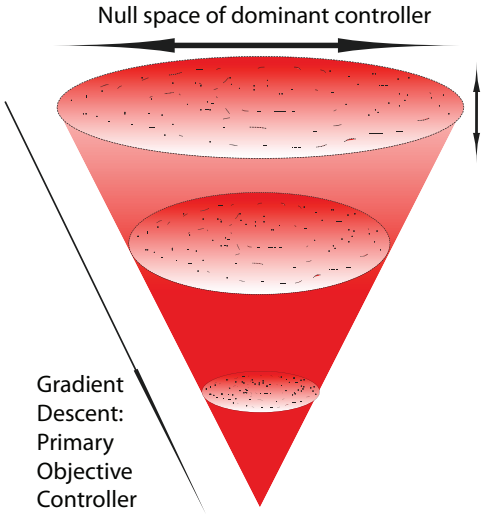

Figure 7: The projection of a secondary objective onto the equipotential manifold of the dominant controller allows to optimize two simultaneous goals [Platt et al., 2002].

Platt introduced the formal approach to incorporate the Moore-Penrose pseudo inverse to the control basis and called it: *null space composition* [Platt et al., 2002]. Null space composition enabled controllers to run independently of each other while pursuing their own goal states. Controllers can be combined hierarchically, where dominant and subordinate controllers exist. The latter are limited to the null space of the dominant controllers,

yet the goal of the subordinate controllers can still be optimized. A simple notation is used to represent this composition and it was said that the subordinate controller is *subject-to* the dominant controller: $\phi_s \lhd \phi_d$. Consider a control basis for assembly in which a robot is trying to insert a truss into a fixture. A force controller can be subject-to a moment controller to concurrently achieve a corrective alignment motion and an insertion motion: $\phi_{force} \lhd \phi_{moment}$. Consider the gradient output of two primitives, ϕ_m, ϕ_f:

$$\begin{aligned} \nabla_{y_m}\phi_m &= e_m(\Gamma_k)^T \nabla_{x_m}\phi_m(s_m(\Gamma_j)) \\ \nabla_{y_f}\phi_f &= e_f(\Gamma_k)^T \nabla_{x_f}\phi_f(s_f(\Gamma_j)) \end{aligned} \tag{7}$$

where the gradient outputs of both primitives must reside in the same domain space, i.e. $Y = Y_1 = Y_2$.

When the gradient of the second controller is projected to the null space of the first gradient, the result is represented as:

$$\nabla_y(\phi_f \lhd \phi_m) = \nabla_y\phi_m + \mathcal{N}(\nabla_y\phi_m^T)\nabla_y\phi_f \tag{8}$$

where

$$\mathcal{N}(\nabla_y\phi_m^T) \equiv I - (\nabla_y\phi_m^T)^T(\nabla_y\phi_m^T) \tag{9}$$

and, I, is the identity matrix, y is an n-dimensional space, and $\nabla_y\phi_m$ is a (n-1) dimensional space orthogonal to the direction of steepest descent [Platt, 2006].

In this way, the "subject-to" constraint, $\phi_2 \lhd \phi_1$, always descends the potential surface of the dominant controller that has not yet converged to a minimum, and maintains the stability of the underlying controller without limiting its actions. A formal presentation of Moore-Penrose pseudo inverse method can be found in Appendix B.

Control Policy Construction

Once there is a number of defined primitives in the set of basis controllers, Φ, it must be determined how to combine them. The size of the set is defined by $\Phi \times 2^s \times 2^e$, giving rise to many possible transitions. While this functionality makes the control basis more powerful and flexible to adapt to new tasks, it is necessary to successfully transition between segmental actions [Huber, 2000].

Closed-loop controllers interact with the environment over time revealing information between the system and the world. The asymptotically stable controllers of the basis tend to equilibria as time goes to infinity: $\frac{\partial \phi}{\partial t} \rightarrow 0, \text{as t} \rightarrow \infty$. The convergence of a controller can be treated as a discrete event and used as criteria to join controllers. This phenomena simplifies the number of possibilities and establishes a framework for controller policy enaction.

Sequences of controllers can be considered as states in a non-deterministic, finite-state automata. Each finite state is an asymptotically stable sequence of controllers and describes patterns of membership across controllers [Brock et al., 2005]. These states can be sequenced to achieve an overall goal. The previously described process is visualized in Figure 8. This thesis utilizes a sequence of controllers composed of position, moment, and force primitives that are presented in detail in Chapter IV.

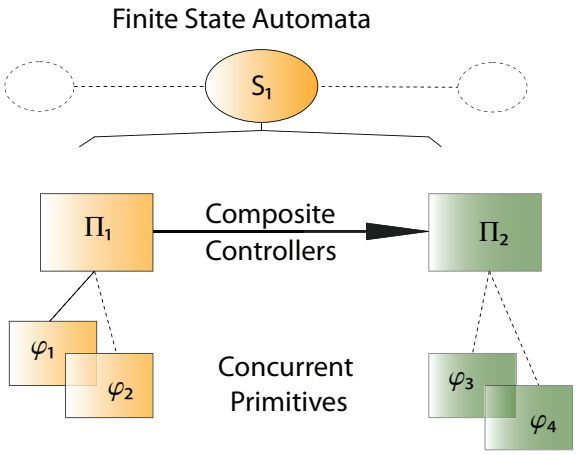

Figure 8: Example of a control policy consisting of a sequence of concurrent controllers.

CHAPTER IV

DEVISING A CONTROL BASIS FOR JOINT ASSEMBLY TASKS

As initially stated in Section II, the assembly tasks involve the insertion of one part into another, *i.e.* the insertion of a truss into a fixture. Such an operation can be carried out successfully if a robot displaces its tool-tip to minimize the moment and force residuals experienced while aligning participating assembly parts. The points of contact between assembly parts in this work are referred to as "contacts". In the past, the control basis approach has been effectively used to displace contacts and minimize residual forces in grasp, manipulation, and bipedal gait tasks [Coelho and Grupen, 1997, Huber, 1998, Platt et al., 2004].

In this Chapter, a control basis set for joint assembly tasks across two cooperative robots is described. The first Section of this Chapter presents controllers necessary for a single robot assembly. These controllers respond to the construction of an assembly process consisting of two stages: (a) a guarded approach, and (b) a compliant insertion. A series of primitive controllers are used, combined, and sequenced to produce the following composites: the "guarded move controller" and the "compliant insertion controller". A control policy that starts with the guarded move controller and transitions to the compliant insertion controller is used to achieve an insertion.

Additionally, another set of controllers was designed to encode behavior particular to a dual-armed and compliant humanoid robot. Two immediate challenges are presented in the humanoid robot to complete the task: (1) to control effectively both robot arms to displace the fixture, and (2) to deal with the elastic nature inherent to the pneumatic muscles in the humanoid. In [Platt, 2006], "virtual contacts" is a technique used to create a single

contact from multiple contacts. The technique is used here to more effectively leverage the contributions of both arms and ease effects related to pneumatic actuators (see Appendix D).

Finally, the design of the presented controller also considered the effects of robots assuming different roles as part of a strategy in a cooperative task. In the literature, cooperative robots often assume a leader or a follower role [Yuan, 2006]. This work assumes robots have active and static roles (these roles are described in detail in Chapter V). The presented controllers are able synthesize both active and static behaviors and enables a robot to switch between these controllers.

Individual Manipulator Assembly

For an insertion task to be executed successfully a robot must be able to displace the assembly part to an optimum location for insertion. If the approach ends at a location outside the interior hole of a fixture, the assembly cannot succeed. Similarly, if the approach is too quick and jams the truss into a fixture, a successful insertion is unlikely. The *Guarded Move Controller* is designed to generate a guarded approach that positions the tool at an optimum location for insertion. Similarly, once an appropriate insertion location has been achieved, controllers must drive the insertion as smoothly as possible. To do so, misalignments must be corrected to decrease the friction, jamming, and wedging phenomena. The *Compliant Insertion Controller* was designed to overcome such misalignments. Before presenting the derivation of the composite controllers (cf. Chapter III), the concept of a wrench residual controller is used to introduce force error minimization.

A wrench is a 6-dimensional generalized vector of forces and torques $\vec{w}_i = [\vec{F}\ \vec{T}]^T$. A wrench vector is generated when an assembly part makes contact

with a mating fixture. A wrench residual ϵ represents the sum over forces and moments generated across n contact points:

$$\epsilon = \sum_{i}^{n} w_i \tag{10}$$

As introduced in Section III, a control primitive is a scalar potential function that represents a control goal. Correct insertion for assembly requires that the wrench residual is minimized. Therefore, the wrench residual potential surface ρ, is defined as the square of the wrench residual:

$$\rho = \epsilon^T \epsilon \tag{11}$$

To reach the goal of the function, greedy descent is used to converge to the attractor of the surface. Descending the surface implies differentiating the wrench residual with respect to the joint configuration of the robot, then displacing the contacts in direction of the gradient vector. Coelho and Grupen [Coelho and Grupen, 1997], noted that local minima sometimes led to spurious states when the wrench residual was minimized. To prevent local minima from occurring, they decomposed the wrench residual into two orthogonal force and moment residuals, such that:

$$\begin{aligned} \rho_{fr} &= \left(\sum_{i=0}^{n} \mathbf{f}_i \right)^T \left(\sum_{i=0}^{n} \mathbf{f}_i \right) \\ \rho_{mr} &= \left(\sum_{i=0}^{n} \mathbf{r}_i \times \mathbf{f}_i \right)^T \left(\sum_{i=0}^{n} \mathbf{r}_i \times \mathbf{f}_i \right) \end{aligned} \tag{12}$$

where $\mathbf{f}_i$ is a unit vector normal to the object surface applied by the i^{th} contact, and $\mathbf{r}_i$ is the location of the i^{th} contact point in a given coordinate frame.

Coelho and Grupen determined that for grasping tasks the force plays a more dominant role. To achieve an effective grasp controller, they descended the gradient of the the force residual controller first, then they descended the gradient of the moment residual second, and finally combined the gradient updates through a control composition policy. Later, Platt proposed a null space projection [Platt et al., 2002] (see Section III) where the result of the subordinate force residual was projected onto the dominant moment residual and both could be minimized correctly. A similar approach is used for the compliant insertion controller used in this work and is introduced next.

Compliant Insertion Controller

For a given assembly task, the robot manipulator holds a truss with an inverted chamfer on the end, as shown in Fig 9. When a force is applied at

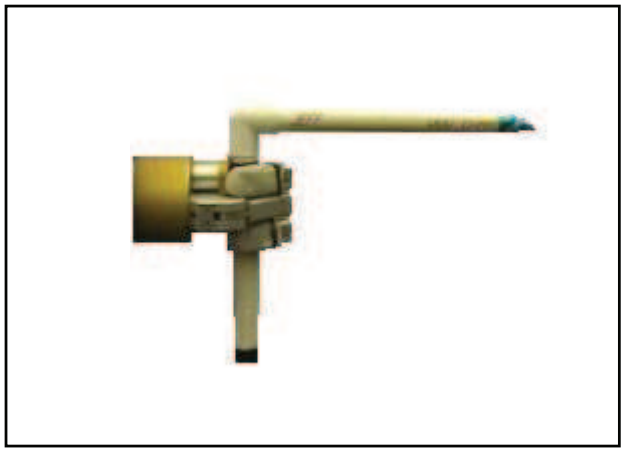

Figure 9: Example of an industrial manipulator holding a truss pipe.

the tip of a truss, the exerted force is primarily experienced as an applied moment by the force-torque sensor, which sits on the wrist of the robotic manipulator. Through the insertion itself, the truss experiences moments as it collides with the walls of the mating part, as illustrated in Figure 10.

Additionally, in order for the "insertion motion" to be carried out, there must be a driving force in the direction of the axis of insertion that pushes the truss until a connection is completed.

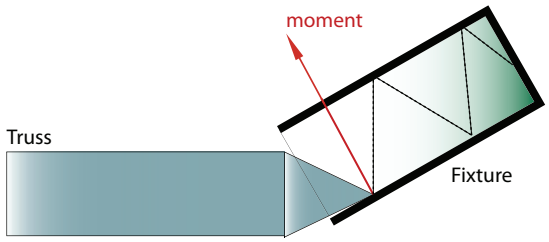

Figure 10: Illustration of contact between a truss and a fixture.

In effect, the insertion process is subordinate to the moments of the task and then to the forces of the task. The former deals with the alignment of the parts, which is crucial for successful task completion. The latter deals with the forward motion that drives the insertion process as misalignments are corrected. With these factors in mind, a composite controller, known as a "Compliant Insertion" controller, was designed. This basis controller is slightly different from the wrench residual introduced earlier. The residual controller designates the moment primitive as the dominant actor and the force primitive as the subordinate actor in correspondence to the task goals. The derivation of this hierarchical component is now presented.

The moment primitive, ϕ_{mr}, uses the sensed moments to update the joint angle configuration of the manipulator and, therefore move, the rigidly held tool to a state where there exist no net moments. The sensor transform, $s_q(\gamma_{moment})$, maps the sensed moments in joint torques. The effector transform, $e_q(\gamma_{torque})$, transforms those updated values into joint coordinates, q. The controller is represented in simplified notation as:

$$\phi_{mr} \left|_{e_q(\gamma_{torque})}^{s_q(\gamma_{moment})}\right. . \tag{13}$$

Similarly, the force residual, ϕ_{fr}, displaces the joint angle configuration of the robot to achieve a reference value. The reference value can be used to implicitly drive the motion of the insertion:

$$\phi_{fr} \mid_{e_q(\gamma_{torque})}^{s_q(\gamma_{force})} (f_{ref}). \tag{14}$$

The objectives of both primitives can be attained through null space composition. The goal vector of the force controller is projected onto the null-space of the moment vector, which allows correct alignment and insertion to take place concurrently:

$$\nabla_q \phi_{mr} + \mathcal{N}(\nabla_q \phi_{mr}^T) \nabla_q \phi_{fr}, \tag{15}$$

where

$$\mathcal{N}(\nabla_q \phi_{mr}^T) \equiv I - (\nabla_q \phi_{mr}^T)^T (\nabla_q \phi_{mr}^T). \tag{16}$$

The sensor and effector transforms have been omitted for clarity. Composite controllers, which result from the use of the null-space operation, can be represented in a simplified notation through the use of a new parameter, π_i. The Compliant Insertion controller is defined as:

$$\pi_{CI} \mid_{e_{CI}(\gamma_{torque})}^{s_{CI}(\gamma_{force})} = \phi_{fr} \mid_{e_{fr}(\gamma_{torque})}^{s_{fr}(\gamma_{force})} (f_{ref}) \lhd \phi_{mr} \mid_{e_{mr}(\gamma_{torque})}^{s_{mr}(\gamma_{force})} . \tag{17}$$

Guarded Move Controller

Prior to an insertion action it is necessary for the assembly fixture to reach an appropriate basin of attraction. The assembly fixture must reach a near optimal location - preferably one in which initial and slight contact is made between the incoming truss and the interior fixture hull. The goal of the guarded move controller is to reach a joint configuration that allows the

potential surface to converge to a state of low moments and forces such that the transition to the compliant insertion controller is smooth.

The guarded move controller is a composite controller consisting of a dominant position controller and a subordinate moment residual controller. The position controller displaces the manipulator and the rigidly held truss to an optimal location for insertion. The subordinate moment controller acts as an identifier to determine whether contact has been made.

The position controller receives its goal cartesian position from the stereo visual system. The latter uses color fiducial marks placed at the tips of the fixtures to estimate 3D cartesian positions. Color segmentation and noise filtering are performed on incoming video and processed to compute image coordinates of the segmented foreground blob that correspond to the marker. The error centroid position of the blob from the right and left images $(\triangle c_r, \triangle c_l)$ is fed through a back propagated neural net (NN_{bp}) to output appropriate updates for camera motor servos. The cameras verge towards the region of interest until the object is centered. A detailed description of this process is found in [**?**], and represented by the following equation:

$$servo = k * \triangle q = k * (NN_{bp}(\triangle c_r, \triangle c_l)). \tag{18}$$

The motors' output pan and tilt angles are used to localize the cartesian coordinates of a blue and a green tool-tip (see Figure 11). The tool orientation is not computed by the visual system. In the experiments in Chapter V, Section V, the orientation of the wrist is assumed to always point approximately parallel to the robot's $\vec{x}$ base-coordinate. This orientation is best for insertion tasks since both robots apply force perpendicularly to the plane on which they are pushing. The cycle is performed sequentially for each of the two tool-tips. The difference in cartesian coordinates between the tips is used

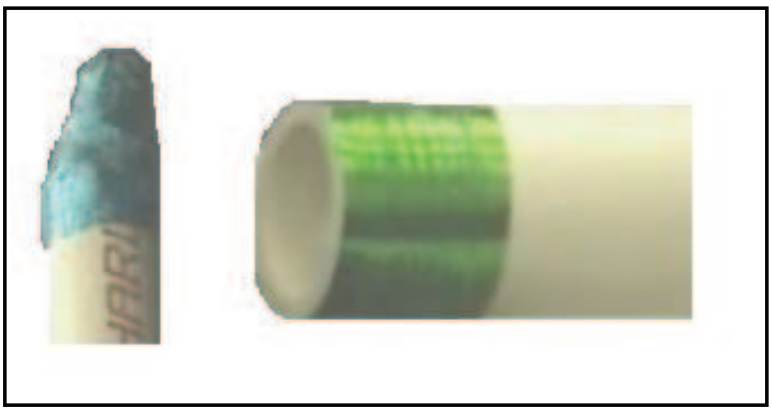

Figure 11: Tool-tips used in experiments. A blue and a green fiducial mark is used for the male and female parts respectively

to update the desired goal position in the corresponding position controller. The guarded move controller drives the assembly tool to the cartesian position generated by the sensor transform $s_p(\gamma_{visual\_sys})$ and returns the current joint configuration of the robot. The latter uses forward kinematics as the effector transform: $e_p(\gamma_{joint})$. The position controller is thus defined as:

$$\phi_p \mid_{e_p(\gamma_{joint})}^{s_p(\gamma_{visual\_sys})} (x_{actual} + \triangle x). \tag{19}$$

The moment residual controller is bound by a sensor transform, $s_{mr}(\gamma_{force})$, that returns the moments experienced by the force sensor, and by an effector transform $e_{mr}(\gamma_{torque})$, that converts torque updates into joint angle updates. The moment residual controller is defined as:

$$\phi_{mr} \mid_{e_{mr}(\gamma_{torque})}^{s_{mr}(\gamma_{force})} . \tag{20}$$

The goal of the guarded move controller is to reach an appropriate location for insertion; namely, one that is close to the fixture's interior hull and where there are no net moments. If contact takes place, the controller displaces the

robot's end-effector to minimize the residual error and transitions to compliant insertion controller, π_{CI}, which in turn compensates for the disturbances through the insertion.

The composite guarded move controller, π_{GM}, is synthesized by having the moment controller be subject-to the position controller:

$$\pi_{GM} \mid_{e_{GM}(\gamma_{cart,moment})}^{s_{GM}(\gamma_{joint,torque})} = \tag{21}$$
$$\phi_{mr} \mid_{e_{mr}(\gamma_{torque})}^{s_{mr}(\gamma_{moment})} \lhd \phi_p \mid_{e_p(\gamma_{joint})}^{s_p(\gamma_{visual\_sys})} (x_{ref}).$$

The two hierarchical components presented in this section are able to generate robust insertion operations for a given manipulator. Our control policy for the task consists of initiating the job with the guarded move controller and as it reaches its basin of attraction, a finite state automata moves the system to the next state where the compliant insertion controller becomes active.

The next section introduces controllers used when two robots are cooperating and coordinating for task execution.

Cooperative Assembly

Thus far the assembly task has been framed under the assumption that only one robot drives the insertion process. This section introduces cooperative work using two robots. Cooperation implies the robots contribute to the overall task achievement in synchronous or asynchronous modes. In some instances, there may only be one "active" robot, in others multiple robots function jointly in the environment. Coordination, on the other hand, implies strategy. In this work there are two scenarios: (a) one robot is an active player, while the other is a passive player: one robot drives the insertion,

while the other holds the mating part stationary, and (b) both robots actively drive their part towards insertion.

Counterbalance Controller

The discussion of the compliant insertion controller mentioned that a reference force was required to drive the insertion of the male truss, and that this motion ends when an opposite force is exerted on to it. In the case of a single robot manipulator, the environment provides the counteracting force. Cooperative assembly requires the other robotic partner to fulfill this role. The counteracting force attempts to hold the mating fixture as rigidly as possible. Otherwise, when one robot drives the insertion, the collaborating robot retracts and the assembly task fails. For this purpose, a counterbalance controller π_{CB} is proposed. The latter is similar to the compliant insertion controller, but it differs in that its reference force is zero so as to always oppose any induced forces in the system:

$$\pi_{CB} \mid_{e_{CB}(\gamma_{torque})}^{s_{CB}(\gamma_{force})} = \phi_{fr} \mid_{e_{fr}(\gamma_{torque})}^{s_{fr}(\gamma_{force})} \lhd \phi_{mr} \mid_{e_{mr}(\gamma_{torque})}^{s_{mr}(\gamma_{force})} . \tag{22}$$

Virtual Contacts

Our robotic testbed consists in part of ISAC, an in-house, dual-arm and pneumatically driven humanoid robot [Rojas and Peters II, 2005]. A detailed description of ISAC and the industrial robot, HP3JC, is presented in Chapter V. ISAC's pneumatic hardware render it naturally compliant. The elasticity of air muscles is advantageous in an assembly task as it provides a spring behavior that eases accuracy requirements. However, the control of pneumatic actuators is non-trivial [Daerden and Lefeber, 2001]. Treating both arms as a redundant manipulator–that is, averaging the contribution each one makes

to the assembly tasks and coordinating similar motions across both arms– simplifies the control problem. The concept of averaging the contribution of sensor and effector resources is known as "virtual contacts" since the contribution of each of the control resources is represented by a single imaginary contact resource.

A formal framework can be derived to parameterize sensor and effector transforms as virtual contacts. Platt parameterized a number of finger contact resources [Platt, 2006]. The sensor transform for the virtual contact, $s_j(\gamma_{vc})$, is simply the average of the output of the individual contact sensor transforms:

$$s_j(\gamma_{vc}) = \frac{1}{n} \sum_{\gamma_i}^{n} s_j(\gamma_i). \tag{23}$$

Similarly, for the effector transform, the output of the virtual contact is the average of the updates contributed by the individual transforms:

$$e_k(\gamma_{vc}) = \frac{1}{n} \sum_{\gamma_k}^{n} e_k(\gamma_k). \tag{24}$$

For ISAC's case, the position and wrench data generated through the use of contact resources in the left and right arm is averaged. The virtual contact parameterizes incoming moment data as:

$$\sigma_{mr}(\gamma_{vc}) = \frac{1}{2}[s_{mr}(\gamma_{left} + \gamma_{right})], \tag{25}$$

where γ_{left} and γ_{right} have rectangular coordinates,

$$m = \begin{bmatrix} \vec{m_x} \\ \vec{m_y} \\ \vec{m_z}. \end{bmatrix}$$

Similarly for the effector transform, the angle updates produced by each of the control resources are averaged over the two control resources:

$$e_{mr}(\gamma_{vc}) = \frac{1}{2}(\frac{\partial \mathbf{m}}{\partial \theta_{\gamma_l}} + \frac{\partial \mathbf{m}}{\partial \theta_{\gamma_r}}). \tag{26}$$

With this new approach, each of the presented controllers can be parameterized to become virtual in nature and applied to the humanoid ISAC. That is, the guarded move controller, the compliant insertion controller, and counterbalance controller, become virtual for ISAC: π_{VGM},π_{VCI}, and π_{VCB}.

$$\pi_{VGM} \mid^{s_{GM}(\gamma_{vc\_visual\_sys},\gamma_{vc\_moment})}_{e_{GM}(\gamma_{vc\_joint},\gamma_{vc\_torque})} =$$
$$\phi_{mr} \mid^{s_{mr}(\gamma_{vc\_moment})}_{e_{mr}(\gamma_{vc\_torque})} \lhd \phi_p \mid^{s_p(\gamma_{vc\_visual\_sys})}_{e_p(\gamma_{vc\_joint})} (x_{ref}),$$

$$\pi_{VCI} \mid^{s_{CI}(\gamma_{vc\_force})}_{e_{CI}(\gamma_{vc\_torque})} =$$
$$\phi_{fr} \mid^{s_{fr}(\gamma_{vc\_force})}_{e_{fr}(\gamma_{vc\_torque})} (f_{ref}) \lhd \phi_{mr} \mid^{s_{mr}(\gamma_{vc\_force})}_{e_{mr}(\gamma_{vc\_torque})},$$

$$\pi_{VCB} \mid^{s_{CB}(\gamma_{vc\_force})}_{e_{CB}(\gamma_{vc\_torque})} =$$
$$\phi_{fr} \mid^{s_{fr}(\gamma_{vc\_force})}_{e_{fr}(\gamma_{vc\_torque})} \lhd \phi_{mr} \mid^{s_{mr}(\gamma_{vc\_force})}_{e_{mr}(\gamma_{vc\_torque})} .$$

CHAPTER V

EXPERIMENTS

Overview

This chapter presents six experiments that demonstrate the effectiveness of the control basis in recasting the assembly process in terms of a sequence of composite controllers across robots. Two sets of three experiments are presented. The first set is preparatory for the second set. For the first set of experiments, the goal is the determination of several controller parameters:

Error gains within controller loops: Controller gains are multiplied by the error inside a controller's loop. They determine the sensitivity of the system towards sensory stimulus.

Reference values for modular controllers: Every controller can take reference values. If they exist, the controller converges towards that reference configuration as its attractor region.

Error thresholds for controller state transition: As part of control policy, a controller must reach the attractor region before sequencing to the next state in the policy.

A qualitative analysis is also included and studies the behavior of the assembly task, its accuracy, and its efficiency.

After determining the controller parameters during the first set of experiments, cooperative assembly experiments were conducted with two robots. These experiments included active-static tasks and active-active tasks. Active-static tasks required one robot drive the insertion while the other held the fixture as rigidly as possible. The term leader-follower was not appropriate

in this context since the second robot did not 'follow' the first in any way. Instead the static robot exhibited an independent reaction based on the experienced stimuli. The active-active tasks had both robots actively drive their assembly parts towards insertion. An analysis of the overall behavior, the force and the moment characteristics, and the efficiency of these tasks is presented. Averaged values are provided and used for comparison across experimental results to highlight benefits and challenges in each case.

The described experiments were run in a laboratory but were uncalibrated. Conditions changed for each trial so that the experiments were performed in a loosely structured environment. One measure consisted of placing the industrial manipulator in random positions near the center of the humanoid robot (i.e. the relative position of both robots in joint tasks varied across experiments). The second measure consisted of running the visual system during different times of the day exposing it to small variations in lighting conditions. The robotic systems responded to current environment conditions during the tasks [Rojas and Peters II, 2009].

Testbed

The testbed consisted of two robotic platforms, an in-house distributed software multi-agent system, and PVC piping.

The robotic team was comprised of two heterogeneous robots: ISAC and HP3JC. The former is Vanderbilt's pneumatic humanoid robot. The latter is a Motoman high accuracy 6 DoF manipulators.

The distributed multi-agent software system is named "Intelligent Machine Architecture" (IMA). The current version is IMA 2.5. The software system encapsulated behavior through modular components. IMA grouped multiple components to produce agents and used the component object model

(COM) and distributed COM (DCOM) communication protocol for inter-component communication. For this work's experiments, multiple agents encapsulated the hierarchical controllers for the different robots and the visual system.

The insertion parts were made from commercially available PVC piping. The male truss was composed of two 0.5 in pipes, connected by a 90 degree elbow connector. At the truss' tool-tip an inverted chamfer was placed to facilitate its entry into a female counterpart. This truss was held by a Barret hand attached to the HP3JC manipulator. The female insertion part, was a 1.0 in pipe, connected through a t-connector to two 1.0 in pipes that are held rigidly by ISAC's end-effectors.

ISAC

ISAC is an anthropomorphic robot [Rojas and Peters II, 2005] and is shown in Figure 12. It's visual hardware includes two Sony XC999 cigar cameras for

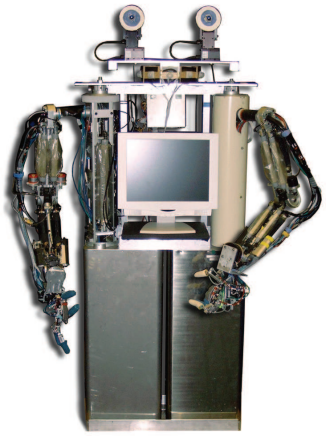

Figure 12: Vanderbilt University's humanoid robot ISAC.

stereoscopic vision. The cameras are compact and lightweight, with a 0.5 inch

colored CCD array. The cameras are mounted on two Direct Perception 17-40 pan-tilt units that provide high-speed and accurate servo control reaching up to speeds of 300 degrees/second [DirectPerception, 2009]. The camera and servo units are connected to a 3.0GHz computer via two co-axial cables to frame grabbing cards and two RS-232 connections respectively.

ISAC has two manipulators, each actuated by 12 pneumatic McKibben artificial muscles. The muscles are linked to replicate human muscles in agonist and antagonist pairs. Each arm is nominally 6-DoF and has a configuration similar to a PUMA[1]. A detailed overview of pneumatic actuators and their history can be found in Appendix D. Each set of air muscles is driven by 12 air-pressured SMC ITV2050 servo valves [SMC, 2009]. The servo and encoder signals are read through the use of three motion control cards by VitalSys [VitalSystem, 2009].

Finally, each of ISAC's end-effectors consist of an ATI six-axis force-torque (F/T) sensor attached to the wrist as well as a machined aluminum part specially designed to hold 1.0 in PVC pipes.

HP3JC

The industrial robot is an HP3JC Motoman 6 DoF model. The robot is a compact, high speed and high-accuracy robot with repeatability at 0.03 mm. The manipulator's hardware controller is a Yaskawa-Motoman NX100 [Motoman, 2009]. The arm's physical configuration is a PUMA variant (Figure 13). The HP3JC has a JR3 six-axis F/T sensor (on loan from NASA JSC) mounted on the wrist [JR3 Inc., 2009] as well as a three fingered Barret Hand. [Barrett Technology, 2009].

[1]The robot has two revolute joints both at the elbow and the wrist. To achieve a spherical wrist and hence a 6DoF arm, the wrist can be rotated 90 degrees about the pitch

Figure 13: Motoman's compact manipulator, the HP3JC.

IMA Architecture

The Intelligent Machine Architecture was developed at the Cognitive Robotics Laboratory [Pack, 1999, Olivares, 2003] as a platform for distributed concurrent programming. It contains agent-based, behavior-based, and reactive algorithms to provide control for intelligent machines. In IMA 2.5, control algorithms are encapsulated within intelligent agents - collections of objects distributed across a network. Agents communicate with each other through Microsoft's COM/DCOM communication protocol.

Preparatory Experiments

This set of three experiments was designed to determine the controller parameters necessary to carry out the three joint assembly experiments.

The first experiment was a static insertion. In this test, the HP3JC inserted a truss on a rigid fixture. This assembly used the guarded move controller (π_{GM}) and the compliant insertion controller (π_{CI}) introduced in

angle. This configuration, however, limits the robots dexterity and was not used for these experiments.

Section IV. The reference position (cartesian location) for the guarded move controller was provided manually in this experiment as was the force reference used in the compliant insertion controller.

The second experiment extended the first to acquire the reference position through the visual system. The purpose was to examine the accuracy of the visual system for insertion tasks.

The third experiment used the results of the previous two experiments and introduced compliance to assembly. ISAC held a female fixture without the use of force sensing. The humanoid only used position control. Given that ISAC is naturally compliant, the goal was to understand the affect of the elasticity of its pneumatic actuators on assembly tasks.

Criteria to determine the success and length of a task is important. A task was considered a failure if the truss held by the HP3JC was unable to enter through the peg and align itself. For all experiments, the timing of the task began when the guarded move controller transitioned to the compliant insertion controller. The clock was stopped when the fiducial mark of the male truss was completely covered by the female fixture – an entry of 4 cm. The metrics used for comparison of experiments were time-to-completion and the absolute value of the maximum moment residual error registered in a task. Note that the moment residual error relates to the alignment of the wrist. Given that the diameter of the fixture is greater than the diameter of the truss, a small misalignment is allowed. This is reflected in the data that shows some residual moment error at the end of successful insertions. Force residual errors are related to the position of the tool-tip and indicate a position change.

Experiment 1: HP3JC Stand-Alone Experiment

This experiment used the HP3JC robot to perform an insertion task under a rigid and static environment. The HP3JC held a male truss and inserted it into a female fixture placed rigidly at a distance. This process is shown through a sequence of images contained in Table V.

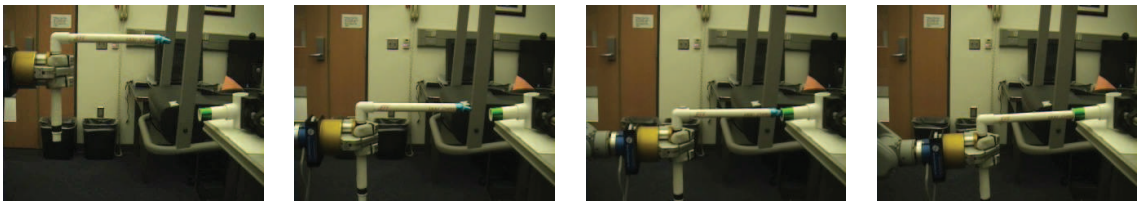

Table 1: Images showing the insertion process for HP3JC on a static and rigid fixture.

The purpose of this first task was to determine baseline performance measures in terms of: (a) the overall behavior of the process; (b) the position controller gains, k_{Pi}, the moment residual controller gains, k_{Ti}, and the force residual controller gains. k_{Fi}; (c) the reference vector for the force subordinate primitive (ref_F) in the compliant insertion controller, π_{CI}; and (d) error thresholds that yield a smooth transition between the guarded move controller and the compliant insertion controller.

For this experiment a total of 11 trials were run. The first trial was an unsuccessful insertion and is presented to show the characteristic of an unsuccessful insertion. The second insertion was successful but slow; the third and fourth trials ran faster, and the last trial approached the fixture from a side instead of straight ahead.

Results

Trials throughout this experiment are classified as: C_MF_00X, where C_MF refer to the use of the cartesian, moment, and force primitives, and X is the trial number. Each controller has gains and reference values pointing in the x-, y-, and z-directions. The positive x-direction points in the direction normal to the face of the F/T sensor and the positive z-direction is upwards. The first trial, Trial C_MF_000, used the following set of controller gains and reference values:

$$\begin{array}{lll} k_{Fx} = 0.00100 & k_{Tx} = 0.2 & ref_{Fx} = 10.0 \\ k_{Fy} = 0.00100 & k_{Ty} = -0.2 & ref_{Fy} = 0.0 \\ k_{Fz} = 0.00025 & k_{Tz} = 0.2 & ref_{Fz} = 1.3 \end{array}$$

These parameters yielded an unstable behavior. Gains in the moment residual primitive were too high. As the truss was inserted into the mating fixture the controller over-compensated and coerced the fixture out of place. Figure 14 shows the JR3 sensor readings along with moment and force residual errors. The plot shows how during the last 50 seconds of the task the torque in the y-direction increases steadily. The torque rose from 0 to an absolute value of 25 in-lbs, which is reflected by the moment residual error. Changes in the force reference values corresponded to an attempt to modify the behavior of the insertion during execution. These reference values affect the speed and direction of the insertion approach. Controller parameter values were updated as follows:

$$\begin{array}{lll} k_{Fx} = 0.00100 & k_{Tx} = 0.05 & ref_{Fx} = 10.0 \\ k_{Fy} = 0.00100 & k_{Ty} = -0.0025 & ref_{Fy} = 0.0 \\ k_{Fz} = 0.00025 & k_{Tz} = 0.01 & ref_{Fz} = 0.5 \end{array}$$

The reference force value in the z-direction compensated for a downward motion associated with the separation of force and moment components in

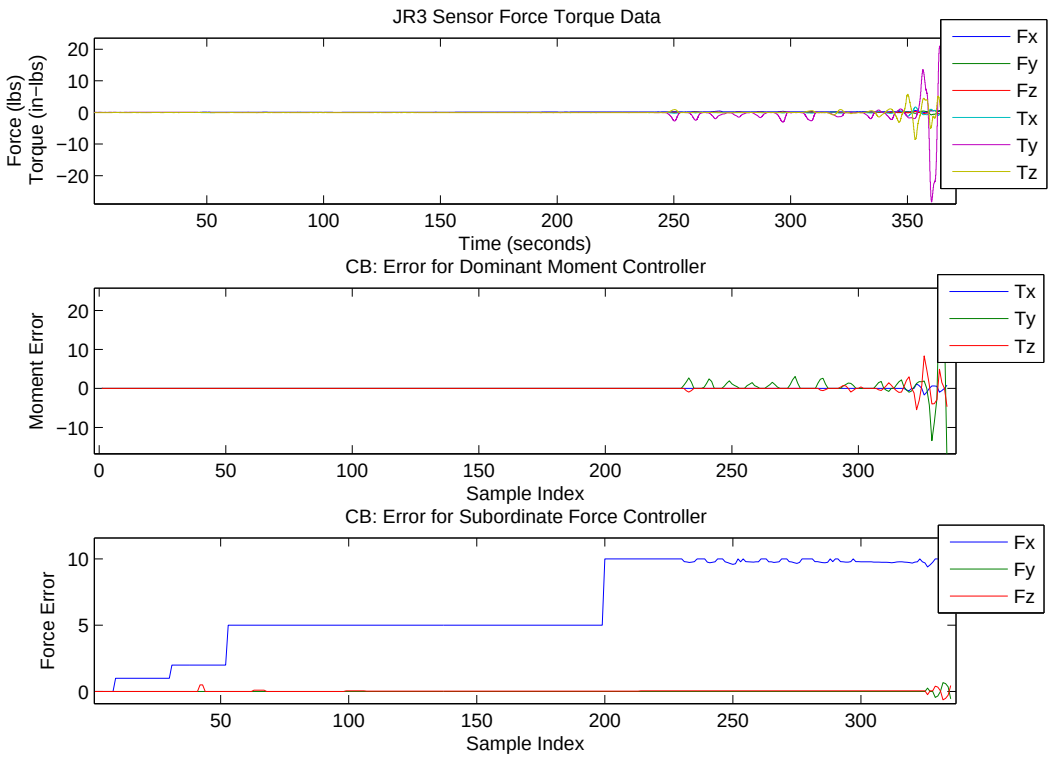

Figure 14: Trial C_MF_000: An unstable insertion. The torque and moment residual error increase as the truss is inserted into the fixture.

the controllers. This separation makes the motion of the first three joints independent of wrist motions. If there were no separation, the Jacobian would update the pitch angle of the wrist.

Trial C_MF_001 is shown in Figure 15. The results indicate a gradual reduction in the sensed torques and the moment residual error after initial contact. The negative force gains shown in the plot were assigned manually online to extract the truss from its fixture once the insertion was completed. In the top subplot, readings show that initial impact between the truss structure and its mating part occured after 430 seconds. The contact generated significant disturbances in the y-torque. The sinusoidal form of this signal reflects the adjustment made by the wrist in the vertical plane as the truss bounces between the upper and lower walls of the inner hull of the female

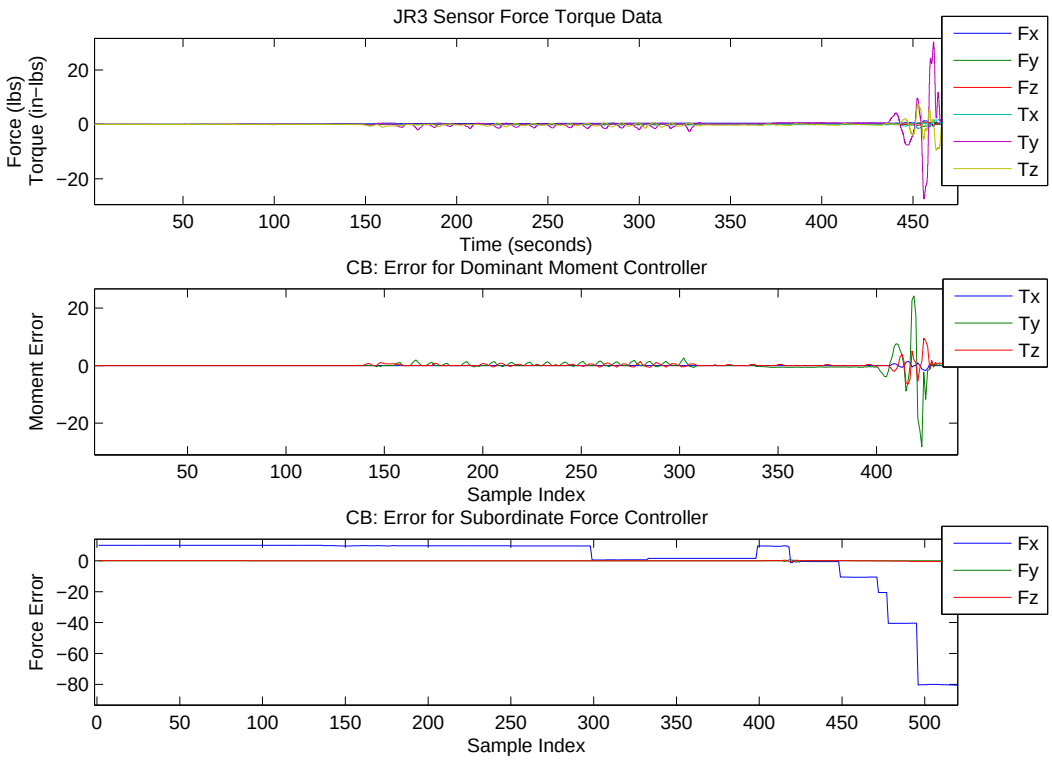

Figure 15: Trial C_MF_001: A successful but slow insertion. Different force reference values were used in the task to study system response.

fixture to align itself. A zoomed version of the plot shown in Figure 16 details the behavior of the moments and the force. The compliant insertion controller, π_{CI}, is able to displace the truss to eliminate the moment residual error after a few seconds. The error presents itself primarily in the y-direction, but there is also a small error in the z-direction. The force reference value was set at 10 lbs to drive the insertion. Around 470 seconds this force was effectively reduced to zero, which indicates a near-complete stop by the robot. The covering of the inverted chamfer that is a fiducial mark is prone to friction and is partially responsible for the slowdown of the insertion process. Larger reference force values were used in future trials to generate a faster forward motion. The position primitive in the guarded move controller reached its attractor region when the goal position was achieved. For this

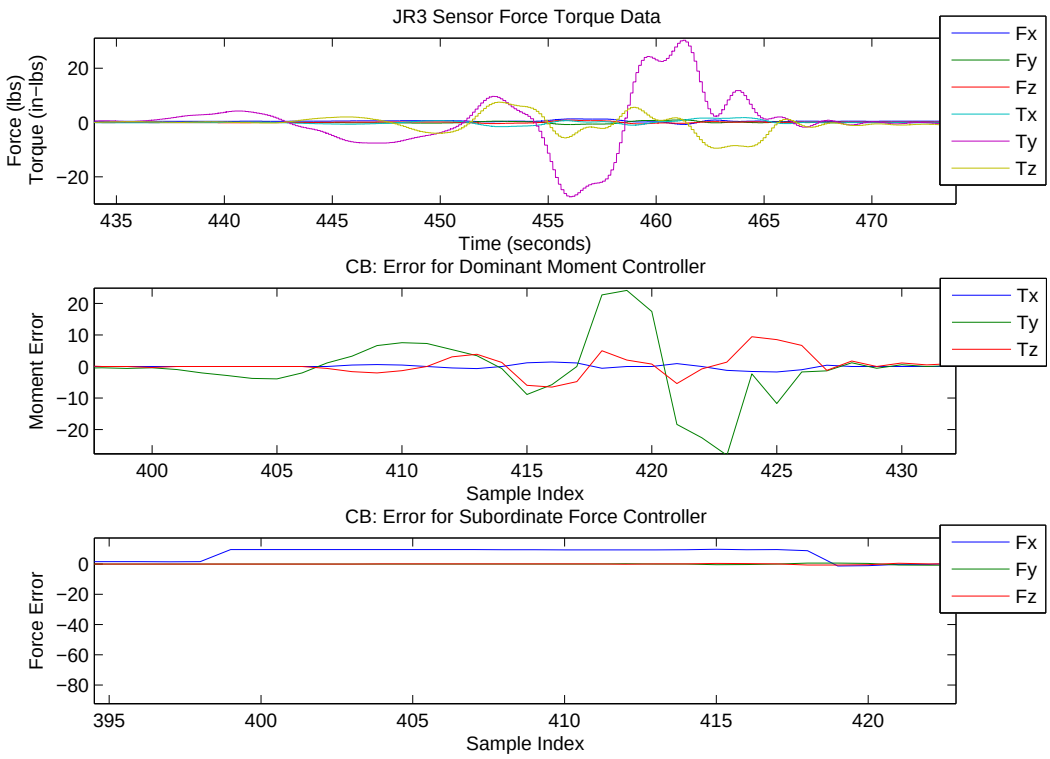

Figure 16: Trial C_MF_001: Zoomed view of torque signals and moment residual error.

experiment, the goal position provided was a short distance away from the actual (and optimal) entry point. π_{GM} reached its intended position easily and transitioned to π_{CI}. Due to the distance, this trial ran for longer periods of time than those seen in other experiments. Extra time was spent having the compliant insertion controller reaching the female fixture. To speed up the system, the reference values were increased. The next successful trial used the following parameters:

$$ref_{Fx} = 20.0,$$
$$ref_{Fy} = 0.0,$$
$$ref_{Fz} = 2.7.$$

The new parameters resulted in a faster and smoother descent of moment error in half the time of the previous trial, as shown in Figure 17. Half-way

through the insertion, the force reference value F_x was attenuated by 50% to study the response of the manipulator's motion. The reduction in value softened the impact during insertion,but increased the time-to-completion.

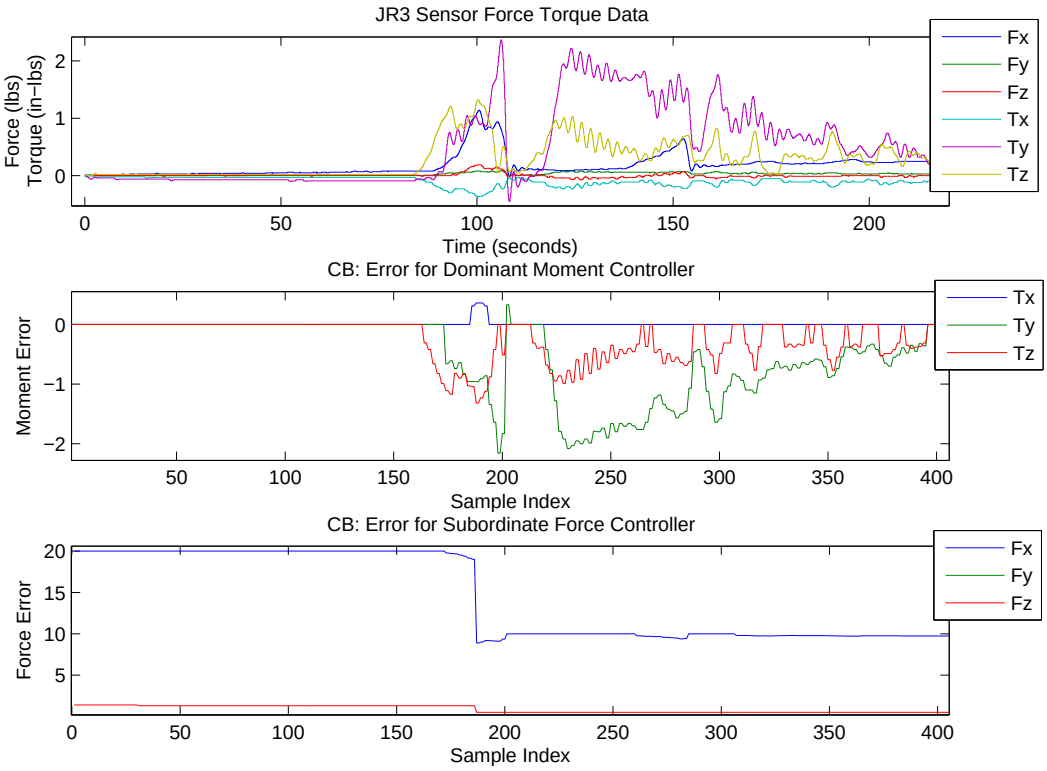

Figure 17: Trial C_MF_003: Faster insertion with smooth decline in torque and moment error data.

Two more trials were run to determine if a faster insertion could be achieved through a different set of force reference values. The force reference values were set to: 40, 0, and 2.7 lbs. in the x-, y-, and z-directions respectively. Figure 18, displays the results for trial C_MF_006. The insertion in this trial ran faster than previous trials, requiring 85 seconds to complete. Sensor readings, however, were not as smooth as readings in prior trials. The force readings registered slightly larger torque signatures due to

the higher reference force values. Nevertheless, the insertion controller reacted favorably to minimize the residual error and successfully complete the insertion.

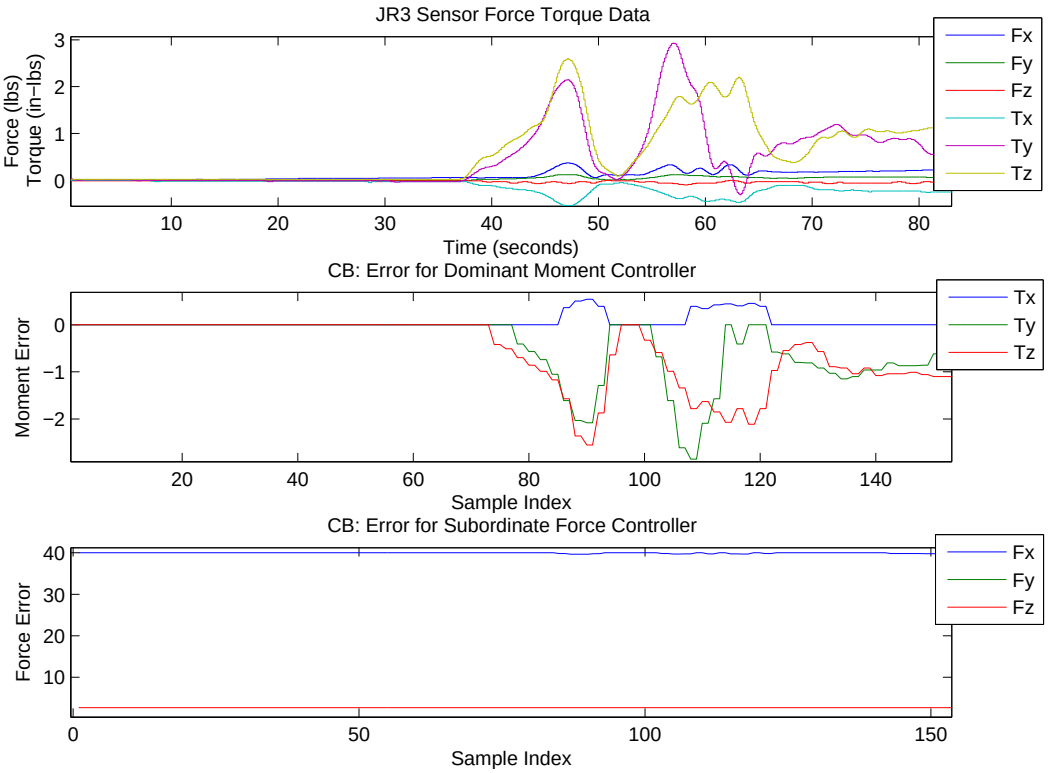

Figure 18: Trial Cart_MF_006: A faster insertion due to higher force reference values. The higher impact is reflected in higher values of torque in the y-direction.

As part of the 11 trials, 4 of these were executed by having the male truss approach the female fixture from a side-approach. Instead of positioning the male truss in front of the fixture, in these trials, it was placed to the side. No updates were necessary for controller gains or error transition thresholds, the reference z-force was slightly modified. Figure 19 shows the z-torque values generated as the manipulator aligned sideways. The sensor experienced 7

in-lbs of moment in the z-direction. The previous trial (with a straight approach), on the other hand, registered a much smaller moment in the same direction, only of approximately 2 in-lbs.

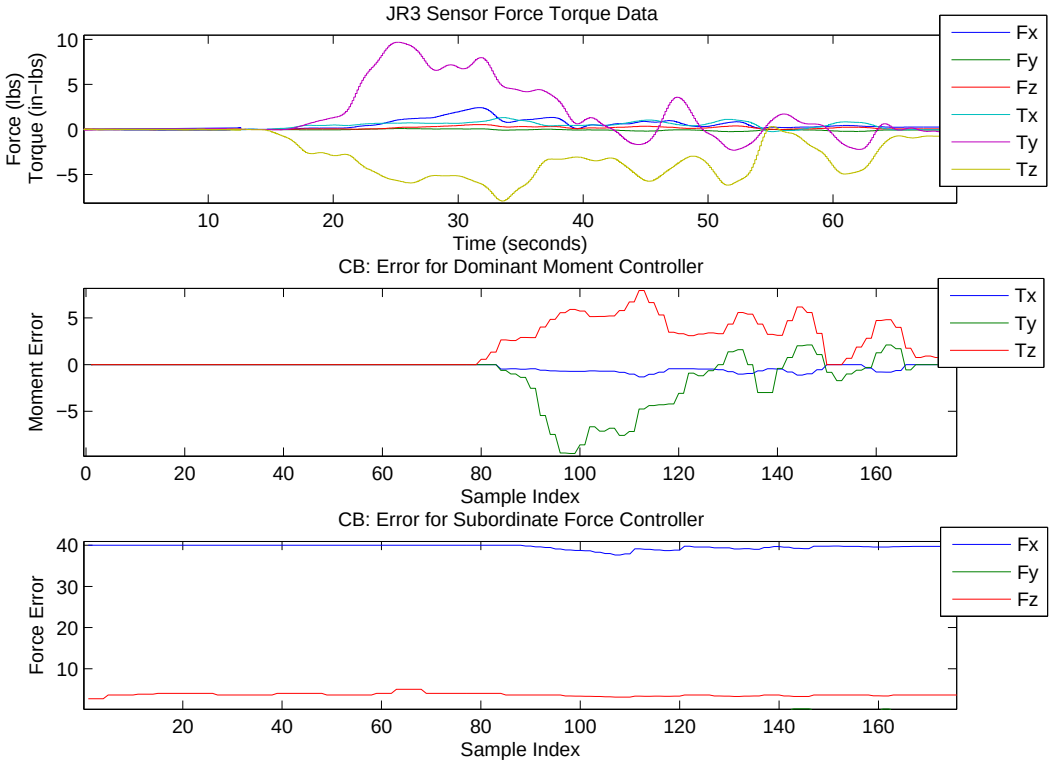

Figure 19: Trial Side_002: Assembly truss approaches fixtures from a side-elevated angle. Consequently, torques in the z-direction are registered.

Summary

A total of 11 trials were run as part of two tests. The results are summarized in Table 2. Successful trials are recorded with an "S" and failed trials are recorded with an "F" in the results category of the table. Set A, consisted of seven trials employed a straight approach between the male truss and the female fixture. Set B, consisted of four trials that employed a side approach. For each trial, the force reference values were recorded. The force reference in the x- and z- directions are shown in the table under the "Fx,z" label.

Similarly, for each trial the maximum absolute values for the moment error in all three directions: x, y, and z are recorded in the table as "Tx", "Ty" and "Tz". The sum of the absolute value of the moment errors was also recorded and labeled as "Max Abs. Error". Time-to-completion and the Max Abs. Error will be primary metrics for comparison. Averaged values for successful trials are found at the bottom of the table and are used to compare across experiments (data for trial C_MF_001 was not used as part of the averaged results).

Results from two experiments show that, generally, with each progressing trial, the time-to-completion decreased or at least stayed the same, as force reference values increased. Absolute moment residual values for set A stayed below 3 in-lbs., while those of set B registered higher average readings for moments in the y- and z-direction. Set B insertions were slightly rougher and required more adjustment on both vertical and horizontal planes.

Experiment 2: Visual System Accuracy

The visual system uses the error between the position of the centroid of a foreground blob that corresponds to a fiducial and the center of the image to trigger the camera pan and tilt servos. The angles, in turn, are used to estimate the 3D cartesian position of the gazed object. The accuracy of the cartesian position relies on how accurately the centroid of the blob can be positioned in the middle of the screen. To accomplish the desired accuracy requires robust noise reduction algorithms and accurate servo steps. Additionally, the visual system does not calculate the cartesian positions until it has verified that the centroid error is under an empirical threshold. A snap-shot of the visual imaging process is shown in Figure 20.

This system recognized colored fiducial marks placed on tool-tips of the

Table 2 - Experiment 1A and 1B							
Experiment 1A and 1B:							
Trial	Result	Fx,z	Time	Max Abs. Error			
		(lbs)	(secs)	Tx	Ty	Tz	Sum
C_MF_000	F	-	-	-	-	-	-
C_MF_001	S	10,0	470	0	20.26	9.29	29.55
C_MF_002	F	-	-	-	-	-	-
C_MF_003	S	20,2.7	220	0.37	2.37	1.32	4.06
C_MF_004	F	-	-	-	-	-	-
C_MF_005	S	40,2.5	82	0.67	3.43	3.08	7.18
C_MF_006	S	40,2.7	75	0.54	2.91	2.6	6.05
Average			*125.67*	*0.53*	*2.90*	*2.33*	*5.76*
Experiment 1B:							
Side_000	F	40,2.7	-	-	-	-	-
Side_001	F	-	-	-	-	-	-
Side_002	S	40,3.6	70	1.31	9.67	7.8	18.78
Side_003	S	40, 3.6	85	1.15	10.55	5.82	17.52
Average			*77.50*	*1.23*	*10.11*	*6.81*	*18.15*

Table 2: Experiment 1: Summary of trial results.

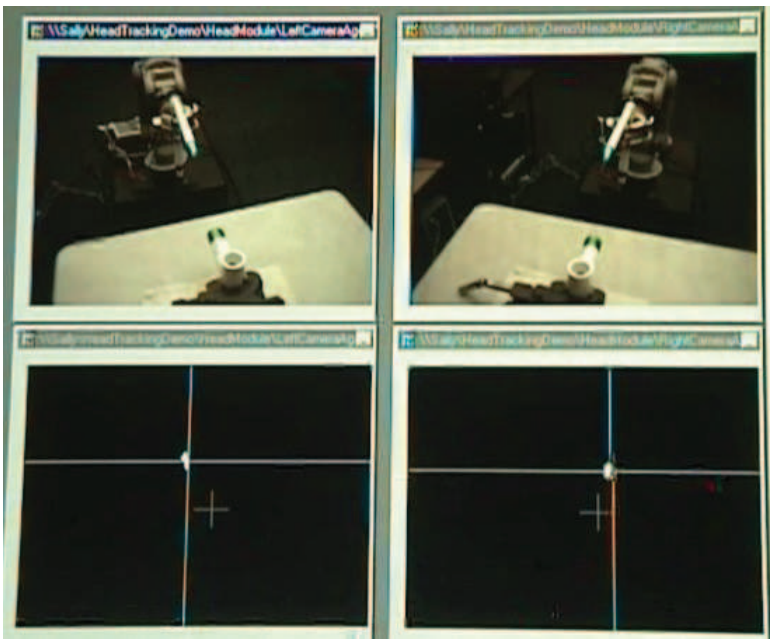

Figure 20: Screen shot of visual system performing color segmentation and tracking of two tool-tips during assembly.

assembly parts. The HP3JC held the truss that used a blue colored tip and ISAC used the fixture that used a green colored tip. First the visual system moved to the blue color fiducial mark. When the system verified the stability of the camera motors it calculated the position. Then it moved to the green color mark. The process was repeated again. A transform was derived and used as a reference position for both robots throughout the remaining experiments.

Results

For the experimental set-up, the HP3JC robot along with the gripped PVC truss was placed in front of ISAC. The corresponding fixture was positioned at: (a) the top of a table nearby ISAC, and (b) the truss held rigidly by ISAC's end-effectors. The first location allowed for easy set-up and a preliminary analysis of the system. The second set-up had both tool-tips in

positions close to those used in the rest of the experiments. In both cases and throughout a number of trials, physical measurements were taken to find the distance between both tool-tips. Results for 8 trials are shown in Figure 21. The averaged computed position in millimeters with reference to the cen-

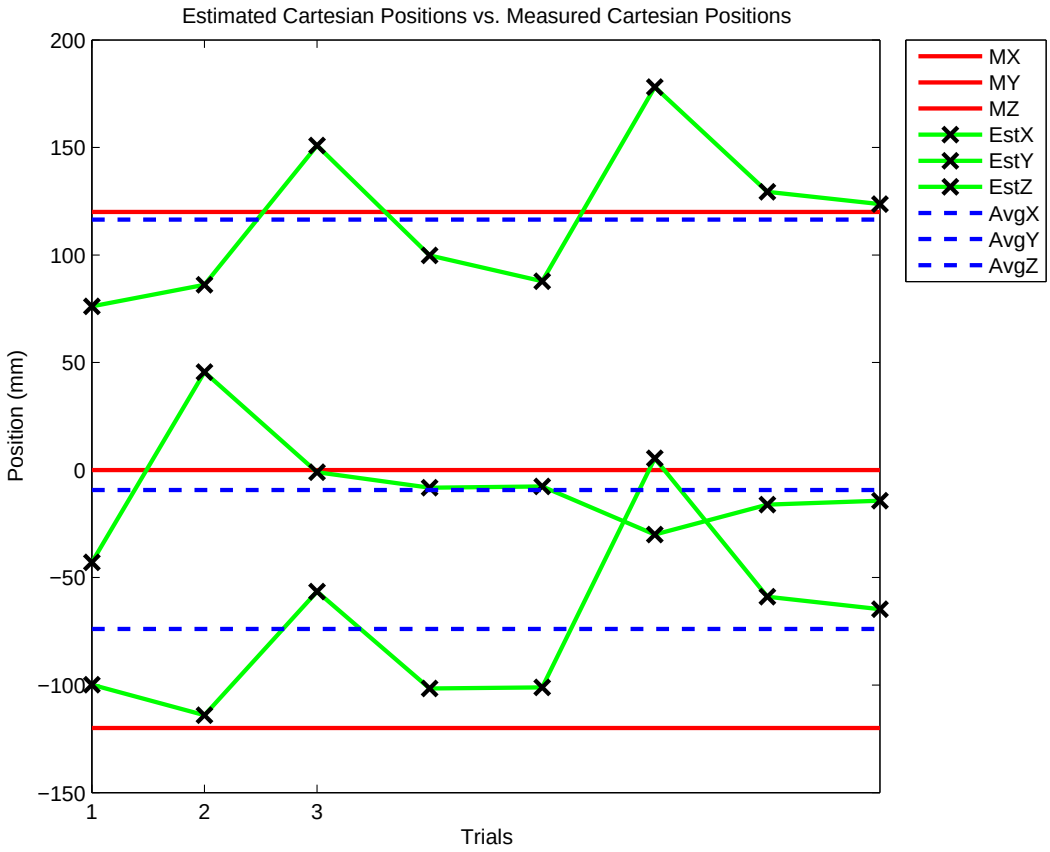

Figure 21: Comparison between computed estimates, measured distances, and average computed positions.

ter of the robot's visual system was: $< 116.4875\vec{x}, -9.3278\vec{y}, -73.9001\vec{z} >$; the averaged error was calculated to be: $< -3.5125\vec{x}, -9.3278\vec{y}, 46.0999\vec{z} >$. The z-coordinate showed the largest margin of error. The cameras presented some jitter motion when the the system recorded positions in space suggesting that the system's stability check was loose. To improve stability, three modifications were made: (a) the velocity and acceleration of each camera was decreased by half to aid the integrity of the color segmentation process,

(b) the error threshold for head stability was decreased, and (c) the magnitude of the standard deviation for the ellipse used to segment the green fiducial mark was increased. Another set of trials were carried out, with better results as shown in Figure 22.

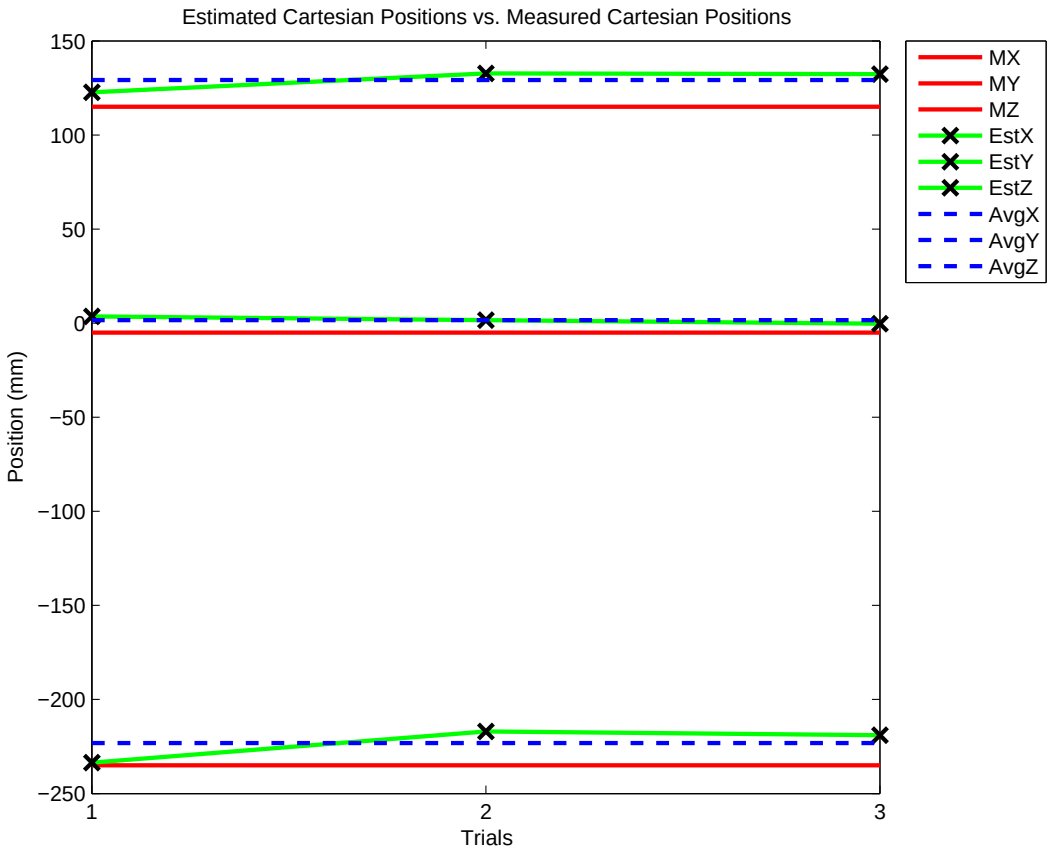

Figure 22: More accurate results after the visual system was refined.

The averaged position for the new set of trials was: $< 129.2595\vec{x}, 1.6289\vec{y}, -223.2044\vec{z} >$ and errors decreased to: $< 14.2595\vec{x}, 6.6289\vec{y}, 11.7956\vec{z} >$. Compared to the previous set of trials, the disparity between computed and measured position was smaller for $\vec{y}$ and $\vec{z}$ and slightly larger for $\vec{x}$. These results seemed to be of good-fit considering that the aperture of the female PVC pipe held by ISAC was of 25.4 mm. Nonetheless, a bias of 20 mm was applied in the negative x-direction to decrease the likelihood of having the male truss held

by the HP3JC to surpass the insertion point of the female fixture during the guarded move approach. The source of error in the x-direction may have been due in part to the color segmentation process. The colored fiducial mark for the HP3JCs covered an inverted chamfer, which was 4 cm long, while the green fiducial was 3 cm long. Given that the centroid was computed for both markers, an approximate 3.5 cm error may have been embedded in the color segmentation process.

The parameter configuration derived was used for the next four experiments. The visual system successfully returned the goal position 90% of the time across the remaining experiments.

Experiment 3: Assembly with a Compliant Robot

The third experiment studied the effect of a compliant robot on the assembly process. Compliant devices are commonly used in the end-effector of stiff robots as described in Section II, but we found no literature reporting on assembly with a compliant robot. While compliant robots are challenging to control, their elasticity can compensate for the high strain forces experienced with industrial manipulators.

This experiment used the industrial HP3JC manipulator, the visual system, and the compliant humanoid robot ISAC. ISAC used rigid end-effectors to hold a female fixture only using position control. The HP3JC robot held the male truss and began the guarded move approach when the visual system computed the reference position. As in experiment 1, the compliant insertion controller was triggered once the reference position was reached.

In this section, a total of seven trials were run and three outcomes are described here. The first is a failed trial, the second is a smooth insertion,

and the last is an example where the truss rammed against the edge of the female fixture. Trials for this third experiment are labeled as Comp_00X.

Results

Initial trials were run with force reference values of $<< 20\vec{x}, 0\vec{y}, 0.5\vec{z} >>$ for a slow entry. Later trials used values twice as large. Trial Comp_005 failed; however, due to an erroneous reference position provided by the visual system. The truss passed over the fixture by a few centimeters and never made contact. Figure 23 shows the resulting force and moment signatures for the industrial robot. This plot shows small readings in moments and no change in forces. The moment readings do not significantly vary over time although they decrease at a steady pace. That was probably induced by the weight of the end-effector as it was displaced over time.

Trial Comp_004 on the other hand is an example of a fast and smooth entry. This run was completed in 43 seconds. The controllers worked effectively to minimize the moment residual error. The results are shown in Figure 24. Torques in the y-direction reached 5 in-lbs, while those in the z-direction reach 2 in-lbs. Both residual errors were minimized to zero over the course of the task. Similarly, no force interjections were experienced such as a force that pushed the manipulator up or down, or even backwards. Compared to the plots in experiment 1 during the rigid insertion, this plot exhibited smoother curvature over the duration of the task due to the gentle adjustments by the compliant robot as the truss was inserted.

Another interesting datum was revealed in trial Comp_007. In this case, the guarded approach by the HP3JC robot forced the truss against the edge of the mating fixture for a few seconds. Over time, the forces experienced by both robots increased steadily and delayed the task's time-to-completion.

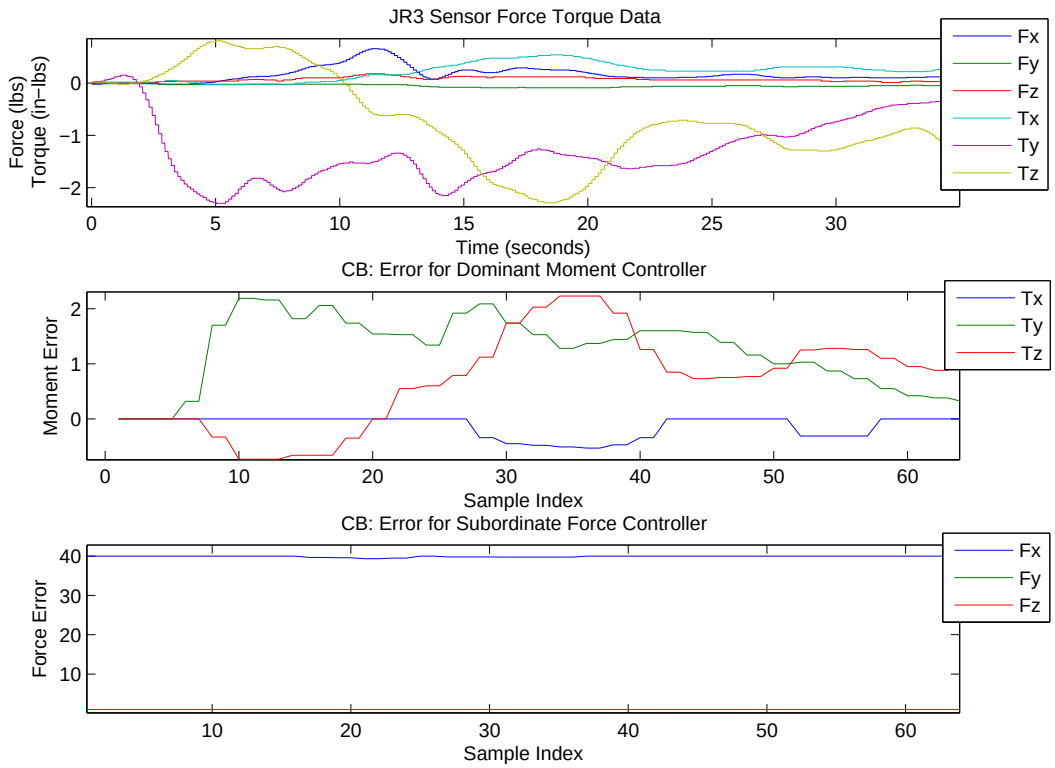

Figure 23: Trial Comp_005: Force and moment plots for the HP3JC robot during a failed insertion where the robot moved past the entry point.

After a brief period, the compliant robot snapped in the right direction and allowed the assembly task to proceed rather quickly. The higher stresses experienced by the industrial robot are shown in Figure 25. The sensor experienced the highest reading for Ty reaching a magnitude of 15 in-lbs. This accumulation reflects the stress experienced by the wrist of the manipulator as it tried to adjust its motion while ramming against the fixture. After a backlash motion, the truss quickly entered the fixture and the sensor's torque readings dropped drastically – under 5 in-lbs – for the rest of the task.

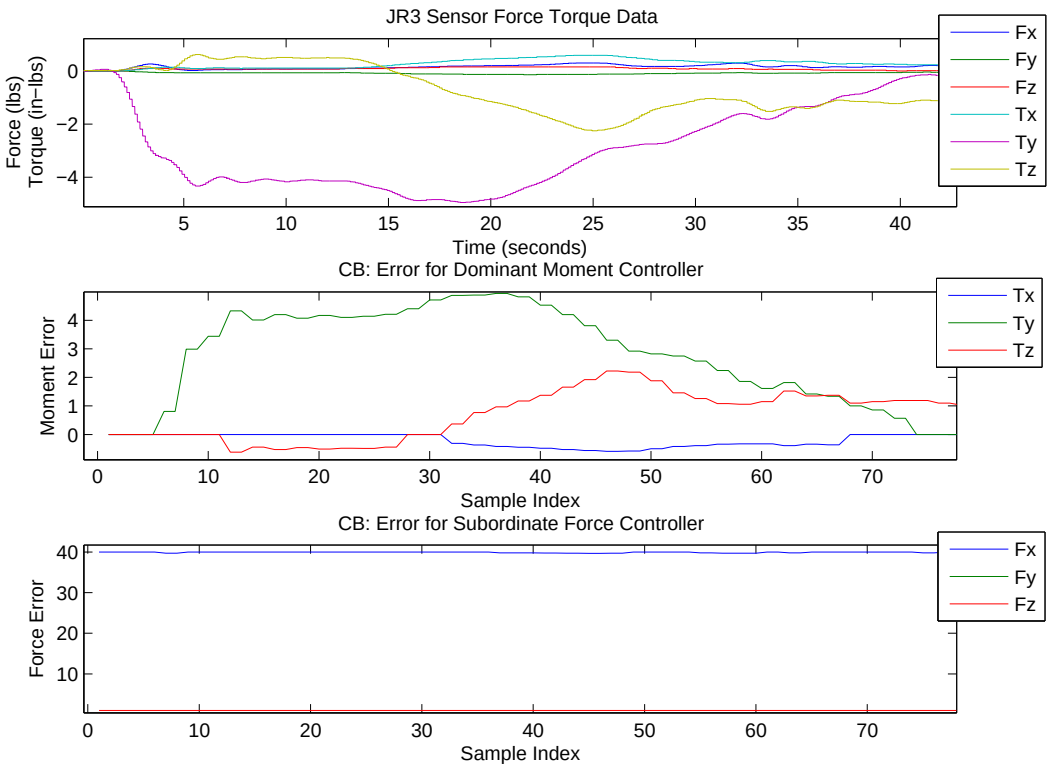

Figure 24: Trial Comp_004: Smooth and faster results than prior runs.

Summary

Integrating compliance into the assembly process enhanced results as compared to those in experiment 1. Seven trials were run, five of which were successful. A summary is presented in Table 3. The average time-to-completion of these trials is 69 seconds compared to the average time of 80 seconds for the trials in experiment 1 that had a side-approach, and the average time of 251 seconds for the trials in experiment 1 that had a straight approach. Two sets of force reference values were consolidated, one set for "fast" insertions, the other for "slow" insertions. The former uses reference values of $< 40\vec{x}, 0\vec{y}, 1\vec{z} >$, the latter uses $< 20\vec{x}, 0\vec{y}, 0.5\vec{z} >$. The average moment readings for this set of trials was very low, only slightly larger than those trials in experiment 1 that had a straight approach due to the ramming of the truss

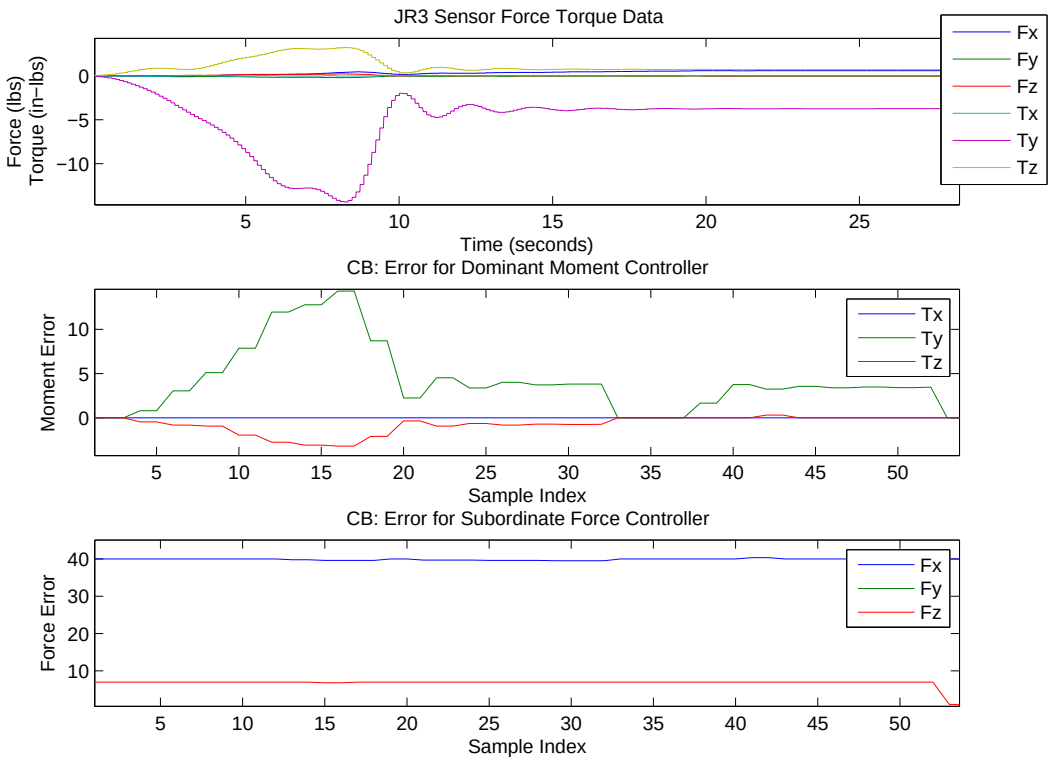

Figure 25: Trial Comp_007: Example of a truss ramming into a female fixture. Higher forces, errors, and increased time-to-completion is experienced.

onto the edge of the mating part for the last trial of this experiment. The compliance of the humanoid robot helped render this last trial successful, without compliance it would have failed and possibly damaged the assembly parts or the robots themselves.

The three experiments presented above were preparatory for the the joint assembly experiments described in the next section. Experiment 1 provided a baseline for controller gains, error transition thresholds, and general reference values for the controllers. Experiment 2 served to test the accuracy of the visual system to ensure a reliable goal position for the active robot. Experiment 3 demonstrated that the use of compliance facilitated the insertion task for the industrial robot.

Table 3 - Experiment 3

Trial	Result	Fx,z	Time	Max Abs. Error			
		(lbs)	(secs)	Tx	Ty	Tz	Sum
Comp_1	F	-	-	-	-	-	-
Comp_2	S	20,.5	95	0	3.86	1.68	5.54
Comp_3	S	20,.5	88	0	5.4	1.45	6.85
Comp_4	S	40,1	43	0.59	4.95	2.22	7.76
Comp_5	F	-	-	-	-	-	-
Comp_6	S	40,1	50	0.4	3.96	2.69	7.05
Comp_7	S	40,1	70	0	14.31	3.19	17.5
Average			*69*	*0.20*	*6.50*	*2.25*	*8.94*

Table 3: Experiment 3: Summary of results.

Cooperative Assembly Experiments

The second set of experiments executed assemblies as part of a coordination and cooperation scheme across robots. Three scenarios were studied. Two of them involved having one robot drive the insertion while the other performed as a static partner. The final experiment consisted of two active robots in which both used force-sensing to drive the insertion. These scenarios were similar to human behavior, when two individuals carry out an insertion task, one person may push while the other holds; similarly, there are times when both people push to speed-up the task.

The following experiments used the π_{GM} and π_{CI} controllers for the industrial robot. ISAC used the virtual-contact counter balance controller $<< \pi_{VCB} >>$ in experiment 4, and the virtual-contact guarded move $<< \pi_{VGM} >>$ and compliance insertion $<< \pi_{VCI} >>$ controllers in experiments 5 and 6. One exception was the exclusive use of the π_{GM} controller for the industrial robot in experiment 5.

For the joint assembly experiments, the same data measurements used for the HP3JC robot were also used for ISAC. The clock for each task; however,

was still maintained by the HP3JC robot, except during experiment 5 when ISAC was the only one using force sensing. Quantitative and qualitative analysis of ISAC's results are presented.

Experiment 4: HP3JC-active and ISAC-static

This experiment designated the HP3JC robot as the active contributor and ISAC as a static holder. In contrast to experiment 3, this set of trials had the compliant robot run a counter-balance controller. The latter aligned the orientation and position of the female fixture to facilitate the entry of the male truss driven by the industrial robot (the counter-balance controller does not update the position of the virtual contact if it does not sense any stimuli from the environment).

For this experiment, three scenarios are initially described here: the first scenario was a wedge situation, the second one a jam, and the third one was a quick insertion that underwent high strains caused by instability in the HP3JC robot. Trials in these experiments were labeled Balance_00X.

Before ISAC's analysis is presented, it is worth noting a few points corresponding to the data related to the compliant robot for this and future experiments:

1. While ISAC uses two force sensors, a virtual contact is used as part of this robot's controllers. The π_{VCI} controller averages the contribution of both sensors and the updated positions of the manipulators; hence, producing only one plot for the moment residual and force residual errors.

2. The moment and force residuals do not match the magnitudes of maximum registered torques or forces in the individual F/T sensor plots.

This too is related to the fact that both sensor readings are averaged before computing any errors.

3. The left and right ATI sensor can experience inversely related forces. If one sensor experiences a positive moment then the other one may experience a negative moment. This results from having both sensors connected by a PVC truss.

4. The legend for all ISAC plots shows Ty before Tx. The ATI sensor had difficulties applying a rotation transformation to the coordinate frame in order to align the sensor frame with the robot frame. Data was read in an order that would represent the appropriate coordinate axis alignment.

Results

As in experiment 1, an initial set of controller gains and reference force values are presented, in this case for ISAC through the use of the π_{VCB} controller:

$$\begin{array}{lll} k_{Fx} = 0.00100 & k_{Tx} = 0.002 & ref_{Fx} = 0.0 \\ k_{Fy} = 0.00100 & k_{Ty} = -0.002 & ref_{Fy} = 0.0 \\ k_{Fz} = 0.00025 & k_{Tz} = 0.002 & ref_{Fz} = 0.0 \end{array}$$

Reference values of zero were used as a reference to always minimize any force residuals to zero. The first trial: Balance_001, was successful, although the responsiveness of π_{VCI} was low – in particular the wrist motion. Moment gains were adjusted and a more responsive set was found to be: $k_{Tx} = 0.2$, $k_{Ty} = -0.2$, and $k_{Tz} = 0.2$. In first trial to be described in this section is Balance_010, where "wedging" occurred. Wedging occurs when a truss makes a two-point contact and the direction of motion prevents the parts from aligning. One of those contacts, exerts forces at the tip of truss inside the

fixture's hull female fixture; the other contact exerts forces at the interface of the edge of the fixture and the body of the truss. Both of these forces seem to push in opposite directions. During the trial, wedging tricked the controller into thinking there was no need for realignment. The robots still moved to minimize the perceived residual errors and achieved the insertion though the alignment was not as desired. The trial lasted 95 seconds and it was longer than all but one trial in experiment 1. The duration was unexpected in light of ISAC running the counter balance controller. However, due to wedging, the task duration was increased. Data for the industrial robot is shown in Figure 26. The force residual plot revealed no significant deviations from

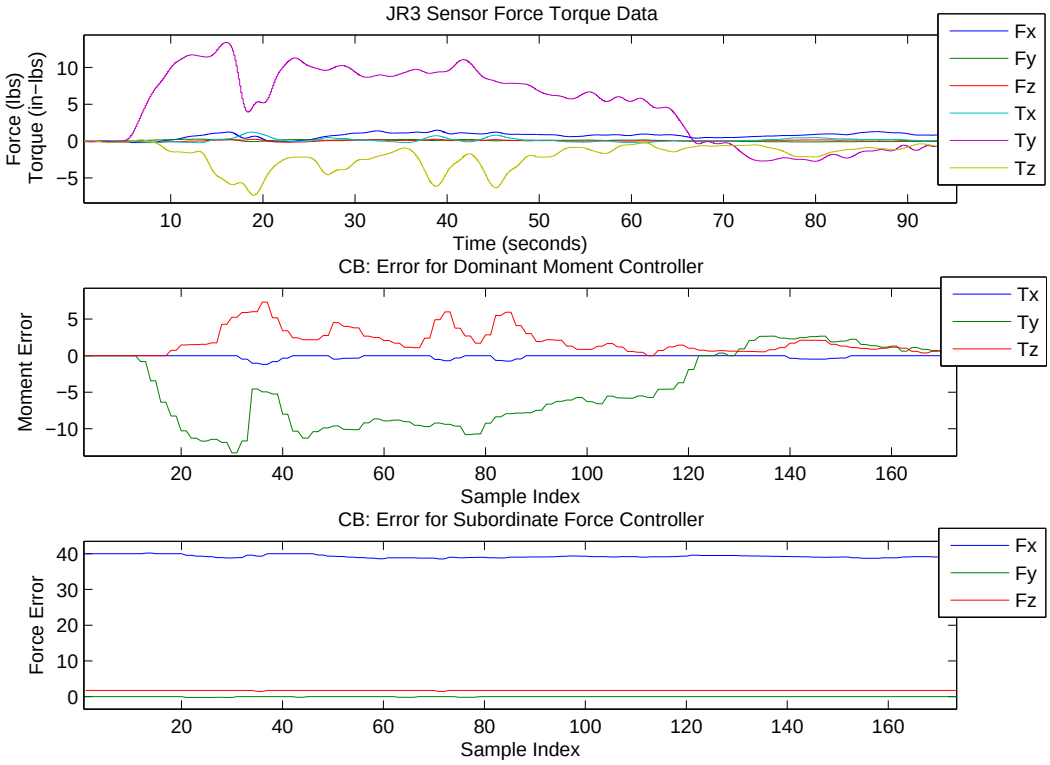

Figure 26: Trial Balance_010A: The HP3JC inserts the truss into the fixture although wedging occurs.

the reference values indicating that the HP3JC did not experience exterior forces that would perturb the path of the truss (*i.e.* force the truss to move

upwards, downwards, backwards, or halt). The moment residual plot also shows a continuous minimization of the residuals, in spite of the wedging condition, conveying that the HP3JC set of controllers did not detect this situation. The force readings for ISAC corresponding to trial Balance_010 are shown in Figure 27. The absolute value of the maximum moment residuals

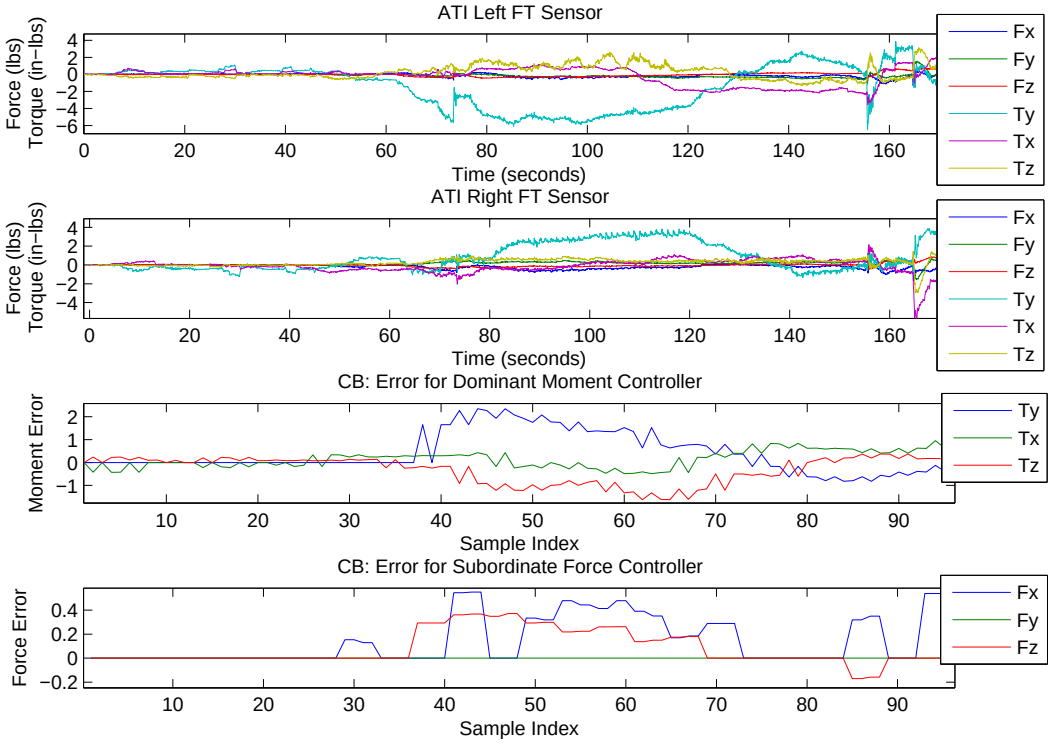

Figure 27: Trial Balance_010B: ISAC's response using a virtual counter balancing controller in a wedge situation.

for ISAC were of: Tx=1.0, Ty=2.4, and Tz=1.6. These were minimized over time. The force residual for the compliant robot presented a more intricate pattern than the one for the industrial robot. The plot describes how the virtual contact's position is affected over time. Due to wedging, the fixture was forced into a backwards and downwards motion. An examination of the force plot shows how the system experienced intermittent forces in the x-direction greater than its reference value of 0. Each of these peaks represents

a backwards motion. For the z-direction, a force greater than zero indicates a downward motion. Note how the four subplots register initial activity, synchronously, at ISAC's clock mark of 60 seconds. This corroborates initial contact and increased errors in the first half of the plot with decreased errors in the second half.

The second trial, Balance_011, yielded a successful insertion and alignment but experienced a jam. During initial contact, the male truss hit the edge of the female fixture and pushed back on it. After some time, the compliant robot snapped so as to continue the insertion. The task required less time than the aforementioned trial but still experienced an above average time-to-completion compared to other trials. For the HP3JC robot, Figure 28 shows similar data to the prior trial. ISAC registered a higher torque

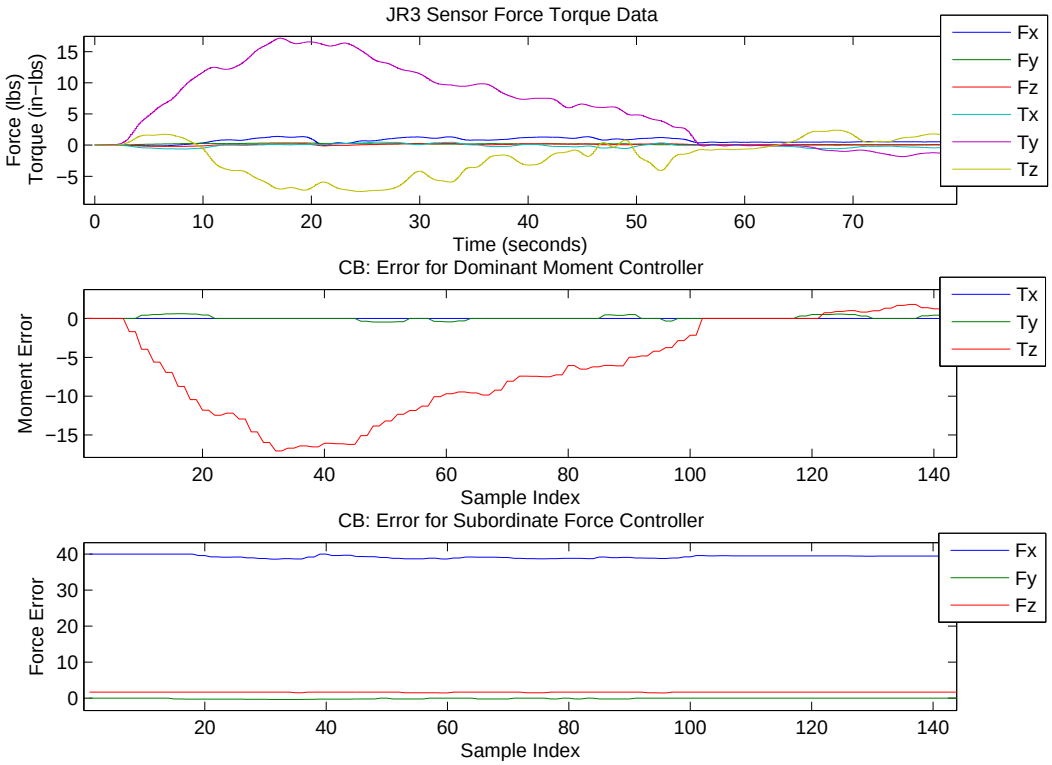

Figure 28: Trial Balance_011A: HP3JC robot efficiently completes the insertion task.

in the y-directions than the prior one due to the impact of the jam. The duration of these forces is shorter for trial 011 than trial 010, particularly for the force in the z-direction. Data is shown in Figure 29.

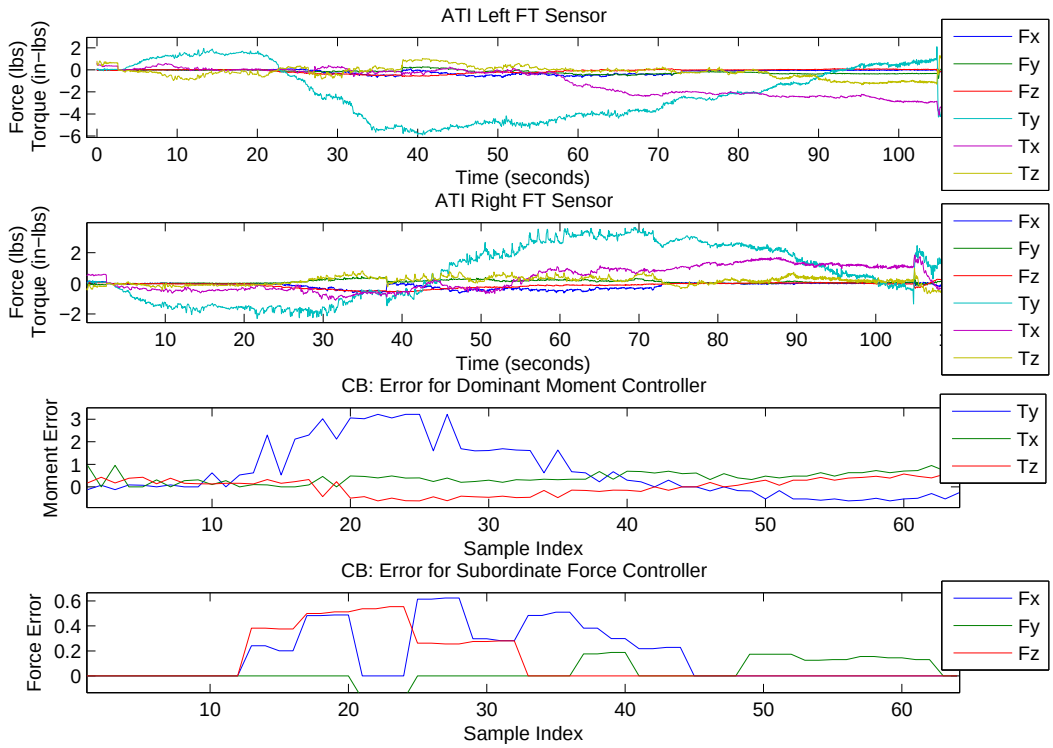

Figure 29: Trial Balance_011B: ISAC successfully aligns the orientation of both end-effectors to assist in the mating of the assembly parts.

The third example, trial Balance_005, presented a unique scenario. As the truss held by the HP3JC entered the fixture, the industrial robot maintained a significant downwards motion creating a difficult situation for ISAC. ISAC; however, adapted well to this behavior and over time ISAC's fixture exerted an increased upward force on the truss. The HP3JC controller responded by moving upwards quickly and in large steps. Then another important downwards motion proceeded. It was remarkable that both robots continued to maintain the insertion in spite of the significant vertical motion registered in this run. This response mimicked the way humans would have behaved in a

similar circumstance and is an attribute of both the controllers and the humanoid robot's compliant nature. The data for the ATI force sensors in trial Balance_005 was corrupted. The force-torque data from both sensor overlapped and was not divisible. The residual plots; however, are still included since they contain very descriptive data and represent a very unique scenario. The residual plots are shown in Figure 30. The force residual plot depicts

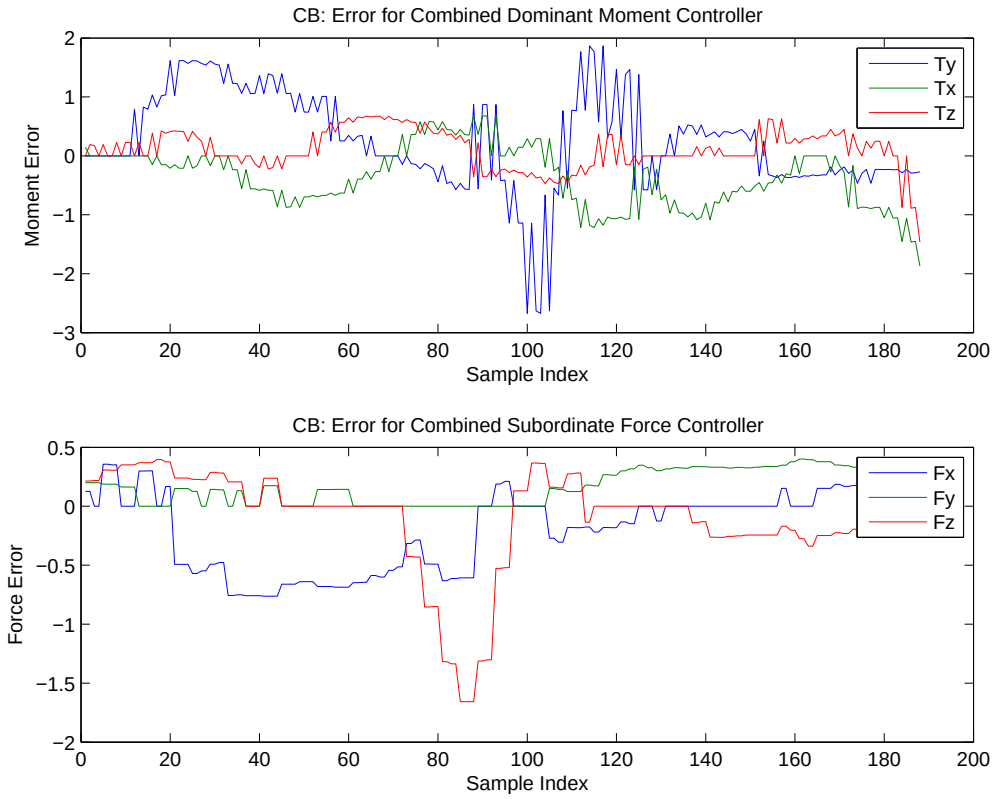

Figure 30: Trial Balance_005B: ISAC exhibits quick reactions to match motions exerted by the HP3JC robot.

the vertical motions of the task clearly. Between readings 0-20, the positive force error denotes a downward motion. There is a sustained and much greater force that drives the arm upwards followed by an equal downwards motion during readings 80-95. Around sample index 85, an asymmetrical correlation between the moment residual error, Tz, and force residual error, Fz, is present. When the moment residual is positive the error of the force is

negative. This inverse relationship illustrates how when the arm is moving up, the wrist is pulled down. ISAC's controller gains and elasticity allowed for a fast response.

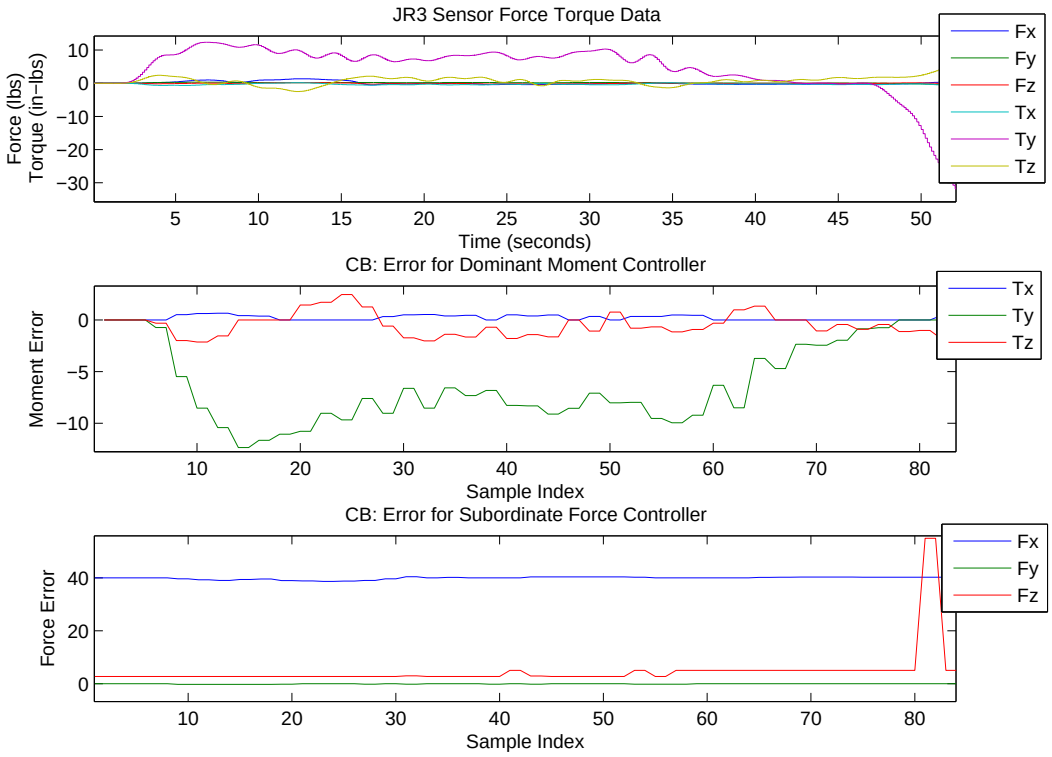

Figure 31: Trial Balance_005A: HP3JC experiences important upward and downward motions.

The experienced moment residual for the HP3JC was minimized over time, as seen in Figure 31. Toward the end of the task; however, both the moment in the y-direction and the force in the z-direction rose. The increment in moment error corresponded to the upward motion that the system experienced during the task. The force plot also shows the downward motion after a few seconds. The correlation between ISAC's results and the HP3JC's result corroborates how both systems underwent an unusual vertical motion as the insertion took place within 57 seconds, the fastest insertion to this point.

Summary

The averaged time-to-completion results for this experiment were unexpected. The average time-to-completion across all trials showed a very small improvement over experiment 3. When trials were separated according to force reference values (Fx=20 for slow insertions and Fx=40 for fast insertions), it was seen how the average time-to-completion for trials with Fx=40 had a higher time to completion. ISAC also experienced higher moment errors than in preceding experiments. Two trials in this experiment experienced delays due to a jam and wedging. It was noted that when wedging took place, the robot's wrists moved slightly upwards as the π_{VCB} controller was triggered. This was a reaction to a build-up of forces on the wrists of the robot caused by the rigid PVC structure connecting both end-effectors. As the wrists rotated upwards, they in turn rotated the orientation of the fixture and prevented a clean entry for the male truss. This position favored wedging, which the controllers and associated control policy were not well suited to detect. As contact was made at two points, such that a wedge was created, a singular and compounded force was sensed and controllers were unable to discern the problematic alignment scenario. The controllers still attempted to minimize net moments and forces, but did not alleviate the wedging condition.

With regards to the industrial manipulator, increased moment errors (as seen by the averaged sum of maximum value moments) were experienced compared to the previous experiment. The moment residual nearly doubled in size, experiencing a 92% increase. This experiment was the first example in which two robots ran force controllers. Table 4 presents a summary of the results for this experiment. Trials 7 - 9 were successful but the data was corrupted.

Given the unfavorable results in the preceding runs, a new batch of trials

Table 4 - Experiment 4												
		HP3JC						ISAC				
Trial	Res	Fx,z	Time	Error				Fx,z	Error			
		(lbs)	(secs)	Tx	Ty	Tz	Σ	(lbs)	Tx	Ty	Tz	Σ
1	S	40,2.7	53	0.5	4.1	2.2	6.9	0,0	38.0	28.3	49.8	116.0
2	F	-	-	-	-	-	-	-	-	-	-	-
3	F	-	-	-	-	-	-	-	-	-	-	-
4	S	-	-	-	-	-	-	-	-	-	-	-
5	S	40,2.7	43	0.7	12.4	2.1	15.1	0,0	149.6	213.9	157.0	520.5
6	F	-	-	-	-	-	-	-	-	-	-	-
10	S	40,1	95	1.2	13.3	7.3	21.8	0,0	67.0	188.4	129.7	385.1
11	S	40,1	80	0.5	17.1	7.4	25.0	0,0	75.7	257.1	49.6	382.5
12	S	20,1	48	0.5	9.9	2.5	12.9	0,0	9.6	22.5	39.4	71.52
Avg			*63.8*	*0.7*	*10.7*	*4.0*	*17.2*		*70.6*	*139.5*	*85.0*	*295.1*

Table 4: Experiment 4a: Summary of results including a wedge and a jam.

was run to achieve clean insertions without jamming or wedging. It was important to see if the time-to-completion of trials without wedging or jamming would yield better performance than those in Experiment 3. Six more trials were run. Three used reference value $Fx = 20$ and three used reference value $Fx = 40$. Special attention was paid at the set-up of the fixture for ISAC. These six trials yielded good results. One trial out of this set is highlighted.

Trial Balance_014 was complete in 54 seconds. This insertion was completed in nearly half the time than trials Balance_010 and 011. Moments in the y-direction were reduced efficiently by both the HP3JC and ISAC, and moments in the z-direction maintained a small presence in both robots. The approach by the HP3JC was a more marked side approach which exerted moments in the z-direction and were not completely removed. The magnitude of these was not of significance and allowed the insertion to take place successfully.

A new average across trials was computed (excluding trials Balance_010

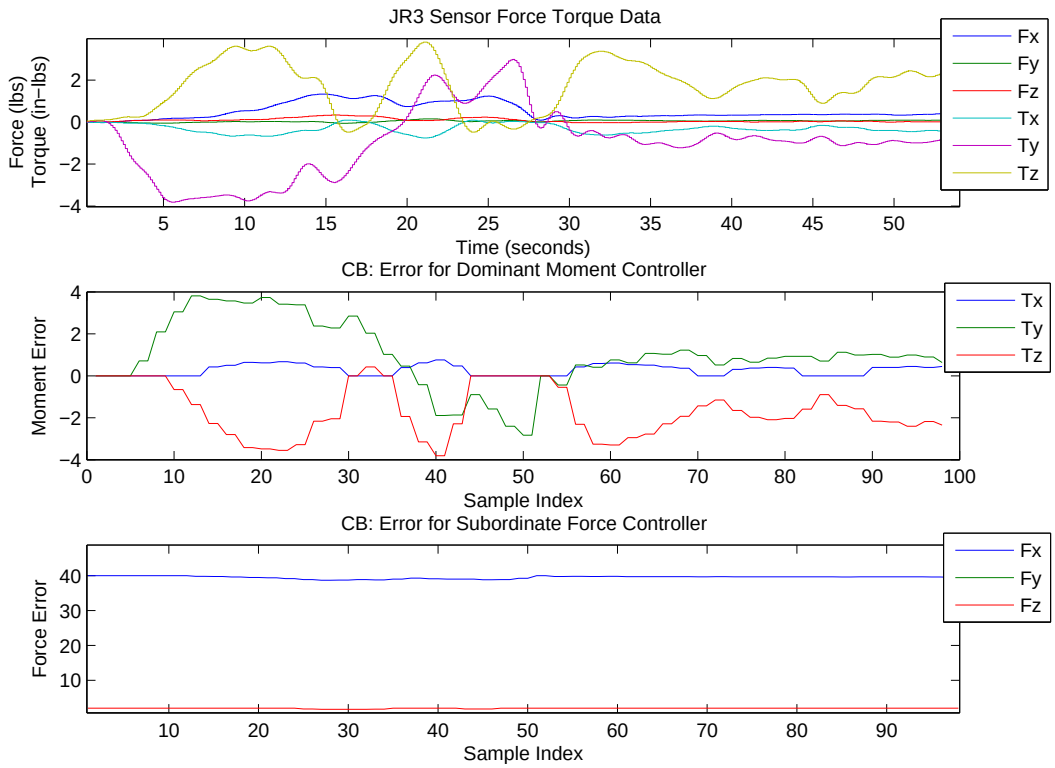

Figure 32: Trial Balance_014A: HP3JC drives a smooth insertion while ISAC runs the counter-balancing controller.

and 011 which had extreme results) and showed in Table 5. The new averaged results follow the trend seen across experiments 1 and 3. The time-to-completion for the overall trials and the sub-categories of $Fx = 40$ and $Fx = 20$ was lower in this experiment than in 3. Similarly, the sum of moment residuals is higher for this experiment than before – even without the wedge. This result suggests that as cooperation increases so are the maximum experienced forces by the robots.

Experiment 5: ISAC-active and HP3JC-static

The fifth experiment evaluated ISAC's ability to lead and drive the insertion. At ISAC's home position the HP3JC robot stands much higher than the base height of the female truss held by ISAC. This experiment was set-up such that

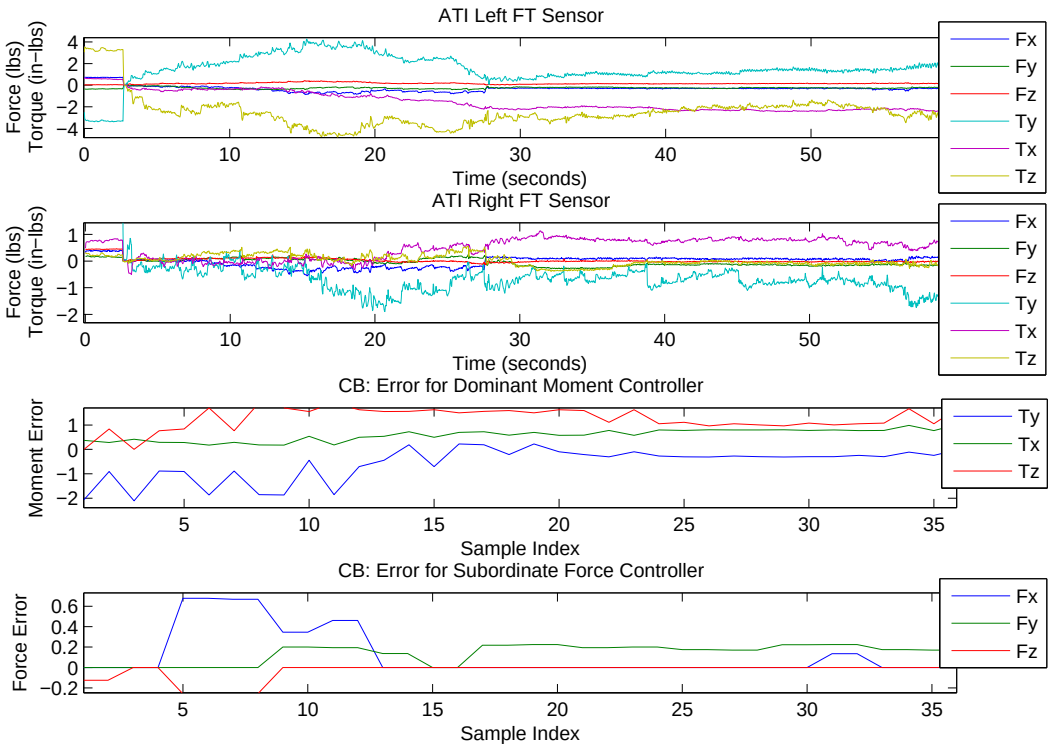

Figure 33: Trial Balance_014B: ISAC cooperates in the joint assembly where no jams or wedging took place.

the industrial robot performed a guarded move approach and then halted in front of the entry point for the insertion. At that time, ISAC's virtual-contact compliant insertion controller, π_{VCI} was activated.

The task dynamics were distinct from prior experiments. Insertions driven by the compliant robot are prone to stiction due to the elastic nature of ISAC's muscles. In this experiment, stiction played a dominant role as opposed to cases where ISAC maintained a static position. Sensor and residual error plots in Figures 37 and 35 present characteristic features of stiction. Similarly, force residual plots present a minimization or canceling of force reference values, which correspond to the robot's slowing down or halting. Stiction phenomena presents characteristic patterns in the sensor and moment residual plots in the form of a quick rise in experienced torque

Experiment 4												
		HP3JC						**ISAC**				
Trial	Result	Fx,z	Time	Error				Fx,z	Error			
		(lbs)	(secs)	Tx	Ty	Tz	Sum	(lbs)	Tx	Ty	Tz	Sum
1	S	40,2.7	53.0	0.5	4.1	2.2	6.9	0,0	0.5	0.4	0.6	1.5
5	S	40,2.7	43.0	0.7	12.4	2.1	15.1	0,0	1.9	2.7	2.0	6.5
12	S	20,1	48.0	0.3	9.9	2.5	12.7	0,0	0.3	0.1	0.5	0.9
13	S	40,2	39	0.9	11.2	4.1	16.2	0,0	3.8	0.8	1.1	5.8
14	S	40,2	54	0.7	3.81	3.56	8.1	0,0	1.0	2.1	1.9	5.1
15	S	40,2	46	0.7	16.1	5.9	22.7	0,0	0.5	1.6	1.1	3.1
16	S	20,1	76	0.0	0.7	1.1	1.8	0,0	0.3	2.2	1.4	3.9
17	S	20,1	72	1.1	16.5	6.6	24.2	0,0	0.9	1.8	0.9	3.6
Avg			*54.0*	*0.6*	*9.3*	*3.5*	*13.5*		*1.1*	*1.5*	*1.2*	*3.8*

Table 5: Experiment 4b: Summary of results with new trials and no wedge and jam.

followed by an immediate drop in it. The quick drop corresponds to a backlash motion experienced by the fixtures once forces overcome friction caused by stiction.

For the HP3JC robot, plots contain two subplots that display the robot's cartesian position and the associated error for the position as part of the guarded move controller. For ISAC, force and moment plots are displayed as in previous experiments. Seven trials were run in this experiment and labeled as ISAC_00X. All of them were successful. Two trials are reported in the next section. The first one is an example of a smooth entry for the humanoid, and the last one shows high stiction in the assembly.

Results

Trial ISAC_005 is an example of a successful insertion driven by ISAC with light stiction. The cartesian plot shown in Figure 34began with no change in position, which corresponded to a wait in time of the π_{GM} controller for the

goal position. The executed trajectory for the industrial robot was non-linear,

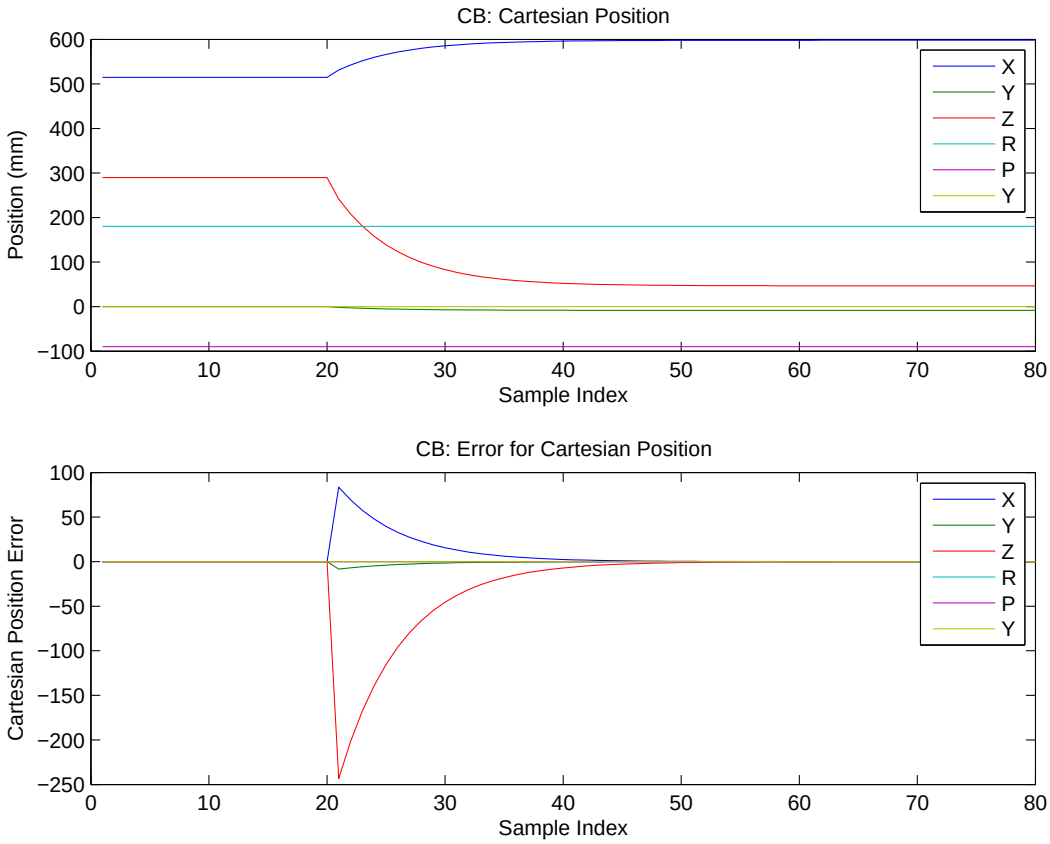

Figure 34: Trial ISAC_002A: HP3JC moves towards its reference position using the guarded move controller.

Figure 34 shows smooth curves for the system's trajectory. The controllers drove the displacement of the end-effector to converge to the attractor region. The top plot shows the change in cartesian position as the HP3JC robot moved to the reference position. In the top sub-plot the x-position increased, representing a forward motion by the robot; and the z-position decreased, representing a decrease in height. All other variables had minimum change. The lower sub-plot depicts how the error for all elements of the position vector converged to zero over time.

In Figure 35, ISAC's clock determined the task's duration. In trial ISAC_005, the task lasted 79 seconds. At clock time 10, a quick rise was

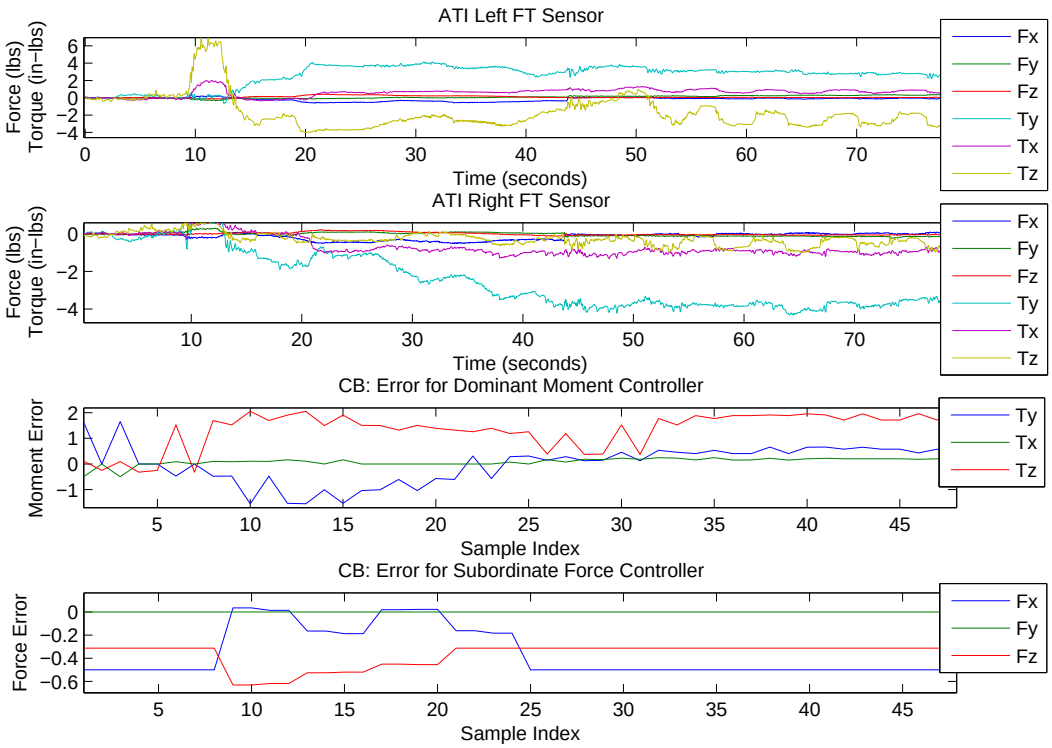

Figure 35: Trial ISAC_002B: ISAC drives the insertion through a virtual compliant insertion controller.

recorded in Tz values and to a lesser degree in the Tx values. This action is reflected in both the moment residual and force residual curves. In the latter, force references of Fx=-0.5, Fy=0, and Fz=-0.31 were used (as in experiment 6). The force residual plot revealed that when stiction began (between samples 7 and 25) that the driving reference force in the x-direction was canceled. This corresponded to a halt in ISAC's forward motion. The moment residual error also increased during this time, further corroborating the phenomena. Once stiction was overcome by the corrective forces of the controllers, the error was minimized. Once the insertion took place the moment error in the z-direction increased due to light stiction on the left sensor. The plot for the left ATI sensor shows a sinusoidal form for the torque in the z-direction from time 50-79 seconds, suggesting a stick-and-slip behavior.

The second example, trial ISAC_004, smoothly reached its reference position as shown in Figure 36. For ISAC, Figure 37 shows rich plots representing

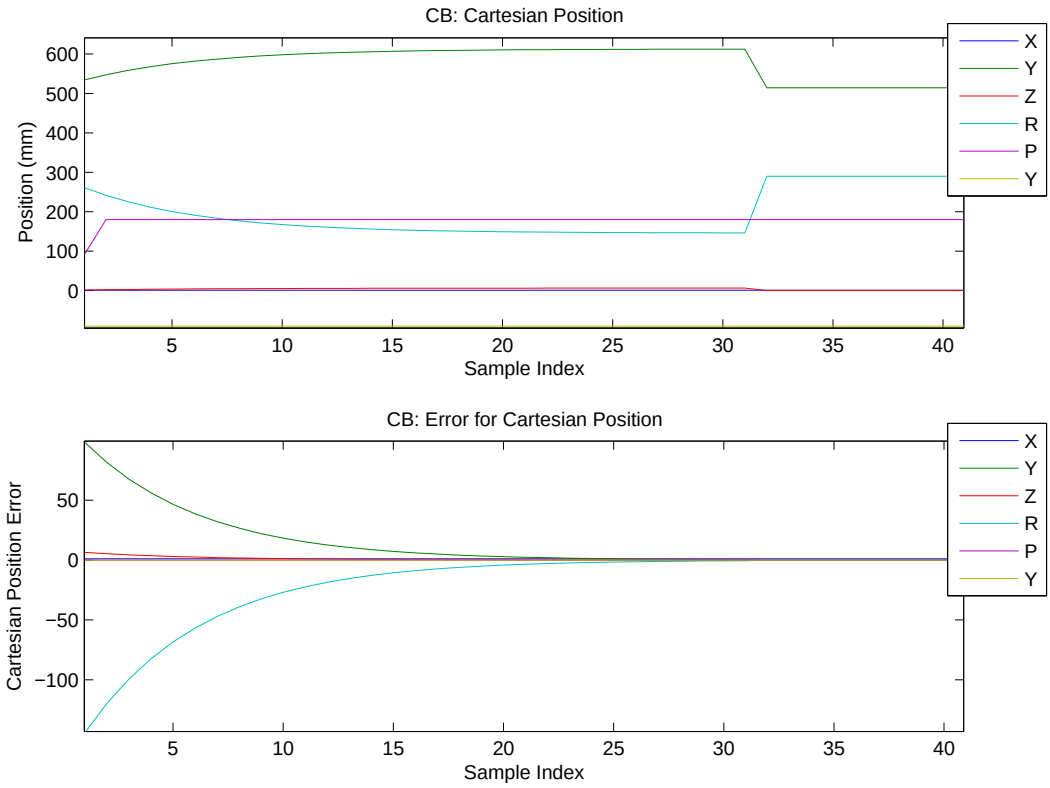

Figure 36: Trial ISAC_004A: HP3JC moves towards its reference position using the guarded move controller.

a few instances of strong stiction points. Both ATI sensor plots registered high torque changes around clock times 200, 280, and 295. A summary is presented in the Table 6.

Clock	Left	Right
(secs)	$\triangle T$	$\triangle T$
200	$\triangle Ty = 6.75$	$\triangle Ty$ = -3.67
280	$\triangle Ty = 4.42$	$\triangle Tx$= 12.94
295	$\triangle Ty = 3.31$	$\triangle Ty = 3.00$

Table 6: Stiction is represented by high changes in torques for trial ISAC_004B

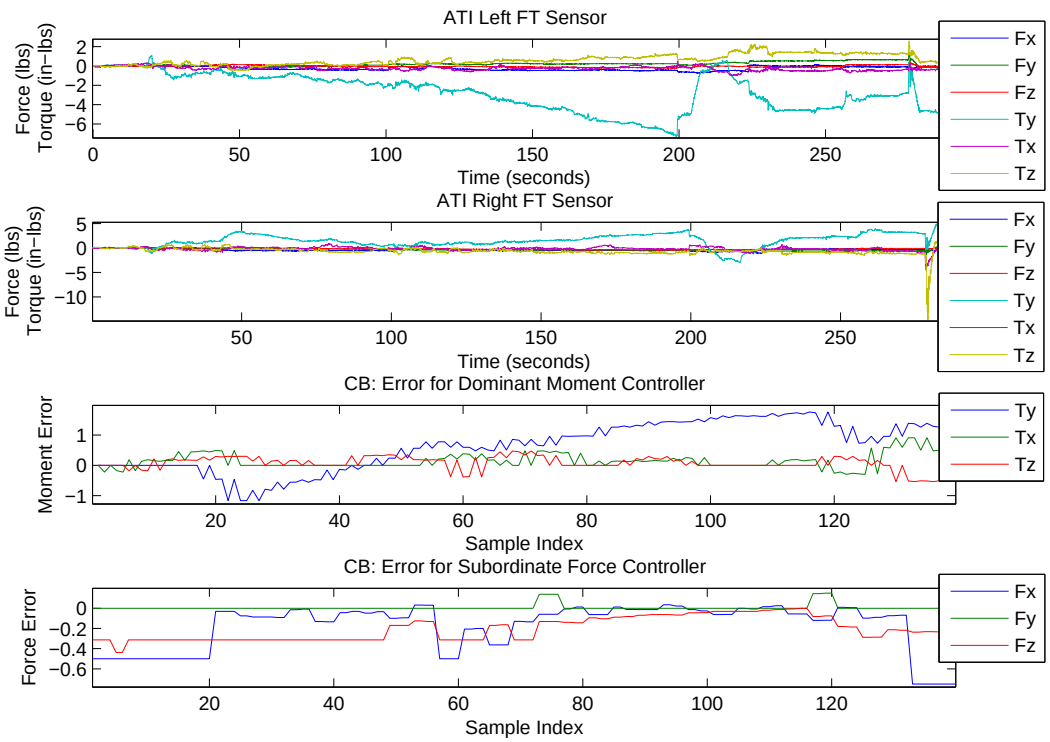

Figure 37: Trial ISAC_004B: ISAC experiences very high stiction points in a few instances.

The force residual plot shows the presence of stiction through two instances in which ref_{Fx} is canceled and ref_{Fz} is minimized over time. At sample index 57, Fx changed quickly from 0 to -0.5 lbs corresponding to a quick forward boost and at sample index 133 Fx changed quickly from 0.07 to 0.75 lbs. The moment residual error minimized the forces twice. The resurgence of force residuals, after being minimized, is related to another set of stiction points. A summary of results for this experiment follows.

Summary

The averaged time-to-completion for these trials was 164 seconds. A higher duration than the average values recorded across experiments for the industrial manipulator. The control of the compliant robot is more difficult than

that of its industrial counterpart. Slower speeds were used to ensure a better system control. With respect to moments residuals (in all three directions and the sum) sensed through the virtual contact, the average values were lower than in the fourth experiment, and the maximum torque values registered by the ATI sensors were generally higher due to stiction. The average sum of the errors was lower than in the previous experiment, which reflects the HP3JC's lack of active participation in the task. A summary of the results is shown in Table 7.

Experiment 5		**ISAC**					
Trial	Result	Fx,z	Time	Max Abs. Error			
		(lbs)	(secs)	Tx	Ty	Tz	Sum
1	S	(-.5,-.3)	253	35.6	119.9	45.4	200.9
2	S	(-.5,-.3)	239	86.1	233.6	72.1	391.8
3	S	(-.5,-.3)	172	78.3	112.3	88.9	279.5
4	S	(-.5,-.3)	296	72.6	140.7	43.3	256.6
5	S	(-.5,-.3)	79	41.0	124.0	164.0	329.0
6	S	(-.5,-.3)	47	84.0	135.0	157.0	376.0
7	S	(-.5,-.3)	63	29.0	93.0	241.0	363.0
Avg			*164*	*61*	*137*	*116*	*314*

Table 7: Experiment 5: Summary of results.

Experiment 6: Two Active Robots

The sixth experiment was the most involved and built on all previous evaluations. Four controllers were used in this experiment. The HP3JC robot used π_{GM} and π_{CI}, while ISAC used π_{VGM} and π_{VCI}. The experiment used the stereo cameras to compute the goal position for the π_{GM} controller. When the guarded move controller received the reference position, the approach motion was triggered. Upon completion of the motion, the controller transitioned to the compliant insertion controller. ISAC, concurrently, executed the π_{VGM}

controller, with a reference position pointing to the home state. When the HP3JC made initial contact with the female fixture, ISAC transitioned to the π_{VCI} controller. A series of images contained in Table 8 illustrate the assembly task.

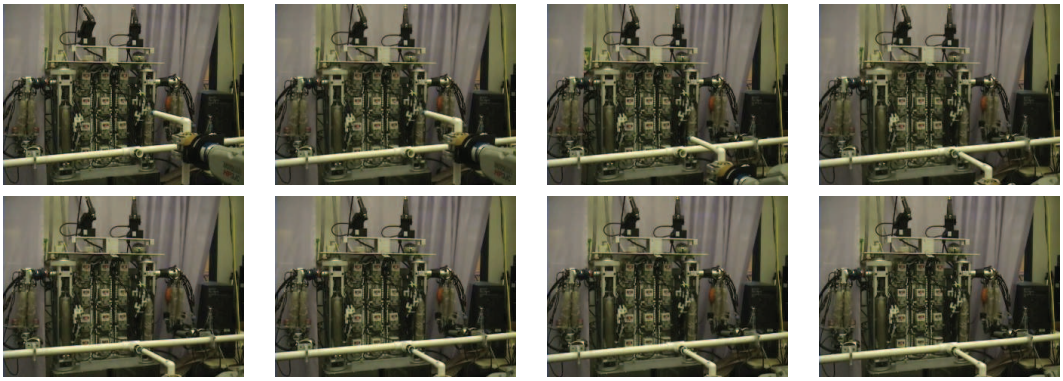

Table 8: Experiment 6: Two heterogeneous robots cooperate to perform a joint assembly using force sensing.

Nine trials were run for this experiment. Six were successful and two are reported in the next section. The first trial used "slow" force reference values, while the second used "fast" values, as defined in Experiment 3. Both trials yielded smooth force readings during the joint robot assembly. Data for these experiments is presented through sensor readings and residual error plots for both robots. Trials are labeled as Two_00X.

Results

Trial Two_007 reported a smooth insertion. The maximum torques experienced by the industrial robot were among the lowest across all trials, only 3 in-lbs and -4 in-lbs for the y- and z-moments respectively. This is due to the force reference parameters used that drove a slower insertion, which took 70 seconds. The sensed force curves were smooth and similar to those

experienced in experiment 3 and reflect the interaction with the compliant robot as shown in Figure 38.

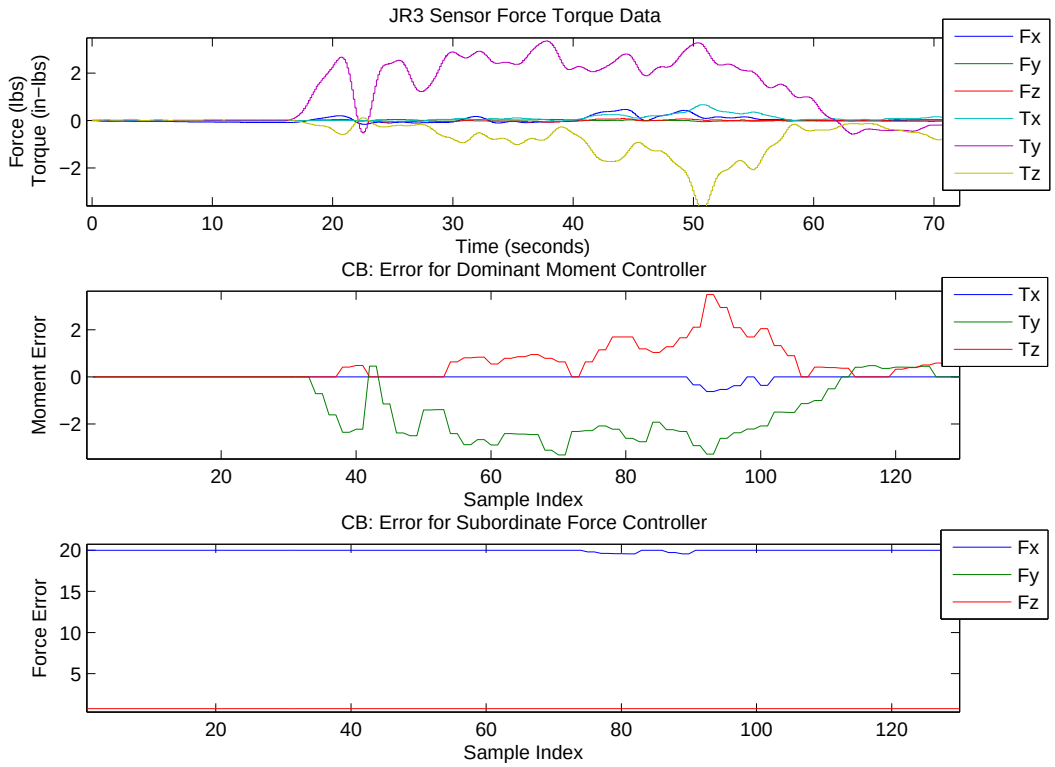

Figure 38: Trial Two_007A: HP3JC force data for a "slow" approach in cooperative assembly task with ISAC.

The moment residual errors for ISAC were smaller than all other trials in all experiments. There were two exceptions, one in experiments 3, and one in experiment 4. Registered residuals were: Tx=0.38, Ty=0.7, and Tz=0.48 in-lbs. The low errors registered for both robots yielded the slowest assembly for all trials in this experiment. Though seemingly counterintuitive, the controllers produced larger update steps when the residuals were also large. This relationship yields to kinds of dynamics: slow insertions with low moment errors and fast insertions with high moment errors. As expected for a low impact assembly, the force plot was minimally affected throughout the trial,

only experiencing a small slow-down in its forward motion between readings 15 and 20, as conveyed in Figure 39.

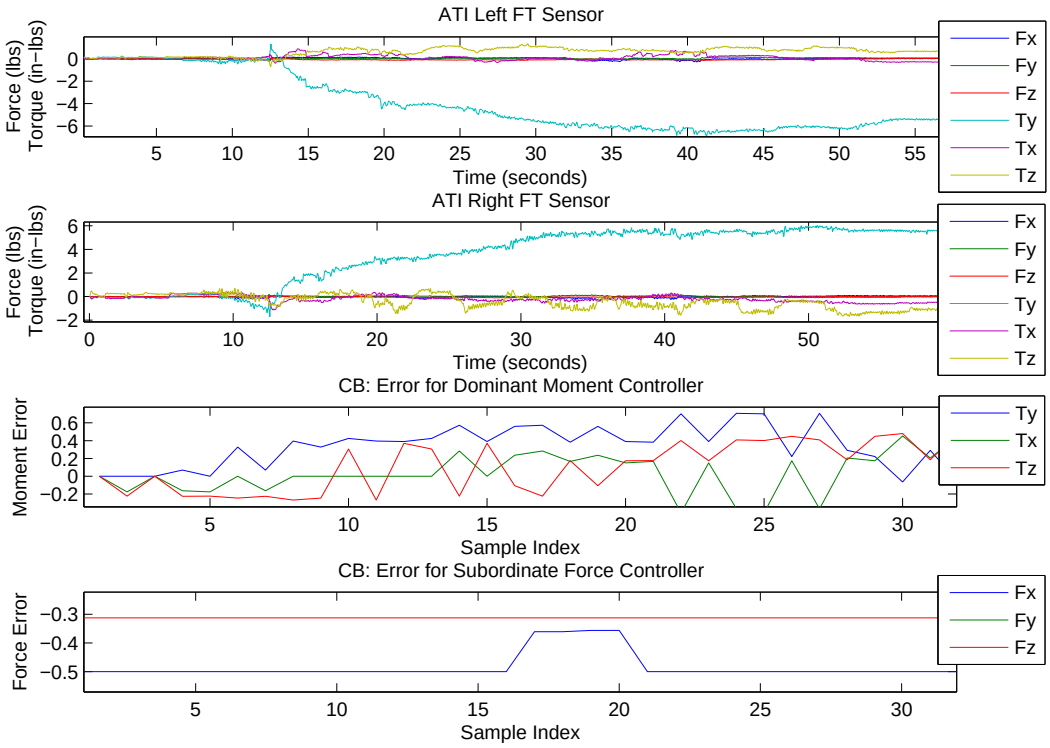

Figure 39: Trial Two_007B: ISAC coordinates its motions to assist in the joint assembly with the HP3JC robot.

Trial Two_001 produced the fastest assembly in all the experiments, requiring only 25 seconds. The speed of the assembly also induced the highest torques on both the HP3JC and ISAC. The plot for the former is shown in Figure 40. ISAC's force plots featured characteristics seen in prior experiments. High and fast rises in torques followed by sharp drops as seen in both the sensor plots and the moment residual plot, around time 110 seconds, show a brief jam experience for the assembly parts. The force residual error showed how both Fx and Fz were canceled suggesting a halt in forward motion as seen in Figure 41.

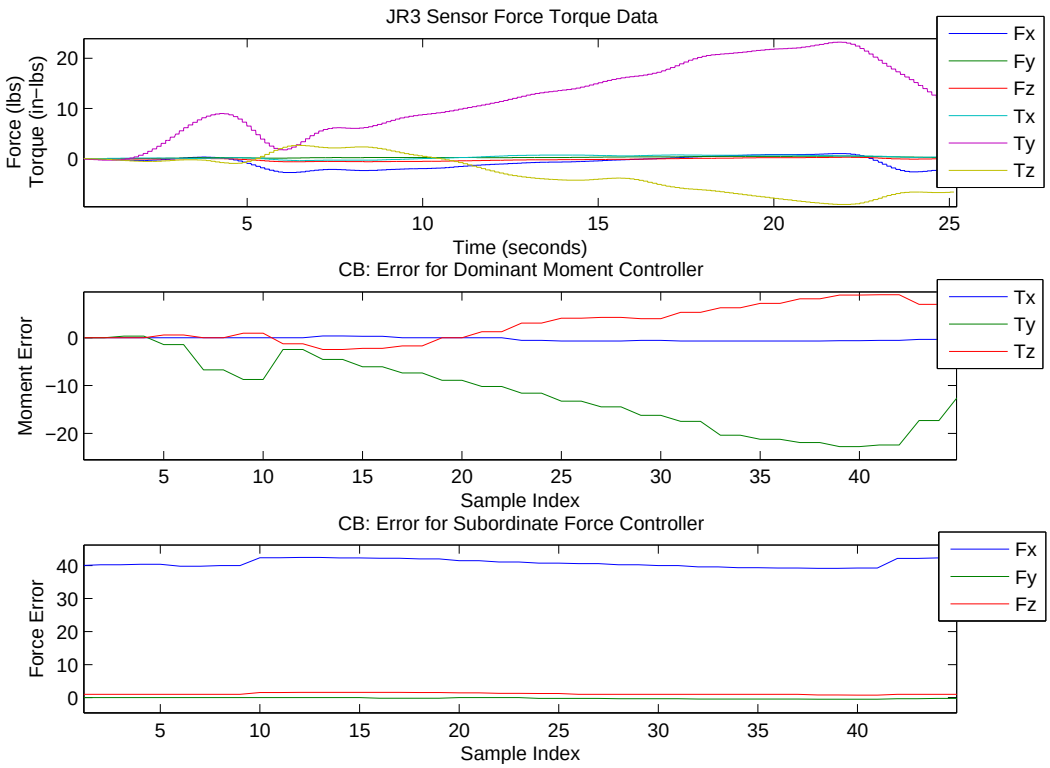

Figure 40: Trial Two_001A: HP3JC increases its speed in the cooperative task with ISAC.

Summary

Experiment 6 yielded the fastest averaged time-to-completion assembly of all experiments. This result is important and provides evidence that the assembly task was more efficient when the two heterogeneous robots coordinated their activity to mate the PVC pipes. Trial 9 was completed with the fastest time of all trials in all experiments. With regard to moments, experiment 6 has larger average moments for the HP3JC than previous experiments (except for when wedging is present as happened in a trial in experiment 4). Similarly, ISAC experienced higher average moments in experiment 6 compared to previous ones. Data suggests that as cooperation levels increase so do the exerted forces across the robots. Even so, the system is able to reach its goal state and achieve assembly in less time than previous experiments.

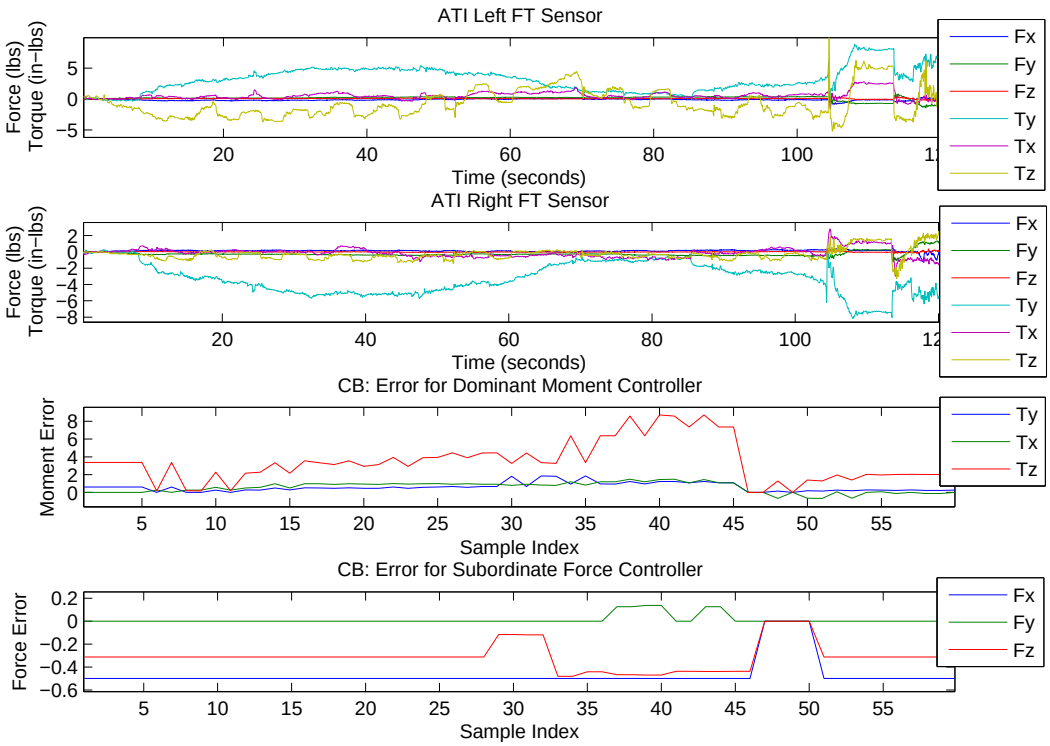

Figure 41: Trial Two_001B: ISAC experiences increased stress as the HP3JC drives truss more speedily.

Summary for the results across 6 successful and 3 failed trials is presented along with averaged values in Table 9.

Analysis

This section provides a comparison of the results. The analysis draws conclusions regarding the relative benefits and weaknesses of the control basis in executing joint assembly tasks through a team of heterogeneous robots and through different coordination schemes. In order to compare the performance of the system three metrics are used: (a) time-to-completion, (b) the sum of the maximum absolute value of the moment residuals in the x, y, and z directions (described as "moment error" throughout the remainder

Experiment 6: Both active												
		HP3JC						**ISAC**				
No	Res.	Fx,z	Time	Max Abs. Error				Fx,z	Max Abs. Error			
		(lbs)	(secs)	Tx	Ty	Tz	Σ	(lbs)	Tx	Ty	Tz	Σ
1	S	40,1	25	0.7	22.8	9.0	32.5	-40,-25	116	357.4	696	1169.4
2	S	20,.5	37	0.0	0.4	5.3	5.8	-40,-25	94.1	130.0	16.2	240.3
3	F	-	-	-	-	-	-	-	-	-	-	-
4	F	-	-	-	-	-	-	-	-	-	-	-
5	S	20,.5	60	0.0	11.0	6.0	17.0	-40,-25	77.9	171.3	204	453.2
6	F	-	-	-	-	-	-	-	-	-	-	-
7	S	20,.5	70	0.0	3.0	4.0	7.0	-40,-25	32.8	56.6	38.4	127.8
8	S	40,2	21	1.2	5.6	6.7	13.5	-40,-25	32.6	144.3	240.7	417.6
9	S	40,2	14	1.3	6.3	5.8	13.3	-40,-25	70.3	172.3	289.7	532.3
Avg			*38*	*0.5*	*8.2*	*6.1*	*14.8*		*70.6*	*172.0*	*247.5*	*490.1*

Table 9: Experiment 6: Summary of results.

of this section), and (c) the force reference parameters. The force reference parameters, more specifically ref_{Fx}, effectively set the task's execution speed and is useful to categorize data into groups belonging to fast insertions or slow insertions.

It is of interest to understand how the time-to-completion correlates to the associated moment error for a given force reference. Five different comparisons are carried out to evaluate the relationships between completion time and moment error. The comparisons are detailed below:

Comparison 1 Compares the averaged times-to-completion and averaged moment errors for the HP3JC robot in experiments 1, 3, 4, and 6. This initial analysis is a blind comparison as it uses values from trial that have different force reference values in the x-direction, ref_{Fx}.

Comparison 2 Carries out the same comparison as in 1, but only looks at average results for trials that used $ref_{Fx} = 40$

Comparison 3 Carries out the same comparison as in 1, but only looks at average results for trials that used $ref_{Fx} = 20$

Comparison 4 Compares the averaged times-to-completion and averaged moment error's for ISAC across experiments 4 and 6. Experiment 5 is not included since the timing for that experiment was inherently different than the other two.

Comparison 5 Same as comparison 2, but in this case the moment errors attained for experiments 4 and 6 for the ISAC robot are averaged with the error moments for the HP3JC robot.

The results of the comparisons are now presented and displayed through the use of bar charts.

Comparison 1

The averaged time-to-completion results from experiments 1, 3, 4, and 6 are plotted along with the corresponding averaged moment errors for the HP3JC robot with disregard for what force reference was used. The results are shown for the aforementioned four experiments in Figure 42.

The plot reveals that as the level of cooperation across robots increases so does the moment error. That is, with each subsequent experiment a greater maximum moment error is registered. As the amount of cooperation increases with subsequent experiments so do the stresses exerted mutually by the robots. The moment error is always minimized although a greater amount of error is accumulated with subsequent experiments. Similarly, data shows that with increased levels of cooperation the task time-to-completion is reduced. Experiment 1 registered one trial with exceptionally high moment

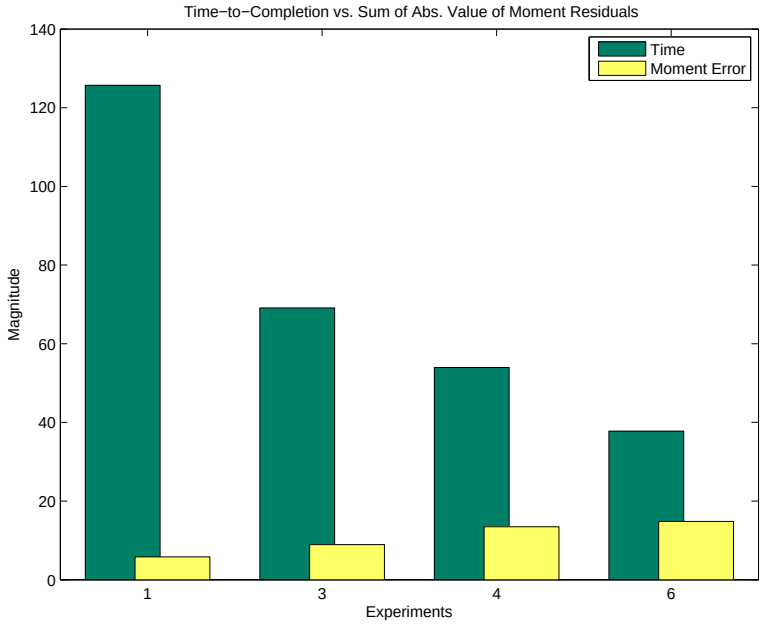

Figure 42: Comparison 1: Average values for all trials for the HP3JC.

errors and time-to-completion that was not considered here. Also, Experiment 4 had one trial that jammed and one that had wedging that had longer than average durations and higher moments that were not considered here.

Experiment 6 was 30% faster than the next fastest experiment and 70% faster than the slowest experiment. With respect to moments errors, experiment 6 had 110% higher moment errors than 4 and 257% higher moment residuals than experiment 1.

Comparison 2

The second comparison is a subset of the 1st and only looks at average values that come from trials that used $ref_{Fx} = 40$. This comparison narrows in on faster trials across experiments. The results are shown in Figure 43.

The trend mentioned in Comparison 1 is seen here as well. The moment error steadily increased across experiments. The averaged moment error in

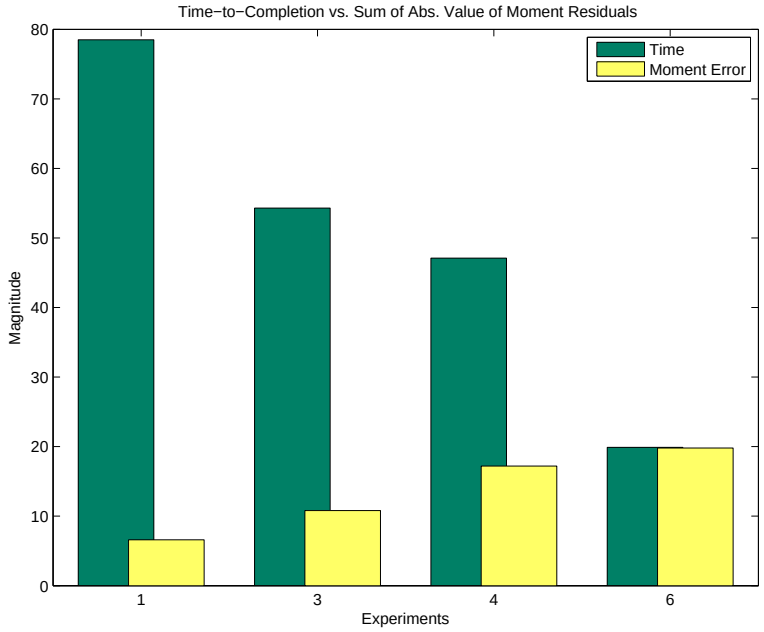

Figure 43: Comparison 2: Average values for all trials consisting of $ref_{Fx} = 40$ for HP3JC.

experiment 6 was 115% higher than experiment 4 and nearly three times greater than in experiment 1. With respect to time, this comparison also shows that with increased cooperation assembly tasks are executed faster. The duration for experiment 6 in this category was 58% faster than that in experiment 4; 63% than experiment 3, and 75% faster than the experiment 1. In this case, by classifying the data according to the same force reference parameter, a heightened degree of efficiency is discerned from the data. The speed increase recorded with subsequent experiments greatly reduces the task's time-to-completion, specially when both robots are active in the assembly.

Comparison 3

The third comparison looks at the slower force reference parameter, $ref_{Fx} = 20$. The results are presented in Figure 44.

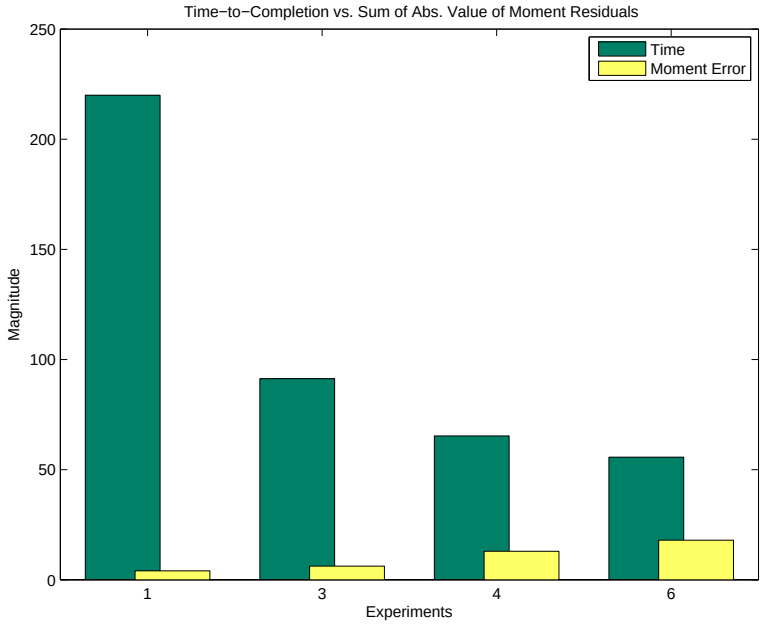

Figure 44: Comparison 3: Average values for all trials consisting of $ref_{Fx} = 20$ for HP3JC.

Even for the slower insertions, the trend found in the previous two comparisons still holds. In this comparison, experiment 6 was 15% faster than experiment 4, 39% faster than experiment 3, and 75% faster than experiment 1. One can see that the increase in speed across experiments is proportional to the numbers recorded in comparison 2. In terms of moment error, experiment 6 was 139% higher than experiment 4, 289% higher than experiment 3 and 442% higher than experiment 1.

Comparison 4

This comparison focuses on performance metrics for ISAC. Data comparisons for ISAC are more challenging due to a number of factors: (1) the number of experiments including ISAC were lower than those for the HP3JC robot and; hence limit the availability of comparable data. (2) Experiment 5 cannot be used since the HP3JC's clock was not used as opposed to experiments 4 and

6. (3) The force reference values for experiments 4 and 6 were different for ISAC. The former had zeroed force reference values for the counter-balance controller, and the latter had force reference values equal to Fx=-0.5, Fz=-0.31 lbs, to drive the insertion. The comparison is made, but is blind in that regard. The results are shown in Figure 45.

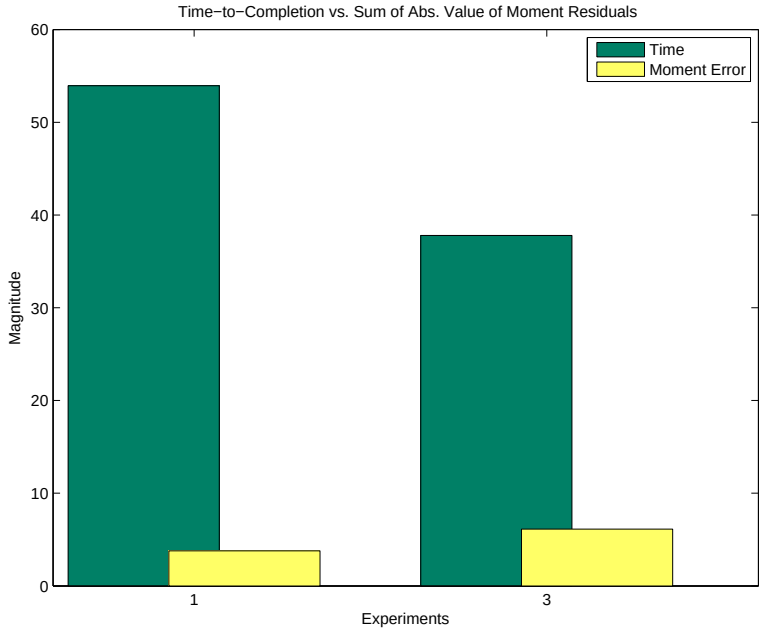

Figure 45: Comparison 4: Average values for all trials for ISAC.

Figure 45, nonetheless, provides the same patterns found in previous comparisons. The task time-to-completion decreases with increased cooperation and moment error increases. Experiment 6 has moment errors 162% higher than experiment 4.

Comparison 5

The last comparison looks at the HP3JC average values that use $ref_{Fx} = 40$ lbs, but averages the moment errors for the HP3JC and ISAC in experiments 4 and 6. This is an attempt to look at the combined contribution of both

robots when they use force sensing in the assembly. Results are presented in Figure 46.

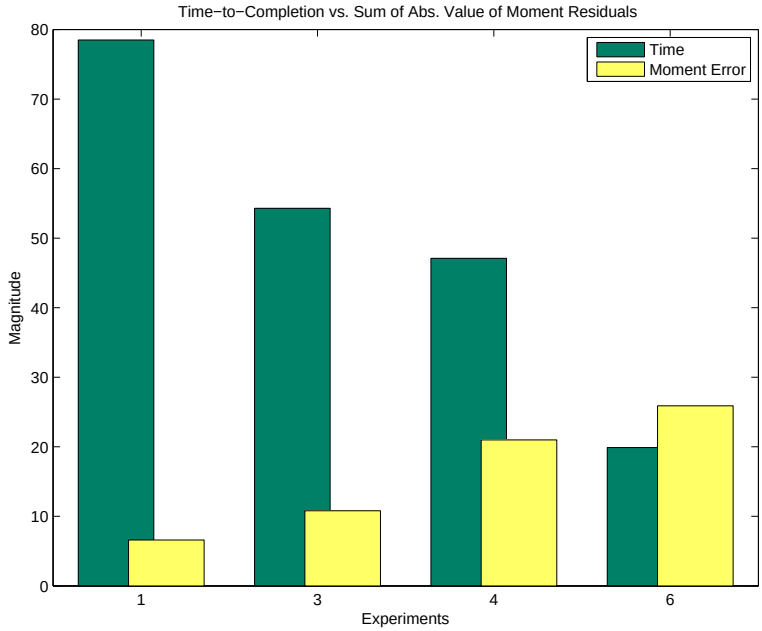

Figure 46: Comparison 5: Average values for all trials consisting of $ref_{Fx} = 40$ for HP3JC and ISAC.

The last comparison confirms the general trend seen throughout the previous comparisons. As before, experiment 4 presents a higher time-to-completion than experiment 3, but in general with each subsequent experiment faster assemblies are achieved albeit with higher stresses. The time benefits are the same as those in comparison 2 and the moment increases are an average of those found in comparison's 2 and 4.

Conclusion

The results suggest that larger moment errors increase the speed with which the controllers update the robot's configurations. Assembly tasks were executed successfully in all experiments, even for the last experiment where

higher moment errors were recorded. In both cases, the controllers were able to mitigate heightened stresses.

The increase in speed recorded by the active-active coordination scheme in experiment 6 cannot be overstated. Experiment 6 recorded 70% faster task completion times than the case where the industrial robot performed the assembly rigidly. More so, the fastest trial lasted 14 seconds as part of active-active coordination scheme. Having said this, it is worth noting that the duration of an insertion task is also a function of the location of the parts before insertion begins. Faster trials occurred when the tool-tip of the truss held by the HP3JC reached a perfect location to easily complete the insertion. Trials in which the tool-tip of the truss was close to the edge of the fixture, or even on the edge itself were delayed.

Moment errors also increased across experiments. These errors represent specific instances during a trial. Factors that contributed to the higher errors are on the one hand: (a) higher initial impacts produced as cooperation increased, (b) larger stresses exerted as one or two robots respond to stimuli in the environment, (c) the elasticity of the compliant robot allows muscles to give some before the sensors experience the strain. On the other hand, there is a trade-off between force and moment controller gains and velocity feedback gains. Lower force and moment gains provide the system with more stability but less responsiveness. Increasing the force and moment gains and lowering the velocity gains increase the amount stiction in the task. In this sense, the control primitives used as part of our basis suffer from a limited response and contribute to the accumulation of error in the tasks.

Data from Experiment 4 showed that in jam scenarios, the controllers successfully completed the insertion albeit in a longer period of time. On the other hand, the same data showed that the controllers did not resolve

wedging phenomena. Jamming scenarios did slow down the task but the controllers along with compliance enabled insertions to complete successfully. With respect to wedging, the controllers allowed the insertion to take place but did not correct the misalignments present in wedging. The controllers designed in this work were well suited for simple low-level assembly tasks but did not resolve wedging phenomena characterized by two contact points.

Finally, it would be of interest to compare the performance of: a) two industrial robots, and b) different heterogeneous robots (as compared to the ones used in this work) performing the same assembly tasks in dynamic environments. This would provide more insight as to which robots are better suited to work in a team scenario and yet provided comparative advantages for a specific task. For our case, the industrial robot was better at driving male truss insertions and doing so with high accuracy. The compliant robot on the other hand was useful at rendering tasks that were at critical points into successful tasks by conforming to the path and alignment of the truss held by the industrial robot in difficult situations.

CHAPTER VI

CONCLUSION

As part of new frontiers in space exploration, innovative robotic control approaches are sought to enable teams of heterogeneous robots to perform autonomous modular truss assembly operations during the window of communication latency common to space operations. Robot teams will operate under variable autonomy modes supervised by human operators to perform material transport, assembly, and maintenance of human life support systems on the moon and martian surfaces.

NASA desires a control architecture that enables the execution of multiple tasks across different robot configurations. The control basis approach is a good candidate as the approach effectively optimizes multiple goals to produce robust behaviors with ease and flexibility. The ability to decompose a complex control problem into sequences and combinations of controllers simplifies the solution implementation very much like distributed modular programming eases code implementation. Challenges concerning this approach relate to the way in which primitive control laws are defined and joined, in [Platt et al., 2006] an efficient approach was presented to autonomously learn effective control policy formations from experience.

This work focused in advancing the capabilities of autonomous heterogeneous robots in the area of low-level automated assembly. It presented a control strategy that enabled independent robots in a loosely structured environments to carry out insertion tasks. The control basis approach is an effective approach to modularize and sequence the assembly process across two heterogeneous robots using force sensing. The designed guarded move controller and compliant insertion controller were successfully implemented

on the industrial HP3JC robot to achieve single robot autonomous assembly. The counter-balance controller and the virtual contact controllers were successfully implemented on the pneumatically driven humanoid robot, ISAC. Position, force, and moment goals were achieved as a series of hierarchical controllers across the robots. This composition enabled the deployment of active-static and active-active coordination schemes for both robots. The use of a compliant robot as part of the heterogeneous team increased the likelihood of success in assembly tasks by accommodating its configuration in problematic situations. The use of a virtual contact helped ease control challenges related the actuation of artificial arms. Finally, the use of two active robots as a coordination scheme yielded faster assemblies and makes a case for use in space construction for future moon and Mars missions.

The contributions made by this work are the following:

1. The implementation of basis controllers that allow the autonomous joining of two mating parts by two independent, sensory-guided heterogeneous robots with articulated arms.

2. The use of independent control bases by two robots, in which controllers reduce contact forces by displacing parts in response to local force, moment, and position feedback.

3. The coordination of a pneumatically actuated and highly compliant humanoid robot with a rigid industrial manipulator.

4. This is the first project of heterogeneous robot teams that jointly perform assembly. At this time, there is no team of autonomous robots that coordinate their work to perform an assembly task via mutual force-torque feedback guidance.

5. The implementation of reactive behaviors on a decidedly non-reactive, point-to-point, pre-programmable, industrial robot arm.

6. The ability to swap leader and subordinate roles in coordination schemes. Active-active and active-static coordination schemes are implemented and possible through inter-robot communication.

7. Experimental results that demonstrated faster completion times when members of the assembly team assume active roles in the task.

This work has shown that a small set of basis controllers consisting of moment, force, and position primitives is able to implement simple low-level assembly tasks through force sensing. This work continues a line of research performed on the control basis approach, which now has been shown to effectively generate: grasping, statically dexterous manipulation, bipedal gaits, and joint assembly tasks. Through the selection of appropriate potential surfaces for primitive controllers, a vast array of tasks have been achieved in multiple robotic testbeds [Huber, 2000, Platt, 2006].

Directions for Future Work

A number of challenges were encountered through the design, implementation, and testing of this work. There a number of important aspects to consider to consolidate the control basis approach for assembly tasks as a viable approach in space construction.

The control primitives designed in this work deal with simple assembly insertions. No consideration was given to insertions with complex geometrical configurations. Further research is required to understand if other primitive or compound controllers are necessary along with different control policies

to perform assembly of complex parts. Even for simple assembly tasks, two-point contact scenarios sometimes yielded wedging that the controllers were unable to discern. This inability prevented the controllers from properly aligning the mating parts. The use of more informative visual data may assist in these cases. It may be of interest to use a visual system that provides pose information. The position controller could include pose information and help align the orientation of the fixtures before and during an insertion.

Additionally, throughout testing it was evident that different force parameters affected the speed and efficiency with which an assembly task was completed. The author believes that an adaptive estimation of these parameters based on the current state of the system may increase the flexibility and robustness of the system. More so, perhaps a three-tier controller that includes position and pose goals may improve performance.

Another issue that has been implemented in other research in autonomous assembly, but not addressed in this dissertation is that of error prevention. A mechanism to detect and recover from errors is crucial in order to increase the system's fault tolerance, particularly if the latter functions as part of a larger multi-player task.

Finally, while this research demonstrated complete insertions under different coordination schemes, no evaluation was done on how performance is affected when coordination schemes are dynamically changed during a task. Dynamically switching coordination schemes in a task could be beneficial if that switch improved the performance. Similarly, no evaluation was done on the relative advantages of having a certain type of heterogeneous robots. A more thorough understanding of how the specialized nature of a particular robot might benefit a task could further the understanding of what robots

to select as part of a team of heterogeneous robots for a given task or sets of tasks.

APPENDIX A

TABLE OF SYMBOLS

This appendix serves as a reference guide to the variety of symbols used in this thesis referring to control law's, controllers, and gradient nomenclature.

The control basis sensor and effector transforms are defined in Table 10.

Transforms	Name
$s_i(\Gamma_k)$	Sensor transform
$e_k(\Gamma_k)$	Effector transform

Table 10: Transforms introduced in Chapter III.

Gradient descent and null space projections are defined in Table 11.

Surface Error Gradient	Name
$\nabla_{x_i}\phi_i$	Error gradient for domain x
$\mathcal{N}(\nabla_y\phi_D^T)\nabla_y\phi_S$	Null space operator

Table 11: Surface error gradients introduced in Chapter III.

Residual Error Parameters are defined in Table 12.

A summary of the controllers used in this dissertation are summarized in Table 13.

Error Functions	Name
ϵ	Wrench residual error function
ϵ_f	Force residual error function
ϵ_m	Moment residual error function

Table 12: Error functions introduced in Chapter IV.

Primitive Controllers	Name
$\phi_p \mid_{e_p(\gamma_{joint})}^{s_p(\gamma_{visual\_sys})} (x_{ref})$	Position controller
$\phi_{fr} \mid_{e_{fr}(\gamma_{torque})}^{s_{fr}(\gamma_{force})} (f_{ref})$	Force residual controller
$\phi_{mr} \mid_{e_{mr}(\gamma_{torque})}^{s_{mr}(\gamma_{force})} (m_{ref})$	Moment residual controller

Table 13: Primitive Controllers.

Compound Controllers for Industrial Manipulator	Name
$\pi_{GM} \mid^{s_{GMC}(\gamma_{joint},\gamma_{torque})}_{e_{GMC}(\gamma_{cart},\gamma_{moment})} =$ $\phi_{mr} \mid^{s_{mr}(\gamma_{moment})}_{e_{mr}(\gamma_{torque})} \lhd \phi_p \mid^{s_p(\gamma_{visual\_sys})}_{e_p(\gamma_{joint})} (x_{ref})$	Guarded Move Controller
$\pi_{CI} \mid^{s_{CI}(\gamma_{force})}_{e_{CI}(\gamma_{torque})} =$ $\phi_{fr} \mid^{s_{fr}(\gamma_{force})}_{e_{fr}(\gamma_{torque})} (f_{ref}) \lhd \phi_{mr} \mid^{s_{mr}(\gamma_{force})}_{e_{mr}(\gamma_{torque})}$	Compliant Insertion Controller
$\pi_{CB} \mid^{s_{CB}(\gamma_{force})}_{e_{CB}(\gamma_{torque})} =$ $\phi_{fr} \mid^{s_{fr}(\gamma_{force})}_{e_{fr}(\gamma_{torque})} \lhd \phi_{mr} \mid^{s_{mr}(\gamma_{force})}_{e_{mr}(\gamma_{torque})}$	Counter Balance Controller

Table 14: Composite controllers used in Motoman's industrial manipulator HP3JC.

Virtual Controllers for dual-arm humanoid	Name
$\pi_{VGM} \mid^{s_{GM}(\gamma_{vc\_visual\_sys},\gamma_{vc\_moment})}_{e_{GM}(\gamma_{vc\_joint},\gamma_{vc\_torque})} =$ $\phi_{mr} \mid^{s_{mr}(\gamma_{vc\_moment})}_{e_{mr}(\gamma_{vc\_torque})} \lhd \phi_p \mid^{s_p(\gamma_{vc\_visual\_sys})}_{e_p(\gamma_{vc\_joint})} (x_{ref})$	Virt. Guarded Move Ctrller.
$\pi_{VCI} \mid^{s_{CI}(\gamma_{vc\_force})}_{e_{CI}(\gamma_{vc\_torque})} =$ $\phi_{fr} \mid^{s_{fr}(\gamma_{vc\_force})}_{e_{fr}(\gamma_{vc\_torque})} (f_{ref}) \lhd \phi_{mr} \mid^{s_{mr}(\gamma_{vc\_force})}_{e_{mr}(\gamma_{vc\_torque})}$	Virt. Compliant Insertion Ctrller.
$\pi_{VCB} \mid^{s_{CB}(\gamma_{vc\_force})}_{e_{CB}(\gamma_{vc\_torque})} =$ $\phi_{fr} \mid^{s_{fr}(\gamma_{vc\_force})}_{e_{fr}(\gamma_{vc\_torque})} \lhd \phi_{mr} \mid^{s_{mr}(\gamma_{vc\_force})}_{e_{mr}(\gamma_{vc\_torque})}$	Virt. Counter Balancing Ctrller.

Table 15: Virtual controllers used in the dual-arm humanoid ISAC.

APPENDIX B

MOORE-PENROSE PSEUDO INVERSE

Multiple goals from concurrent controllers can be optimized by projecting the output goal of a subordinate controller unto the null-space of the locally-linear gradient dominant controller [Platt, 2006]. In the control basis approach, the operation is referred to as having the subordinate controller be "subject-to" the dominant controller.

The derivation presented here was originally shown in [Platt, 2006], and is presented here for convenience. An illustrative example is appended at the end of this section. Consider two primitive controllers whose outputs are desired velocities in joint angle configuration space, $\mathbf{q}$. The first controller outputs velocity $\dot{\mathbf{q}}_\mathbf{d}$, while the second one outputs velocity $\dot{\mathbf{q}}_\mathbf{s}$. A way to integrate the result from both such that their goals can be optimized is by ensuring that the controller results are orthogonal to each other. This could be understood as having the velocity of the secondary controller run tangent to the goal function of the primary controller. If the goal state of the dominant controller is defined as: $\phi_d(\mathbf{q}_\mathbf{ref}) = \mathbf{q}$ and the gradient of the output of the controller is defined as: $\nabla\phi_d(q_{ref}) = \dot{q}$, then one could say that a velocity $\dot{\mathbf{q}}'$ is orthogonal to the gradient output of the controller $\nabla_\mathbf{x}\phi_d$ if their dot product is zero:

$$\nabla_\mathbf{x}\phi_d^T.\dot{\mathbf{q}}' = 0$$

Now consider, if the output of the subordinate controller is: $\nabla_x\phi_2 = \dot{q}_s$ and, a second and different value for a velocity $\dot{\mathbf{q}}'_\mathbf{s}$ and produces a dot product of zero with the dominant controller: $\nabla_\mathbf{x}\phi_d^T\dot{\mathbf{q}}'_\mathbf{s} = 0$. Then we would like to find

the velocity $\dot{\mathbf{q}}'_{\mathbf{s}}$ that minimizes:

$$f(\dot{\mathbf{q}}'_{\mathbf{s}}) = \frac{1}{2}(\dot{\mathbf{q}}_{\mathbf{s}} - \dot{\mathbf{q}}'_{\mathbf{s}})^T(\dot{\mathbf{q}}_{\mathbf{s}} - \dot{\mathbf{q}}'_{\mathbf{s}})$$

The velocity $\dot{\mathbf{q}}'_{\mathbf{s}}$ can be found via the Lagrange multiplier method. The gradient of the function to be minimized is set equal to the product of a constant and the gradient of the constraint:

$$\begin{aligned} \frac{\partial f(\dot{\mathbf{q}}'_s)}{\partial \dot{\mathbf{q}}'_s} &= \lambda \frac{\partial(\nabla_{\mathbf{x}}\phi_d^T \dot{\mathbf{q}}'_s)}{\partial \dot{\mathbf{q}}'_s} \\ -(\dot{\mathbf{q}}_s - \dot{\mathbf{q}}'_s) &= \lambda \nabla_{\mathbf{x}}\phi_d \\ \nabla_{\mathbf{x}}\phi_d^T(\dot{\mathbf{q}}'_s - \dot{\mathbf{q}}_s) &= \lambda \nabla_{\mathbf{x}}\phi_d^T \nabla_{\mathbf{x}}\phi_d \end{aligned} \tag{27}$$

Recalling that$\nabla_{\mathbf{x}}\phi_d^T \dot{\mathbf{q}}'_{\mathbf{s}} = 0$, the equation reduces to:

$$-\nabla_{\mathbf{x}}\phi_d^T \dot{\mathbf{q}}_s = \lambda \nabla_{\mathbf{x}}\phi_d^T \nabla_{\mathbf{x}}\phi_d \tag{28}$$

We can solve for λ:

$$\lambda = -(\nabla_{\mathbf{x}}\phi_d^T \nabla_{\mathbf{x}}\phi_d)^{-1} \nabla_{\mathbf{x}}\phi_d^T \dot{\mathbf{q}}_s \tag{29}$$

Substituting back into equation 27 yields:

$$-(\dot{\mathbf{q}}_s - \dot{\mathbf{q}}'_s) = -\nabla_{\mathbf{x}}\phi_d (\nabla_{\mathbf{x}}\phi_d^T \nabla_{\mathbf{x}}\phi_1)^{-1} \nabla_{\mathbf{x}}\phi_d^T \dot{\mathbf{q}}_s \tag{30}$$

Solving for $\dot{\mathbf{q}}'_s$ produces:

$$\begin{aligned} \dot{\mathbf{q}}'_s &= \dot{\mathbf{q}}_s - \nabla_{\mathbf{x}}\phi_d (\nabla_{\mathbf{x}}\phi_d^T \nabla_{\mathbf{x}}\phi_d)^{-1} \nabla_{\mathbf{x}}\phi_d^T \dot{\mathbf{q}}_s \\ &= (I - \nabla_{\mathbf{x}}\phi_1 (\nabla_{\mathbf{x}}\phi_d^T \nabla_{\mathbf{x}}\phi_d)^{-1} \nabla_{\mathbf{x}}\phi_d^T) \dot{\mathbf{q}}_s \end{aligned} \tag{31}$$

Observing that $\nabla_{\mathbf{x}}\phi_d(\nabla_{\mathbf{x}}\phi_d^T\nabla_{\mathbf{x}}\phi_d)^{-1}$, is the *pseudo-inverse* of $\nabla_{\mathbf{x}}\phi_d^T$, yields:

$$\begin{aligned}\dot{\mathbf{q}}_s' &= (I - (\nabla_{\mathbf{x}}\phi_d^T)^{\#}\nabla_{\mathbf{x}}\phi_d^T)\dot{\mathbf{q}}_s \\ &= \mathcal{N}(\nabla_{\mathbf{x}}\phi_d^T)\dot{\mathbf{q}}_s \end{aligned} \tag{32}$$

where

$$\mathcal{N}(\nabla_{\mathbf{x}}\phi_d^T) = I - \nabla_{\mathbf{x}}\phi_d(\nabla_{\mathbf{x}}\phi_d^T\nabla_{\mathbf{x}}\phi_d)^{-1}\nabla_{\mathbf{x}}\phi_d^T$$

And, $\mathcal{N}(\nabla_{\mathbf{x}}\phi_d^T)$ is the null space projection matrix. It guarantees that the result is orthogonal to the primary controller goal function, $\nabla_{\mathbf{x}}\phi_d$. Equation 32 projects the subordinate controller velocity $\dot{\mathbf{q}}_s$, unto the null space of the gradient of the dominant controller, $\nabla_{\mathbf{x}}\phi_d^T$.

Illustration

By looking at the null space matrix operator one can see that it is composed of two operations. There is a vector outer product which produces a matrix. There is also an inverted inner product which effectively serves as a normalization factor. We can prove that this matrix operator projects unto the null space.

Consider a 2D case where the vector $g(\vec{x,y})$ is set equal to the control basis output ϕ_d:

$$\vec{g}(x,y) = \nabla_{\mathbf{x}}\phi_d$$

The vector representation of $\vec{g}(x,y)$ is visualized as the column vector:

$$\vec{g}(x,y) = \begin{bmatrix} g_x \\ \\ g_y \end{bmatrix} \tag{33}$$

In substituting 33 into the null space representation of 32 the following matrix

representation is obtained:

$$\mathcal{N}(\nabla_{\mathbf{x}}\phi_d^T) = I - \frac{1}{g_x^2 + g_y^2}\begin{bmatrix} g_x^2 & g_y g_x \\ g_y g_x & g_y^2 \end{bmatrix} \tag{34}$$

The null space of a vector is defined to be any vector x such that the product $Ax = 0$. A vector of the form $A = [l_x l_y]'$ is sought such that $A[g_x g_y] = 0$. It's simple to see that if we set:

$$\begin{bmatrix} l_x & = & g_y \\ l_y & = & -g_x \end{bmatrix} \tag{35}$$

And substitute 35 into 32 the result = 0, *i.e.* $g_y g_x^2 - g_y g_x^2$.

APPENDIX C

HISTORY OF SPACE ROBOTICS

In this section, a wide overview of space robotics from its inception is included. It contains a description of early machines produced by NASA and other space agencies consisting of probes, orbiters, telescopes, and others. The summary is based on Angelo's work [Angelo, 2007].

NASA began it's exploratory space efforts with the Pioneer space probes. All in all there were 13 probes launched beginning in 1958 and ending in 1978. These were space robots designed to first reach the moon and later to reach other planets in the solar system. The Pioneer probes served primarily as instrumentation devices that sent researchers telemetry data on interplanetary phenomena like cosmic radiation, magnetic and electric fields, amongst other data. The Pioneer 4 probe was the first NASA robot to achieve an earth-moon trajectory. Russian lunar probes known as *Luna's*, always achieved their goals before those of their American counterparts, where Luna 2 was the first to space craft to land on the moon, and Luna 3 was the first to take pictures of the moon. Pioneer 5 visited the interplanetary space between the Earth and Venus; and Pioneer 10 & 11 twin robots, were the first to to visit Jupiter, Saturn, and the first to leave the solar system, Pioneer 13 was a multi-probe craft that entered the Venusian atmosphere and had one probe land on Venus' surface.

With the creation of the Jet Propulsion Laboratory, a second generation of space probes was born and known as the *Ranger probes*. The Ranger probes were designed to prepare the way for the Apollo project by testing spacecraft navigational performance and photographing the surface of the moon. These probes were launched in the first half of the 1960's. It wasn't until probes 7-9

that completely successful missions were achieved and returned thousands of lunar surface images that allowed for the advancement of scientific knowledge of the moon.

Next, NASA developed the *Surveyor landers* and launched them between 1966 and 1968. These robots were versatile spacecrafts used to study soft-landing techniques as a precursor to the Apollo project. Surveyor 1 landed on the moon in 1966 and helped establish that lunar soil would be adequate to support the Apollo crafts. The third probe was able to dig a trench using a robotic manipulator fixed with a shovel and discover that the load-bearing strength of the lunar soil increased with depth. Surveyors 5-7 provided amongst other things information on the chemical composition of the lunar soil and on-surface navigation data.

It is worth noting that in early 1970's the Soviets launched a number of spacecraft with mobile rovers, namely the Lunokhod 1 and 2. Both of these rovers were deployed on the lunar surface. The first rover covered 6.5 miles of lunar surface providing soil analysis from a number of locations 20,000 images. The second version was more impressive. The rover was radio-controlled from Earth, it traveling around 23 miles and also provided soil analysis and numerous images.

JPL conducted a parallel mission denoted the Mariner Project. This effort studied the inner planets of the Solar System. Mariner 2, was launched in 1962 and was the first robot spacecraft to fly by another planet. Mariner 2, studied Venus and discovered data related to surface temperatures and pressures, atmospheric characteristics, rotation nuances, cosmic dust density, amongst others. Mariner 4, was the next successful launch, in 1964, and it's target was to study planet Mars. Mariner 4, traveled the interplanetary space for 8 months before arriving to Mars to then provide the first close-up

pictures of another planet up to that point. Mariner 9, was launched in 1971 and orbited Mars becoming the first man-made robot to orbit another planet. Mariner 10, then became the first spacecraft to use a gravity-assist boost to send it from one planet to another. This orbiter was able to fly by Venus to later, in 1974, encounter Mercury. To this date, this is the only spacecraft that has visited the innermost planet in our solar system.

The next mission, in 1975, would entail an intense search for life on Mars, and would be known as the Viking mission. The latter consisted of two orbiters and two lander spacecrafts.

After Viking, would come the spacecrafts that would visit the most giant planets. In 1977 the twin crafts Voyager 1 and 2 were launched, taking advantage of the very sporadic alignment of Jupiter, Saturn, Uranus, and Neptune. The former visited the first 2, while the latter flew by all of them.

In the next two decades to come, important advances in sensor, computer, and aerospace engineering would allow a new generation of sophisticated aircraft that would significantly advance the scientific investigation of outer space. In 1995, The Galileo space mission began when the aircraft was deployed in low Earth orbit by the *Atlantis* space shuttle. The robot's goal was to study Jupiter and it's surrounding moons. To do so, the mission would employ gravity-assisted flybys through Venus, Earth, and Mars. Galileo had a detachable atmospheric probe that would gather data of the Jovian atmosphere. In a two year lapse, the spacecraft would perform 10 flyby's of Jupiter's major moons. In late 1997, focused examination of Jupiter's moons Europa and Io would proceed. In 2000, extended missions to Ganymede and Callisto were carried out, in this case with a special collaboration with the Cassini capsule.

The Cassini/Huygens mission consisted of the former as an orbiter and

the latter as a probe. The Huygen's probe would be attached to the Cassini capsule and would remain dormant until it approached its final destination. This was a joint effort between the NASA space agency and the European Space Agency to study the largest of Saturn's moons, Titan. Titan is the only moon in the Solar system with a dense atmosphere that precludes Earth observers from seeing its surface. So, it was Cassinni/Huygen's mission to enter this natural satellite and provide data of it's atmospheric composition, distribution of trace gases and aerosols, winds and temperatures, and the composition of the surface. A noteworthy fact of the Cassini orbiter is it's on-board intelligent machinery. Given that Saturn is 1.43 billion km away from Earth, the one-way speed-of-light time from Saturn to Earth is of 84 minutes. For this reason, real-time control of the orbiter is not a possibility and the orbiter must function properly while unsupervised.

We conclude this overview by presenting NASA's launch four space labs that would investigate the full portions of the electromagnetic spectrum. This project was known as the Great Observatories Program. The latter eventually deployed four telescopes. The *Hubble Telescope* was the first to be launched in 1990 and was designed to observe light in the visible, ultra-violet, and near-infrared spectrum. The second telescope was the *Gamma Ray Observatory*. It was launched in 1991 with the purpose to observe high-energy gamma rays from violent process in the universe. The third facility was the *Advance X-ray Astrophysics Facility* and put into Earth's orbit in 1999. this observatory examined X-ray emissions from suppernovas and the accretion disks around suspected black holes. The fourth craft in this group was the *Space Infrared Telescope Facility*, it was launched in 2003 and captured infra-red data from the formation of galaxies, stars, and planets.

The use of advanced robotic manipulators, cranes, and agents is further covered in II.

APPENDIX D

ARTIFICIAL MUSCLES

Artificial muscles, especially McKibben muscles used in both industry and biomedical engineering have overwhelming benefits as compared to other actuators like servo motors[Yaman, 2000].

Historically, manipulators of all varieties have been characterized by a high degree of stiffness which improves the positioning accuracy, but makes the arm difficult to control when it is in contact with a dynamic surface. Maintaining contact with a dynamic surface requires compliance. Robot designs usually trade one for the other: accurate position control or accurate force control. A stiff manipulator can deliver a strong force to a surface with relatively small joint displacements. These systems can become unstable when interacting with rigid surfaces as a manipulator would insist on reaching a certain location yet the physical constraints of the environment would preclude that task [Williamson, 1995].

To mimic the low stiffness of human appendages, some researchers have developed light, compliant actuators that possess high force-to-weight ratios and low friction. These actuators mitigate the effects of inertia and backlash and facilitate force control since they are able to deform on contact. The following section presents a historical account of compliant muscles, which are used in this thesis.

General Characteristics

Since the 1930's different kinds of artificial muscle actuators have been built. In [Daerden and Lefeber, 2002], Daerden ascribes a number of characteristics

to artificial muscles consisting of: (a) pneumatic or hydraulic actuators, (b) overpressure or underpressure performance, (c) braided or embedded membranes, and (d) stretching or rearranging membranes. A description of the two most important types of pneumatic muscles: braided and pleated follows.

Braided pneumatic muscles consist of an air-tight elastic inner tube covered by a braided sleeving (weave, braid, or sleeve). The braid fibers run helically about the muscle's long axis. When pressurized, the tube expands radially, pressing against the sleeve. The force produced by the expansion of the membrane is counteracted by the tensional force in the braiding. Braided muscles, then, only operate in overpressure where the force generated at the interface between the inner tube and the braid is translated into force on the load. The rubbing of the inner membrane against the weave is a source of friction, that also exhibits stiction. So, when the muscle is inflated, the rubbing of both surfaces creates a sticking effect. Commonly, when the muscle is inflated and deflated, the sticking effect precludes the system from returning to its original state, an effect known as hysteresis.

Pleated pneumatic muscles were developed within the last decade by Daerden and Lefeber [Daerden and Lefeber, 2002] and shown in Figure 47. Pleated membranes are said to be of the "rearranging type". The axial pleats of the muscle, unfold when the muscle is pressurized, leading to a radial expansion but a shortening in the axial direction. Another significant characteristic is the negligible effect of membrane stresses perpendicular to the axis. As a result, a muscle requires small amounts of energy to expand and the absence of the friction seen in the sleeved muscles minimizes hysteresis.

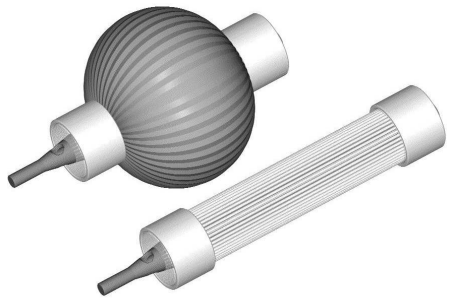

Figure 47: Pleated Muscle, fully stretched and inflated [Daerden and Lefeber, 2002].

Pneumatic Actuators

The current section provides a historical overview of pneumatic actuators, beginning with their motivation and continuing with their evolvement over time. A detailed description of the behavior and characteristics is presented along with an evaluation of its disadvantages. The section provides insight into the advantages and challenges posed in their use for manipulation tasks in robots.

History of Pneumatic Actuators

J. L. McKibben developed the pneumatic actuator for use in orthotic rehabilitation [Klute et al., 1999]. Friendly actuators were desired for orthopedic patients. The rigidity of electric and hydraulic drives would not comply with human motion. On the other hand, the pneumatic actuator elicited the desired compliance and did not compromise actuating power. These pneumatic muscles were used to actuate orthotics in the 1950s for polio patients [Nickel et al., 1963], see Figure 48. Since then different types of pneumatic

actuators have been developed and have been used in factory floor automation [Daerden and Lefeber, 2002], biomedical engineering [Yaman, 2000], and humanoid robotics [Rojas, 2004].

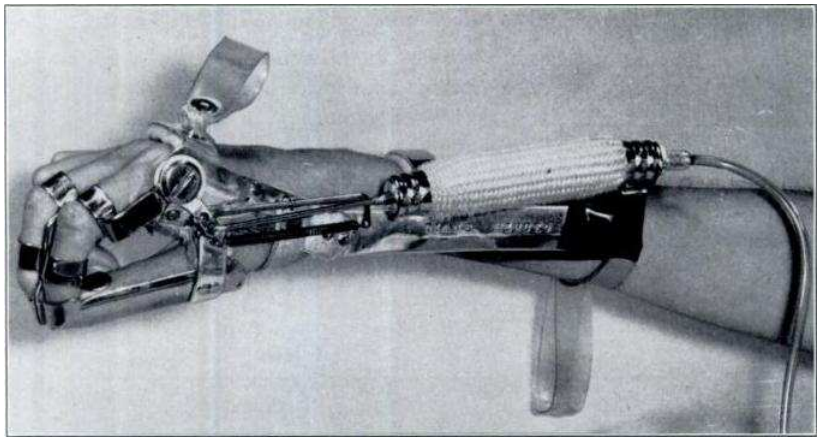

Figure 48: Pneumatic actuator for use in patient [Nickel et al., 1963]

In the 1960's McKibben muscles for orthotics were replaced by smaller and more accurate electric motors. Interest did not resurface until two decades later when Bridgestone Corporation redesigned them and distributed them as actuators for industrial painting robots [Chou and Hannaford, 1996]. Inspired by the previous use of PAMs in orthotics, Kawamura combined two Bridgestone arms to make the first humanoid robot expressly designed for interaction with people [Kawamura et al., 1995]. Other groups work with this technology and continue to develop more robust models and ways to control them [Ozkan et al., 2000, Yaman, 2000, Schreder, 2003]. The Shadow Robot Company developed its own version of a pneumatic artificial muscle [Shadow Company, 2007] and shown in Figure 49. Their model exhibits an improved inner membrane that reduces stiction and hysteresis allowing the muscle to operate more smoothly than previous McKibben models. Festo is

Figure 49: Shadow Muscle [Schreder, 2003]

another company that produces pneumatic muscles for industrial use. Festo produced muscles are comprised of intermingled thread and inner membrane to minimize coulomb friction [Festo, 2007]. Also, researchers at the Massachusetts Institute of Technology (MIT) created series elastic actuators that consist of traditional electric motors with a compliant load sensor (spring) positioned between the gear's train output and the load. The MIT design, reduces motor inertia and friction at the output while increasing the fidelity of force control and force control stability over typical electric drives [Yobotics, 2007].

Physical Description

Klute and Hannaford [Klute and Hannaford, 1998] describe pneumatic artificial muscles as actuators made from an inflatable, tubular inner bladder sheathed with a nylon double helix weave that shortens lengthwise when expanded radially, see Figure 50. The tubular inner bladder and the nylon

weave are clamped with fittings at both ends, one of which contains an air intake as shown in Figure 50.

Figure 50: Braided pneumatic muscle [Shadow Company, 2007]

Physical Behavior

Daerden [Daerden and Lefeber, 2002] provides an excellent description of PAMs; his research is referred to throughout this chapter. As the inner membrane is inflated, the actuator contracts along the axis of the tube. Similarly, as it deflates it expands along the same axis. If one end is fixed, the other moves a load in an approximately linear fashion generating a force.

An experiment of Daerden's clarifies the behavior of the PAMs [Daerden and Lefeber, 2002]. Consider a vertically oriented muscle fixed at the top end with a mass, M, attached to the other end. The pressure in the membrane is increased from an initial value of zero. At zero gauge pressure the volume in the muscle is minimal, V_{min}, and its length maximal, l_{max}. If the pressure is increased to p_1, the muscle expands radially and exert a pulling force of magnitude MG, where G is the gravitational pull. The volume of the membrane increases to V_1, and its length contracted to l_1. This tendency continues if the pressure is increased to a new level p_2. This behavior is depicted below in Figure 51

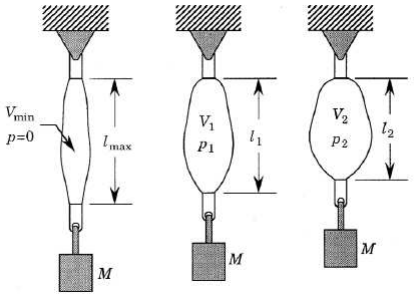

Figure 51: Muscle behavior as pressure is increased [Daerden and Lefeber, 2002]

Physical Properties

Air muscles are uniquely compliant among actuators. This is a result of two constituent factors: the actuator operates on the basis of gas compressibility and its inner bladder is elastic. Even if the gas pressure remains unchanged, an applied force that changes the length produces a spring-like behavior in the rubber material of the bladder. The elasticity of the membrane enhances the compliance of the actuator beyond the compressibility of the gas (especially true at lower pressures). This particular behavior is what distinguishes the air muscle from other actuators and makes it similar to the spring-like motion of the human limbs [Rojas and Peters II, 2005].

Static Load Characteristics

The length of a pneumatic actuator is a function of the applied pressure, the external load, and the contractile characteristics of its materials. Consider a muscle at pressure p over a time interval, dt, which leads to an increase in volume, dV. The muscle will have done pdV work and the actuator's length will have changed by dl (< 0 for shortening). The mass, M, produces a

load, F, that is displaced over the same distance requiring an amount of work, $-Fdl$. Disregarding the work needed to deform the membrane and assuming quasi-static conditions one can write,

$$F = -p\frac{dV}{dl} \tag{36}$$

As the air muscle contracts, the cylindrical shape of the muscle degenerates because of membrane deformation. This requires a correction factor to the contraction ratio, the relative change in length of the muscle with respect to its original length.

$$\epsilon = \frac{(l_o - l)}{l_o} \tag{37}$$

To show the force-contraction relationship, Daerden and Lefeber [Daerden and Lefeber, 2001] define the contraction ratio as the the change in length with respect to the maximum length l_0, shown in Equation 37. The static load characteristics as a function of contraction *percentage* (*i.e.* a contraction of 10% denoting a shortening to 9/10th of the maximum length) are shown in Figure 52. Each curve plots the value of degenerated muscle force as a function of the contraction ratio for a constant pressure value. Different pressure values act as scaling factors in the family of curves. The figure contains typical curves for PAMs, although the curve can be modified slightly based on the elastic properties of the particular membrane.

Antagonistic Pairs

As with the skeletal system, pneumatic artificial muscles were designed to work as antagonistic pairs. Two muscles are coupled around a wheel, one actuator is the agonist or active muscle while the other is the antagonist muscle. This coupling provides stability to the system by countering the

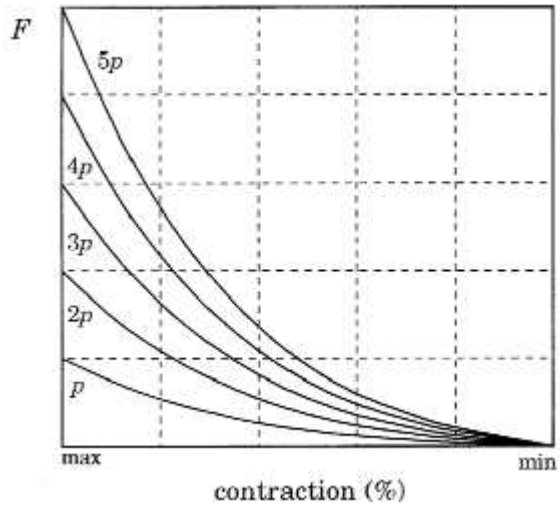

Figure 52: PAM isobaric force-contraction diagrams [Daerden and Lefeber, 2002]

motion of the opposing muscle. Force is thus generated by applying an equal but opposite change in pressure to both air muscles. Driving the system this way provides enough stiffness for stable operation of the muscles throughout their workspace. Figure 53, represents the differential pressure

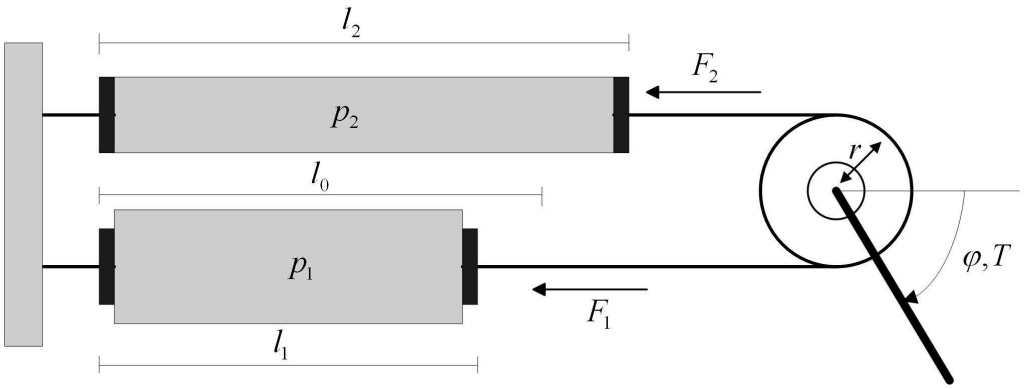

Figure 53: Antagonistic set-up [Schreder, 2003]

as: $\triangle p = \frac{1}{2}(p_2 - p_1)$; the torque as: $T = (F_2 - F_1)r$; and the angle as: $\phi = \frac{l_2 - l_1}{r}$. In [Ozkan et al., 2000], Ozkan derived equation 38 by expanding the Bridgestone Model equation (shown in next section) to represent a coupled system. This equation shows that pressure is proportional to the change in torque in the coupled system and inversely proportional to the contraction ratio.

$$P_{ki} = P_{oki} \pm \left[\frac{\tau_i}{2r(\beta_{ki} - \alpha_{ki}\epsilon_i)} - \frac{\gamma_{ki}}{(\beta_{ki} - \alpha_{ki}\epsilon_i)} \right] \tag{38}$$

where

$i =$ *the joint number*

$k =$ *the muscle index*

$P_0 =$ *the equilibrium pressure*

$\pm =$ *positive for agonist, negative for antagonist*

$\tau_i =$ *the torque for the joint*

$P_{ki} =$ *is the resulting pressure for muscle at the ith joint.*

Advantages and Disadvantages

As a result of their constituent materials, pneumatic muscles are lightweight and have a high force to weight ratio when compared to electric motors. Other significant features include easy replacement and safety due to their natural compliance. This technology, nonetheless, affords non-trivial difficulties. As part of its compliant nature, non-linearities in the system are significant, increasing the complexity to control the system. For example, an inherent challenge in the control of pneumatic actuators is hysteresis.

Pneumatic Actuator Models

Mathematical models of pneumatic actuators show the relationships between force, pressure, and contraction. In particular, these models derive joint torque as a function of change in pressure and contraction. Several models have been derived and a good overview is found in [Schreder, 2003].

Schulte presented the first static model [Schulte, 1961]. The Bridgestone Company followed when they commercialized the "rubbertuator" [Tondu et al., 1994]. In 1994, Chou and Hannaford developed a model that accounts for the wall thickness of the shell and the bladder [Chou and Hannaford, 1994]. The latter has been a foundation for many later models. Later, Caldwell *et al.* used an adaptive controller that estimates polynomial parameters to create a model [Caldwell et al., 1995]. Cai and Yamamura soon constructed a dynamical model [Cai and Yamamura, 1996]. Repperger used a second order nonlinear differential equation and adaptive methods to approximate the model [Carbonell et al., 2001]. Tsagarakis and Caldwell, improved the model by considering distortion effects at the termination nodes and radial pressure loss as a consequence of elasticity [Tsagarakis and Caldwell, 2000].

The Schulte Model

Schulte published a static physical model of the McKibben actuator in 1961 [Schulte, 1961]. The muscle force is proportional to the pressure, diameter of the actuator, and weave angle at rest.

$$F = \frac{\pi D^2 p}{4}(3\cos^2(\Theta) - 1) \tag{39}$$

where

F = *actuator force*,

π = *3.142*,

p = *internal pressure*,

Θ = *weave angle at rest*, and

D = *diameter of the actuator when* Θ *is 90 degrees.*

The Bridgestone Model

Two decades later the Bridgestone corporation published their static air muscle model. Similar to Schulte's, the force is proportional to the pressure of the muscle and its diameter, but uses a contraction ratio as opposed to a weave angle.

$$F = D_o^2 p[4(a(1-\epsilon)^2 - b)], \tag{40}$$

where

F = *actuator force*,

p = *internal pressure*,

ϵ = *contraction ratio*,

a = *muscle specific coefficient*,

b = *thread length*, and

D = *effective diameter at rest.*

Both models are similar, the Bridgestone can be converted into the Schulte through the following substitutions: $a = \pi\frac{3}{4}\frac{l_o^2}{b^2}$, $b = \frac{\pi}{4}$, $l = \cos\Theta$, $\epsilon = \frac{l_o - l}{l_o}$, and $D = D_0$.

The Chou and Hannaford model

Chou and Hanaford used a static model based on the conservation of energy. The force of the muscle is a function of the work done, pdV, and the change in actuator length, dl:

$$F = -p\frac{dV}{dl} \tag{41}$$

The volume of the cylinder is approximated by a perfect cylinder:

$$V = \frac{1}{4}\pi D^2 l \tag{42}$$

where $l = \cos\theta$ and $D = \frac{b\sin\theta}{n\pi}$. Hence:

$$V = \frac{b^3}{4\pi n^2}\sin^2\theta\cos\theta, \tag{43}$$

where b is the thread length, θ is the angle between the thread and the longitudinal axis (90 degrees at rest), and n is the number of turns in the thread.

By substituting equation 43 into equation 41, the resulting force is expressed as:

$$F = -p\frac{dV}{dl} = -p\frac{dV/d\theta}{dl/d\theta} = \frac{b^2(3cos^2\theta - 1)}{4\pi n^2} \tag{44}$$

At rest, θ is 90 degrees. This information is used to introduce a variable for the diameter at rest, D_0, where $D_0 = \frac{b}{n\pi}$. Hence, the force equation is simplified to:

$$F = \frac{\pi D_0^2 p}{4}(3cos\theta - 1) \tag{45}$$

Finally, the Schulte model was derived similarly except that the model con-

siders wall thickness, d of the shell. The volume is expressed as:

$$V = \frac{1}{4}\pi(D - 2d)^2 l \tag{46}$$

Using the modified volume in equation 46 gives:

$$F = \frac{\pi D_0^2 p}{4}(3cos\theta - 1) + p\pi \left[D_0 d \left(2\sin\theta - \frac{1}{\sin\theta} \right) - d^2 \right] \tag{47}$$

The model demonstrates that hysteresis is velocity-independent, and is predominantly caused by coulomb friction within the actuator.

[Alford and Belyeu, 1984] Alford, C. and Belyeu, S. (1984). Coordinated control of two robot arms. *Proceddings of the IEEE International Conference on Robotics and Automation*, 1:468–473.

[Ambrose et al., 2000] Ambrose, R., Aldridge, H., Askew, R., Burridge, R., Bluethmann, W., Diftler, M., Lovchik, C., Magruder, D., and Rehnmark, F. (2000). Robonaut: Nasa's space humanoid. *Journal of Intelligent Systems and Their Applications*, 15(4):57–63.

[Angelo, 2007] Angelo, J. A. (2007). *Robot Spacecraft*. Facts On File, Inc. An imprint of Infobase Publishing.

[Arimoto et al., 1987] Arimoto, S., Miyazaki, F., and Kawamura, S. (1987). Cooperative motion control of multiple robot arms or fingers. *In the Proceedings of the IEEE International Conference on Robotics and Automation*, 4:1407–1412.

[Asada and Kakumoto, 1988] Asada, H. and Kakumoto, Y. (1988). The dynamic rcc hand for high-speed assembly. *Proceedings of the IEEE International Conference on Robotics and Automation*, 1:120–125.

[Asada and Leonard, 2005] Asada, H. and Leonard, J. (Fall 2005). Introduction to robotics. *MIT OPENCOURSEWARE (ocw.mit.edu)*.

[Barrett Technology, 2009] Barrett Technology (2009). Barrett hand. `http://www.barretttechnology.com/`.

[Boon-Cheong and Chutatape, 1992] Boon-Cheong, T. and Chutatape, O. (1992). Mms and interprocess communication for multiple robot assembly system. *Proceedings of the IEEE International Symposium on Industrial Electronics*, 2:799–803.

[Brock et al., 2005] Brock, O., Fagg, A., Grupen, R., Platt, R., Rosenstein, M., and Sweeney, J. (2005). A framework for learning and control in intelligent humanoid robots. *International Journal of Humanoid Robots*, 2(3):301–336.

[Brogardh, 2007] Brogardh, T. (2007). Present and future robot control development–an industrial perspective. *Journal of Annual Reviews in Control*, 31(1):69–79.

[Brookshire et al., 2004] Brookshire, J., Singh, S., and Simmons, R. (2004). Preliminary results in sliding autonomy for assembly by coordinated teams. *In the Proceedings of the IEEE Transaction on Robots and Systems*, 1:706–711.

[Cai and Yamamura, 1996] Cai, D. and Yamamura, H. (1996). A robust controller for manipulator driven by artificial muscle actuator. In *IEEE Conference on Control Applications*, pages 540–545.

[Caldwell et al., 1995] Caldwell, D., Medran-Cerda, G., and Goodwin, M. (1995). Control of pneumatic muscle actuators. In *IEEE Control Systems Magazine*, volume 15, pages 40–48.

[Carbonell et al., 2001] Carbonell, P., Jiang, Z., and Repperger, D. (2001). A fuzzy backstepping controller for a pneumatic muscle actuator system. In *International Symposium on Intelligent Control*, page 353358.

[Chen et al., 2007] Chen, H., Zhang, G., and Zhang, H. (2007). Integrated robotic system for high precision assembly in a semi-structured environment. *Journal of Assembly and Automation*, 27(3):247–252.

[Chou and Hannaford, 1994] Chou, C. and Hannaford, B. (1994). Static and dynamic characteristics of mckibben pneumatic artificial muscles. In *International Conference on Robotics and Automation*, volume 1, pages 281–286.

[Chou and Hannaford, 1996] Chou, C. and Hannaford, B. (1996). Measurement and modeling of mckibben pneumatic artificial muscles. In *IEEE Transactions on Robotics and Automation*, volume 12, pages 90–102.

[Coelho and Grupen, 1997] Coelho, J. A. and Grupen, R. A. (1997). A control basis for learning multifingered grasps. *Journal of Robotic Systems*, 14(7):554 – 557.

[Culbert et al., 2003] Culbert, C., Rochlis, J., Rehnmark, F., Kortenkamp, D., Watson, K., Ambrose, R., Diftler, R., and Ward, B. (2003). Activities

of the nasa exploration team human-robotics working group. *Technical Report*.

[Daerden and Lefeber, 2001] Daerden, F. and Lefeber, D. (2001). The concept and design of pleated pneumatic artificial muscles. *International Journal of Fluid Power*, 2(3):41–50.

[Daerden and Lefeber, 2002] Daerden, F. and Lefeber, D. (2002). Pneumatic artificial muscles: Actuators for robotics and automation. *European Journal of Mechanical and Environmental Engineering*, 47:10–21.

[Diftler et al., 2005] Diftler, M. A., Mehling, J. S., Strawser, P. A., Doggett, W. R., and Spain, I. M. (2005). A space construction humanoid. *Proceedings of 2005 5th IEEE-RAS International Conference on Humanoid Robots*.

[DirectPerception, 2009] DirectPerception (2009). Pt 46-17 camera units. `http://www.dperception.com/products_family_ptu-d46-17.html`.

[Doggett, 2002] Doggett, W. (2002). Robotic assembly of truss structures for space systems and future research plans. *In Proceedings of the 2002 Aerospace Conference*, 7:3589–3498.

[Donald, 1987] Donald, B. R. (1987). Robot motion planning with uncertainty in the geometric models of the robot and environment: A formal framework for error detection and recovery. *Proceedings of the IEEE Transactions on Robotics and Automation*, 3:1588–1593.

[Festo, 2007] Festo (April2007). Festo muscles. `http://www.festo.com/INetDomino/us/en/223b033aa5570bd9c1256be90037be52.htm`.

[Glosser and Newman, 1994] Glosser, G. D. and Newman, W. S. (May 1994). The implementation of a natural admittance controller on an industrial manipulator. *In the Proceedings of the IEEE International Conference on Robotics and Automation*, 2:1209–1215.

[Gottschlich and Kak, 1989] Gottschlich, S. N. and Kak, A. C. (1989). A dynamic approach to high-precision parts mating. *Proceedings of the IEEE Transactions On Sistems, Man, and Cybernetics*, 19(4):797–810.

[Hayati, 1986] Hayati, S. (1986). Hybrid position/force control of multi-arm cooperating robots. *In Proceeding of the International Conference on Robotics and Automation*, pages 82–89.

[Heger et al., 2005] Heger, F. W., Hiatt, L. M., Sellner, B., Simmons, R., and Singh, S. (2005). Results in sliding autonomy for multi-robot spatial assembly. *In Proceedings of the 2005 ISAIRAS Conference*.

[Hogan, 1985] Hogan, N. (1985). Impedance control: An approach to manipulation: Part i, ii, iii. *ASME Journal of Dynamic Systems, Measurement, and Control*, 107:1–24.

[Huber, 1998] Huber, M. (1998). A control for learning locomotion gaits. *7th. International Symposium on Robotics and Applications*.

[Huber, 2000] Huber, M. (2000). *A Hybrid Architecture for Adaptive Robot Control*. Ph.d. dissertation, University of Massachusetts.

[Huntsberger et al., 2005] Huntsberger, T., Stroupe, A., and Kennedy, B. (Oct. 2005). System of systems for space construction. *In the Proceedings of the IEEE International Conference on Systems, Man and Cybernetics*, 4:3173–3178.

[Inuoe, 1981] Inuoe, H. (1981). Force feedback in precise assembly tasks. *In Artificial Intelligence: An MIT Perspecrive*, 2:219–241.

[Ishida, 1977] Ishida, T. (1977). Force control in coordination of two arms. *In the Procedings of the 5th International Conference on Artificial Intelligence*, pages 717–722.

[Jameson and Leifer, 1987] Jameson, J. and Leifer, L. (Sept. 1987). Automatic grasping: An optimization approach. *Proceedings of the IEEE Transactions on Systems, Man, and Cybernetics*, 17(5):806–813.

[Jong-Hann and Li-Chen, 1993] Jong-Hann, J. and Li-Chen, F. (1993). An adaptive control scheme for coordinated multimanipulator systems. *In the Proceedings of the IEEE Transaction on Robotics and Automation*, 9(2).

[JR3 Inc., 2009] JR3 Inc. (2009). Six axis fsensor. `http://www.jr3.com`.

[Kawamura et al., 1995] Kawamura, K., II, R. P., Bagchi, S., Iskarous, M., , and Bishay, M. (1995). Intelligent robotic systems in service of the disabled. In *IEEE Transactions on Rehabilitation Engineering*, pages 3.1:14–21.

[Klute and Hannaford, 1998] Klute, G. and Hannaford, B. (1998). Fatigue characteristics of mckibben artificial muscle actuators. In *Proceedings of the International Intelligent Robots and Systems IROS*, pages 1776–82.

[Klute et al., 1999] Klute, G., Hannaford, B., and Czemiecki, J. (1999). Mckibben artificial muscles: Pneumatic actuators with biomechanical intelligence. In *Proceedings of the International Conference on Advanced Intelligent Mechatronics*.

[Kumar and Waldron, 1988] Kumar, V. R. and Waldron, K. J. (1988). Force distribution in closed kinematic chains. *In the Proceedings of the IEEE Journal Robotics and Automation*, 4(6):657–664.

[Lee and Smith, 1984] Lee, C. S. G. and Smith, R. H. (1984). Force feedback control in insertion process using pattern analysis techniques. *In Proceedings of the American Control Conference*, pages 39–44.

[Liu et al., 1996] Liu, Y. H., Arimoto, S., and Ogasawara, T. (1996). Decentralized cooperation control: Non-communication object handling. In *IEEE International Conference on Robotics and Automation*, pages 2414–2419.

[Maples and Becker, 1986] Maples, J. A. and Becker, I. J. (1986). Experiments in force control of robotic manipulators. *Proceedings of the IEEE Transactions on Robotics and Automation*, 2:695–702.

[Mason, 1981] Mason, M. (1981). Compliance and force control for computer controlled manipulators. *Trans. IEEE Sys., Man. Cyber.*, pages SMC–11(6):418–432.

[Mathewson, 1994] Mathewson, B. B. (1994). *Integration of Force Strategies and Natural Admittance Control*. PhD thesis, Case Western University.

[Motoman, 2009] Motoman (2009). The hp3jc industrial manipulator. `http://www.motoman.com`.

[Mukaiyama et al., 1996] Mukaiyama, T., Kim, K., and Hori, Y. (1996). Implementation of cooperative manipulation using decentralized robust position/force control. *In the Proceedings of the 4th International Workshop on Advanced Motion Control,*, pages 529–534 vol.2.

[Nakamura et al., 1989] Nakamura, Y., Nagai, K., and Yoshikawa, T. (1989). Dynamics and stability in coordination fo multiple robotic mechanisms. *International Journal of Robotics Res.*, 8(2):44–61.

[Namvar and Aghili, 2005] Namvar, M. and Aghili, F. (2005). Adaptive force-motion control of coordinated robots interacting with geometrically unknown environments. *In the Proceedings of the IEEE Transactions on Robotics*, 21(4):678–694.

[Namvar and Aghili, 2006] Namvar, M. and Aghili, F. (2006). Adaptive force control of robots in presence of uncertainty in environment. *In the Proceedings of the 2006 American Control Conference*, pages 3253–3258.

[NASA, 2006a] NASA (2006a). International space station: Canada arm. `http://www.nasa.gov/mission_pages/station/structure/index.html`.

[NASA, 2006b] NASA (2006b). Nasa's humanoid: Robonaut. `http://robonaut.jsc.nasa.gov`.

[NASA, 2007] NASA (2007). Nasa's small business innovative research (sbir). `http://sbir.gsfe.nasa.gov/SBIR/sbirsttr2003/solicitation/SBIR`.

[Newman et al., 2001a] Newman, W., Branicky, M., Pao, Y., Birkhimer, C., Chhatpar, S., Wei, J., and Zhao, Y. (2001a). Intelligent strategies for compliant robotic assembly. *In the Proceedings of the IEEE International Conference on Robotics and Automation.*

[Newman et al., 2001b] Newman, W. S., Zhao, Y., and Pao, Y. H. (2001b). Interpretation of force and moment signals for compliant peg-in-hole assembly. *In the Proceedings of the IEEE International Conference on Robotics and Automation*, 1:571–576.

[Nickel et al., 1963] Nickel, V., Perry, J., and Garrett, A. (1963). Development of useful function in the severely paralyzed hand. *Journal of Bone andJoint Surgery*, (5):45A:933–952.

[Oda, 2000] Oda, M. (2000). Experiences and lessons learned from the ets-vii robot satellite. *In the Proceedings of the IEEE International Conference on Robotics and Automation*, pages 914 – 919.

[OḰeefe, 2004] OḰeefe, S. (2004). The vision for space exploration. Technical report, National Aeronautics and Space Administration.

[Olivares, 2003] Olivares, R. E. (2003). The intelligent machine architecture version 2.5: A revised development environment and software architecture. Master's thesis, Vanderbilt University.

[Ozkan et al., 2000] Ozkan, M., Inoue, K., Negishi, K., and Yamanaka, T. (2000). Defining a neural network controller structure for a rubbertuator robot. *Neural Networks*, pages 13:533–544.

[Pack, 1999] Pack, R. T. (1999). *IMA: The Intelligent Machine Architecture*. Ph.d. dissertation, Vanderbilt University, 2201 West End Avenue, Nashville, Tennessee 37235.

[Peshkin, 1990] Peshkin, M. A. (1990). Programmed compliance for error-corrective manipulation. *Proceedings of the IEEE Transactions on Robotics and Automation*, 6(4):473–482.

[Peters II et al., 2003a] Peters II, R. A., Campbell, C. L., Bluethmann, W. J., and Huber, E. (2003a). Robonaut task learning through teleoperation. In *IEEE International Conference on Robotics and Automation*, Taipei, Taiwan.

[Peters II et al., 2003b] Peters II, R. A., Hambuchen, K. A., and Bodenheimer, R. E. (2003b). Motion transformations of the sensory ego-sphere. Technical Report CIS-03-11, Center for Intelligent Systems, Vanderbilt University, Nashville, TN.

[Peters II and Jenkins, 2006] Peters II, R. A. and Jenkins, O. C. (2006). Uncovering manifold structures in robonaut's sensory-data state space. *In the Proceedings of the IEEE-RAS International Conference on Humanoid Robots*.

[Peters II et al., 2006] Peters II, R. A., Jenkins, O. C., and Bodenheimer, R. E. (2006). Sensory-motor manifold structure induced by task outcome: experiments with robonaut. In *Proceedings of the IEEE/RAS International conference on Humanoid Robots (Humanoids 2005)*, pages 484–489, Genoa, Italy.

[Pires and da Costa, 1998] Pires, J. N. and da Costa, J. M. G. S. (1998). Running an industrial robot from a typical personal computer. *IEEE International Conference on Electronics, Circuits and Systems*, 1:267–270.

[Platt et al., 2002] Platt, R., Fagg, A. H., and Grupen, R. A. (2002). Nullsapce composition of control laws for grasping. *In the Proceedings of the IEEE International Conference on Intelligent Robots and Systems.*

[Platt et al., 2004] Platt, R., Fagg, A. H., and Grupen, R. A. (2004). Manipulation gaits: sequences of grasp control tasks. In *Proceedings of the IEEE International Conference on Robotics and Automation*, volume 1, pages 801–806.

[Platt et al., 2006] Platt, R., Grupen, R., and Fagg, A. (2006). Improving grasp skills using schema structured learning. *In the Proceedings of the IEEE International Conference on Development and Learning.*

[Platt, 2006] Platt, R. J. (2006). *Learning and generalizing control-based grasping and manipulations skills.* PhD thesis, University of Massachusetts Amherst.

[Prisma Lab, 2007] Prisma Lab (2007). Cooperative control schemes. `http://www.prisma.unina.it/ramsete/coop.htm`.

[Raibert and Craig, 1981] Raibert, M. and Craig, J. (1981). Hybrid position/force control of manipulators. *In the Transactions of the ASME Journal of Dynamic Systems, Measurement, and Control*, 103:126–133.

[Rehnmark et al., 2005] Rehnmark, F., Ambrose, R. O., Kennedy, B., Diftler, M., Mehling, J., Bridgwater, L., Radford, N., Goza, S. M., and Culbert, C. (2005). Innovative robot archetypes for in-space construction and maintenance. volume 746, pages 1070–1077.

[Rehnmark et al., 2003] Rehnmark, F., Bluethmann, W., Huber, E., Rochlis, J., and Ambrose, R. (2003). Useful interactions between human and robotic agents performing a cooperative assembly task. *Space*.

[Rhodes et al., 1990] Rhodes, M. D., Will, R. W., and Wise, M. A. (1990). A telerobotic system for automated assembly of large space structures. *The 21st Century in Space – American Astronautical Society*, pages 111–117.

[Rojas, 2004] Rojas, J. (2004). Sensory integration with articulated motion on a humanoid robot. Master's thesis, Vanderbilt University.

[Rojas and Peters II, 2005] Rojas, J. and Peters II, R. A. (2005). Sensory integration with articulated motion on a humanoid robot. *Journal of Applied Bionics and Biomechanics*, 2(3-4):171–178.

[Rojas and Peters II, 2009] Rojas, J. and Peters II, R. A. (2009). Preliminary results in force guided assembly for teams of heterogeneous robots. *SPIE's Defense, Security, and Sensing. Accepted and pending publication.*

[Schimmels and Peshkin, 1990] Schimmels, J. M. and Peshkin, M. A. (1990). Accommodation matrices for error-corrective assembly. *Proceedings of the IEEE Transactions on Robotics and Automation*, (714-719).

[Schreder, 2003] Schreder, J. (2003). Position control of a humanoid robot arm actuated by artificial muscles. Master's thesis, Universitt Karlsruhe.

[Schulte, 1961] Schulte, H. (1961). The characteristics of the mckibben artificial muscle. In *The Application of External Power in Prosthetics and Orthotics*, Washington D.C. National Acamy of Sciences - National Research Council.

[Sellner et al., 2005] Sellner, B., Simmons, R., and Singh, S. (Dec. 2005). *Multi-Robot Systems. From Swarms to Intelligent Automata Volume III. Proceedings from the 2005 International Workshop on Multi-Robot Systems*. Springer Netherlands.

[Shadow Company, 2007] Shadow Company (2007). Shadow muslces. `http://www.shadow.org.uk`.

[Shahinpoor and Zohoor, 1991] Shahinpoor, M. and Zohoor, H. (9-11 Apr 1991). Analysis of dynamic insertion type assembly for manufacturing

automation. *Proceedings of the IEEE International Conference on Robotics and Automation*, 3:2458–2464.

[Simmons et al., 2007] Simmons, R., Singh, S., Heger, F. W., Hiatt, L. M., Koterba, S. C., Melchior, N., and Sellner, B. P. (2007). Human-robot teams for large-scale assembly. In *Proceedings of the NASA Science Technology Conference.*

[SMC, 2009] SMC (2009). Air servo valves. `http://www.alliedelec.com/Search/ProductDetail.aspx?SKU=499-0654`.

[Son et al., 1996] Son, J., Howe, R., and Hager, G. (Nov. 1996). Preliminary results on grasping with vision and touch. *In the Proceedings of the IEEE Conference on Intelligent Robots and Systems*, 3:1068–1075.

[Stemmer et al., 2007] Stemmer, A., Albu-Schffer, A., and Hirzinger, G. (2007). An analytical method for the planning of robust assembly tasks of complex shaped planar parts. *In IEEE International Conference on Intelligent Robots and Systems*, pages 317–323.

[Stroupe et al., 2006] Stroupe, A., Okon, A., Robinson, M., Huntsberger, T., Aghazarian, H., and Baumgartner (April 2006). Sustainable cooperative robotic technologies for human and robotic outpost infrastructure construction and maintenance. *Journal of Autonomous Robots*, pages 113–123.

[Sun and Mills, 2002] Sun, D. and Mills, J. K. (2002). Adaptive synchronized control for coordination of multirobot assembly tasks. *In the Proceedings of the IEEE International Conference on Robotics and Automation*, 18(4):498–510.

[Thomas et al., 2007] Thomas, U., Molkenstruck, S., Iser, R., and Wahl, F. M. (2007). Multi sensor fusion in robot assembly using particle filters. *Proceedings of the IEEE Transactions on Robotics and Automation*, pages 3837–3843.

[Thomas et al., 2005] Thomas, U., Wahl, F. M., Maass, J., and Hesselback, J. (2005). Towards a new concept of robot programming in high speed assembly applications. *In IEEE International Conference on Intelligent Robots and Systems*, pages 3827–3833.

[Tondu et al., 1994] Tondu, B., Boitier, V., and Lopez, P. (1994). Naturally compliant robot-arms actuated by mckibben artificial muscles. *Systems, Man, and Cybernetics*, 3:2635–2640.

[Tsagarakis and Caldwell, 2000] Tsagarakis, N. and Caldwell, D. (2000). Improved modelling and assessment of pneumatic muscle actuators. In *IEEE Conference on Robotics and Automation*, page 36413646.

[VitalSystem, 2009] VitalSystem (2009). Control and data acquisition pci cards. `http://www.vitalsystem.com/web/motion/motionLite.php`.

[Walker, 1990] Walker, M. W. (1990). Adaptive control of manipulators containing closed kinematic loops. *In the Proceedings of the IEEE Transactions on Robotics and Automation*, 6(1):10–19.

[Watson, 1981] Watson, P. C. (1981). The remote center of compilance system and its applications to high speed assemblies. *In Industrial Robotics: Fundamentals, Robotics, Int. SMe*, 1:404–414.

[Whitney, 1987] Whitney, D. (1987). Historical perspective and state of the art in robot force control. *The International Journal of Robotics Research*, (1):6:3–14.

[Williamson, 1995] Williamson, M. (1995). Series elastic actuators. Master's thesis, Massachusetts Institute of Technology.

[Xi et al., 96] Xi, N., Tarn, T. J., and Bejczy, A. K. (96). Intelligent planning and control for multirobot coordination: An event-based approach. *In the Proceedings of the IEEE Transaction on Robotics and Automation*, 12(3):439–452.

[Yaman, 2000] Yaman, A. (2000). Load independent trajectory control for an artificial muscle. Master's thesis, Bogazii University.

[Yobotics, 2007] Yobotics (2007). Series elastic actuators. `http://yobotics.com/actuators/description/description.htm`.

[Yoshikawa, 1987] Yoshikawa, T. (1987). Dynamic hybrid position/force control of robot manipulators – description of hand constraints and calculation of joint driving force. *In the Proceedings of the IEEE Journal of Robotics and Automation*, RA-3(5):386–392.

[Yoshikawa, 1993] Yoshikawa, T. (1993). Coordinated dynamic hybrid position/force control for multiple robot manipulators handling one constrained object. *In the Proceedings of the IEEE Journal of Robotics Research*, 12(3):219–230.

[Yoshikawa and Nagai, 1987] Yoshikawa, T. and Nagai, K. (1987). Manipulating and grasping force in manipulation by multifingered hands. *In the Proceedings of the IEEE International Conference on Robtics and Automation*, pages 1998–2004.

[Yuan, 2006] Yuan, P. (2006). An adaptive feedback scheduling algorithm for robot assembly and real-time control systems. *In the Proceedings of the IEEE International Conference on Intelligent Robots and Systems*, pages 2226–2231.